Snap-Through of a Shallow Arch Subjected to Random Excitation

by

Thiwa Penketgorn

Dissertation submitted to the Faculty of the

Virginia Polytechnic Institute and State University

in partial fulfillment of the requirements for the degree of

Doctor of Philosophy

in

Civil Engineering

APPROVED:

K. B. Rojiani, Chairman

R. H. Plaut

R. M. Barker

R. K. Kapania

T. M. Murray

February, 1988

Blacksburg, Virginia

Snap-Through of a Shallow Arch Subjected to Random Excitation

by

Thiwa Penketgorn

K. B. Rojiani, Chairman

Civil Engineering

(ABSTRACT)

The motion of a shallow arch subjected to random loading is investigated. It is expected that the arch will vibrate about its initial stable configuration under low intensity loading, but will snap back and forth about its horizontal axis under high intensity loading. The parameter of interest is the time of first snap-through of the shallow arch under random load. This is defined as the time taken for the arch to snap to the other side of the horizontal axis. The statistics of the time to first snap-through, such as the mean time to failure as well as its probability distribution, are determined. Most of the work treats one response mode.

In the first part of the study, the critical random loading for dynamic snap-through of the shallow arch was investigated using the method of computer simulation. The random excitation was assumed to be a stationary white-noise process. The primary object was to determine the critical power spectral density parameter of the random excitations. The vanishing or diminishing of the average frequency of snap-through was used to estimate this parameter. An exact value of the critical random loading parameter could not be obtained using this criterion since it was based on numerical integration of the non-linear equation of motion and computer simulation which is expensive and time-consuming. However, the critical value or range of critical values of intensity of random excitations could be estimated with a reasonable degree of accuracy.

The second part of the study dealt with the first-passage problem. The exact solution of the first-passage problem is available for only a limited class of problems. In this study, the solution was obtained using numerical approximation techniques and computer simulation. For an oscillator subjected to white noise, the displacement and velocity process are governed by the Fokker-Planck-Kolmogorov (FPK) equation. The finite difference method was used to

solve the derived FPK equation of the energy envelope of the equation of motion of the arch subjected to white-noise excitation. Solution were obtained in terms of the mean time to failure, and the probability distribution function of the time to failure.

A computer program for the Monte Carlo simulation of the response of the arch subjected to random loads was also developed. A large number of records of the random excitations were simulated and these were used as input in the numerical integration of the equation of motion. The Runge-Kutta method was used to obtain the time history of the displacement response, and the time at which the response exceeded the critical threshold was recorded. Statistics of the time to first snap-through were obtained and these were then used to select an empirical distribution model for the first-passage time. The results of the approximate analysis were compared with those from the simulation. Results of both methods were in close agreement.

The effect of including more than one mode in the equation of motion was also studied. Multi-mode approximations of up to four modes were considered in the analysis. It was found that the results of the multi-mode approximations are significantly different from the one-mode approximation. The effect of nonstationary random excitation on the time to first snap-through was also investigated using computer simulation.

Acknowledgements

I would like to thank the Civil Engineering Department and all professors in the structural engineering division. Special thanks are due to Dr. Rojiani and Dr. Plaut for their advice and guidance in finishing this dissertation. I also thank Dr. Barker, Dr. Kapania, and Dr. Murray for serving on the advisory committee. The success of this study is partly due to the VPI computer facilities and computer time.

I am very fortunate to have many good friends surrounding me, and I would like to take this opportunity to acknowledge their kindness and friendship. First, I would like to acknowledge the kindness of Preecha and Kanokporn Mapunya and their family. Although I am actually very far from home, I always feel warm from the love of my family which gives me strength and encouragement to keep on trying. My special thanks go to my mother and a little lady named Nattaya.

Finally, I would like to thank the Thai Government, especially the Royal Thai Army, for letting me continue my study and for their support.

Table of Contents

List of Illustrations

List of Tables

Chapter I

Introduction

1.1 General

The dynamic stability of shallow structures, such as shells and arches, under deterministic loadings has been studied by many researchers. However, the behavior of real structures in most cases is governed by various uncertainties due to the imperfections of structures and the stochastic nature of actual loads. For instance, dynamic responses of elastic shallow structures subjected to ground acceleration caused by earthquakes possess uncertainties in the earthquake excitation which is random in nature, and in the variability of complex geometry and material properties of structures. A deterministic framework is unrealistic for the study of structures subjected to random loads. As a result, the concepts of probability and mathematical statistics should be used in investigating the behavior of shallow structures under random excitations.

Probability theory has been widely applied in safety and performance analysis of structures. In dealing with uncertainties in structural design, the probabilistic framework is believed to provide a more rational approach than the deterministic framework. Probability theory is closely related to the concepts of reliability and stability of structures, as pointed out by Bolotin [11]. The reliability or the probability of safe performance is equal to one minus the probability of failure. An acceptable design is the one with a sufficiently small probability of

failure. The probability distributions of parameters of interest, which describe the behavior of the structure, must therefore be determined and used to evaluate the probability of safe performance of the structure. The reliability of the structure under any disturbances is associated with the probability that these parameters of interest stay in a "safe" region in the parameter space. Therefore, the measure of reliability is the probability that all parameters stay within the specified safe region.

1.2 Purpose and Scope

The purpose of this study is to investigate the dynamic stability of a shallow arch subjected to random excitations. The problem involves the failure of the arch due to dynamic snap-through. There are two basic topics that may be addressed in studying the dynamic behavior of shallow arch under stochastic loads. The first one is concerned with the probability of first snap-through at a given time. The second one is the determination of the probability distribution of time of first snap-through starting from a given initial condition. The parameter of interest in the second problem is the time to first snap-through. This class of problem is also known as the first-passage time problem in probability theory.

This study considers a shallow arch with deterministic properties, that is, known initial arch curvature and arch rise. The arch is assumed to be simply supported and to have a constant cross-section. The initial arch rise is small; therefore, the arch is shallow and capable of exhibiting dynamic snap-through instability under loads. The load applied to the arch is taken to be a zero-mean random process. There is no initial static load, and the motion of the arch is assumed to start from rest.

The equation of motion for this problem is governed by a stochastic differential equation in time and space with non-parametric random loading, and is nonlinear due to the initial shape of the arch. The techniques used for the determination of the response of a nonlinear system excited by random loads are as follows: (a). the exact Markov vector approach, and

(b). several approximation techniques, such as the approximate solution of the Fokker-Planck equation, the perturbation method, the equivalent linearization method, closure methods, and the method of Monte Carlo simulation.

An exact solution to the first-passage probability for this type of nonlinear system is not yet available. In this study, the energy envelope process of the response is used to approximate the Fokker-Planck-Kolmogorov (FPK) equation of the amplitude response process [76]. The FPK equation for the energy envelope process, with suitable boundary conditions, is then solved numerically using the implicit finite difference method. This approximation technique is restricted to the system excited by stationary white noise only.

A computer simulation procedure is developed to generate the response of the shallow arch subjected to white-noise excitation, and the statistics of the first-passage probability, such as the mean time to failure, are determined using the Monte Carlo method. Results obtained from Monte Carlo simulation are then compared to those of the energy envelope approximation to examine the reliability of the approximation technique for this problem.

Since the approximation techniques can be used only for the system excited by a stationary wide-band random process such as a white noise, the simulation method is used to obtain estimates of the probability distribution of the first-passage time for the shallow arch subjected to nonstationary random disturbances of the earthquake type. The nonstationary earthquake excitation is represented by the product of a stationary white noise and a deterministic function of time.

1.3 Organization

In Chapter 2, a review of the literature and current research related to this study are presented. The reviewed papers are related to dynamic instability of a shallow arch, theory of nonlinear random vibrations and the first-passage time problem, and stochastic models of earthquake excitation.

In Chapter 3, the features of the shallow arch to be considered and the governing equation of motion are described and formulated. The failure criterion and the first-passage time problem of the shallow arch are also stated.

In Chapter 4, the approximation technique used to solve the first-passage probability of the nonlinear Fokker-Planck-Kolmogorov equation is described. The random excitation is assumed to be a stationary white-noise process.

In Chapter 5, the Monte Carlo simulation procedure is detailed and used to obtain the probability of the first-passage time. The random load is also assumed to be a stationary white noise.

In Chapter 6, the results obtained from Chapters 4 and 5 are discussed and compared. Monte Carlo simulation is then used to estimate the first-passage probability of a shallow arch subjected to nonstationary random excitation of an earthquake type. The nonstationary random excitation considered in this study is a modulated white-noise process.

Chapter 7 presents the conclusions of this study.

Chapter II

Literature Review

2.1 Dynamic Instability of a Shallow Arch

The critical transverse loading of a shallow arch depends upon the dimensions and rigidity of the arch, the end conditions, the initial curvature of the arch, and the type of load distribution [27]. There are two possibilities for instability of shallow arches: an inextensional buckling, and an extensional buckling. For sufficiently steep arches, the instability will be an inextensional buckling. For shallow arches, the induced axial thrust due to the bending of the arches is significant and the arches will exhibit an extensional buckling; therefore, the shallow arches are capable of failure by the snap-through phenomenon.

Snap-through of a shallow arch under deterministic loadings has been studied by many researchers. The critical static load for snap-through of a shallow arch was investigated by Fung and Kaplan [27] and others. The dynamic snap-through of the arch is more relevant to this study. The stability criteria used for dynamic snap-through of shell-type structures are generally based on the Budiansky and Roth criterion [12] or the Hsu sufficient condition [37].

In the study of dynamic snap-through of shallow arches under deterministic loading, the arches with deterministic initial curvature, mostly circular and sinusoidal, having simply supported or clamped boundary conditions have been investigated. For deterministic dynamic

loads, investigations dealing with shallow arches have included step loads [26,40,59,60], impulse loads [40,60,68], and harmonic loads [25,61].

Although there have been several studies on the response of shallow arches subjected to stochastic loadings, most of the work has dealt with the stochastic response of shell-type structures, where the governing equation of motion is similar to the arch problem. Ariaratnam and Sankar [5] studied the dynamic snap-through of a shallow arch subjected to random loading. The equation of motion was derived using Lagrange's equation, and for a single mode approximation, the equation has the following form:

$$\ddot{q} + c\dot{q} + \omega_o^2(q + \varepsilon_1 q^2 + \varepsilon_2 q^3) = f(t) \tag{2.1}$$

where q is the generalized coordinate giving a measure of transverse deflection, c is a damping coefficient, ω_o is the natural frequency of a corresponding linearized equation, ε_1 and ε_2 are the constant coefficients of the nonlinear terms, and $f(t)$ is the generalized time-dependent forcing function.

A similar equation governing the dynamic response of shell-type structures was also derived by Bolotin [11], in which a thin, elastic curved panel subjected to a random transverse force was considered. Bolotin [11] considered the random force, $f(t)$, to be a stationary white-noise process, and obtained an approximate solution to the mean time to first snap-through using the Galerkin technique.

If the random force $f(t)$ is assumed to be a wide-band random process, the system response $(q, \dot{q})$ can be approximated by a Markov vector process. The probability distribution of time of first snap-through or the first-passage probability is governed by the backward Kolmogorov equation, and the moments of time to first snap-through are governed by the generalized Pontriagin-Vitt equations [8,11]. For most studies, the probability of time for first snap-through is the main objective, and the mean time to first snap-through is the single important parameter of interest [5,8,11,65,76]. For a nonlinear system, as in the case of this study, an analytical solution of the probability distribution is not yet available.

Ariaratnam and Sankar [5] assumed that the random load, $f(t)$, was a stationary, wide-band random process. The response process was approximated by a Markov process which subsequently gave the Fokker-Planck equation, which described the diffusion process of the response. They solved the problem and obtained the probability of first snap-through for the arch in a given time interval.

Pi, Ariaratnam, and Lennox [65] considered a long cylindrical panel subjected to random loading. Using a single mode approximation, an equation of motion similar to Eq. (2.1) was obtained. Computer simulation was used to generate a wide-band random process for the stochastic loading function, $f(t)$, and the nonlinear differential equation was solved using a fifth order Runge-Kutta procedure. The results obtained were the probability density function for the time of first snap-through and the mean time to first snap-through.

Kuak and Lennox [56] considered a cylindrical shell under a wide-band random excitation, and obtained the probability distribution of the first-passage time using the finite element method and the method of weighted residuals [58]. Other numerical techniques, such as the finite difference scheme and Monte Carlo simulation, have also been used to obtain estimates of the first-passage probability [28,76].

A similar type of problem was recently considered by Seide [78,79], where the responses of initially buckled beams subjected to uniform random pressure were investigated. The equation of motion obtained for the initially buckled beams was similar to that given by Eq. (2.1) for the shell-type structures. Responses of the buckled beams were determined using the equivalent linearization technique of the random vibrations and the computer simulation method. The load was assumed to be a wide-band stationary random process having a constant power spectrum and a zero mean. Seide also investigated the snap-through of initially buckled beams, and the critical power spectral density parameters of the random loads were also estimated.

The dynamic snap-through of a shallow arch subjected to random loading is related to the first-passage problem of the theory of probability and random vibrations. The next section

will review the related literature involving solution techniques for nonlinear random vibration and the first-passage probability.

2.2 Nonlinear Random Vibrations and First-Passage Time Problems

The failure of a shallow arch under random excitation is associated with the occurence of the first "snap-through". Therefore, the time to first snap-through, which is also known as the first-passage time, is the parameter of interest.

The governing equation of motion of a shallow arch subjected to random loadings is nonlinear with a restoring spring force of softening type. A similar nonlinearity is found in the vibrational system called the Duffing oscillator. The response of the Duffing nonlinear system under random excitations has been studied extensively. However, the exact solution of the first-passage time problem is not yet available.

Reviews of methods of nonlinear random vibration analysis have been given by Caughey [16], Crandall [21], and Iwan [48]. Recently, techniques for solving nonlinear random vibration problems were summarized by Roberts [74] and To [90]. The most powerful method for nonlinear random vibration problems is based on the Markov vector approach, where the corresponding Fokker-Planck equation which governs the joint probability distribution of the displacement and velocity responses of a nonlinear system can be solved [63]. However, the exact solution of the Fokker-Planck equation is only available for a certain class of systems [15,23]. Techniques for solving nonlinear random vibrations rely mostly on approximate methods, which include an approximate solution of the Fokker-Planck equation, the perturbation method, the equivalent linearization method, the Gaussian and non-Gaussian closure methods, and the methods of computer simulation.

Since the exact solution for most practical problems is not available, various techniques have been developed to obtain the approximate solution of the Fokker-Planck equation. These approximation techiques include the method of iterative solution [41,57], the method of

eigenfunction expansion [6], the Galerkin method [94], and the method of stochastic averaging [75].

For the solution of weakly nonlinear systems, the perturbation method has been used extensively [19,63]. The perturbation method was developed from the classical asymptotic method for deterministic vibration. However, there are considerable difficulties in the application of the perturbation method when linear viscous damping is absent from the vibrational system.

The equivalent linearization method is widely used and has become a very popular method in nonlinear random vibrations [14,46,47,49]. In this method, the nonlinear system is replaced by an appropriately equivalent linear system, providing that the ensemble average of the difference of the two systems is minimized. The response of the nonlinear system is approximated by the solution of the equivalent linear system.

The Gaussian and non-Gaussian closure techniques have been developed from a class of closure techniques [22,50], where it is assumed that the moment equations are closed regarding the statistical structure of the response. The Gaussian technique assumes that the response statistics are Gaussian, which is the same assumption that is used in the perturbation method and the equivalent linearization method. The non-Gaussian method takes into account the non-Gaussian statistics of the response. The response of the nonlinear system is approximated from the moment equations up to a finite order of moments.

The techniques of computer simulation, one of which is known as the Monte Carlo method, have been developed due to the inefficiency of the other approximate methods in solving highly nonlinear systems and the non-existence of an exact solution [82,92]. The Monte Carlo method is also used frequently to examine the reliability of an approximate method for certain nonlinear systems where exact solutions are not available. The procedure of computer simulation generally begins with the generation of a random forcing function. Then, the governing equation of motion of the nonlinear system is solved numerically and the response realizations are obtained. Finally, the statistics of the response are determined from a large number of realizations. To obtain reliable results it becomes necessary to use a large

number of realizations. This makes the Monte Carlo simulation method expensive and time-consuming. However, it is generally applicable, especially when the nonlinear systems can not be solved by other approximate methods.

Due to the availability of fast digital computers and efficient techniques for generating the random forcing function, a large number of realizations of system responses can be generated. Therefore, the Monte Carlo simulation method has been extensively used in nonlinear random vibrations [20,28,83,84,87,92,96].

The response statistics obtained using the previously mentioned approximation methods are usually given in terms of the moments of the response, such as the root mean square response or the autocorrelation function. However, the probability of the first passage time can not be obtained directly using these methods, except for the computer simulation method. It is known that the approximate solution of the first-passage problem for linear oscillators subjected to a stationary white-noise process is completely established [70,71]. However, the first-passage time problem for nonlinear systems is still in need of much research. The nonlinearity of the system is obviously important in the first-passage problem, since a small magnitude of nonlinearity can significantly influence the solution of the probability of the first-passage failure when the critical level is high [71].

The earlier relevant works on the first-passage time problem of nonlinear systems are studies by Goldberg, et al. [28], and Toland and Yang [91]. Goldberg, et al [28] used a computer simulation technique to estimate the first-passage probability of simple nonlinear systems subjected to a nonstationary random disturbance of an earthquake type. Toland and Yang used an approximate numerical technique to diffuse probability in the phase plane to determine the first-passage time probability distribution of linear and nonlinear vibrational systems excited by a stationary white-noise process. Results of both studies were limited due to the lengthy computation procedure.

In the application of numerical techniques in solving the first-passage time probability, the appropriate boundary conditions must be correctly specified and the problem must be well posed [97]. For nonlinear systems excited by a white-noise process, the numerical approxi-

mation techniques that have been used are: the finite element method [9,56], a discrete random walk model approximating the Fokker-Planck-Kolmogorov equation [72,91], the implicit finite difference scheme solving the Fokker-Planck-Kolmogorov equation of the energy envelope process [76], the Monte Carlo simulation method [28,65], and the application of the Galerkin technique and the perturbation method in solving the backward Kolmogorov equation [88]. The method of Monte Carlo simulation is often used to assess the reliability of the proposed approximation techniques.

For a system with nonlinear restoring force, the equation of motion is generally of the form

$$\ddot{X} + \beta\dot{X} + G(X) = f(t) \tag{2.2}$$

where $X(t)$ is the displacement response, β is a small parameter which may be regarded as a damping coefficient, $G(X)$ is a nonlinear function, and $f(t)$ is a stationary white-noise excitation.

The energy envelope process $V(t)$ of the response process of Eq. (2.2) is defined as

$$V(t) = \frac{\dot{X}^2}{2} + U(X) \tag{2.3}$$

where the first term on the right-hand side is the kinetic energy and the function

$$U(X) = \int_0^X G(\xi)d\xi \tag{2.4}$$

is the potential energy.

It has been shown that, for sufficiently light damping, the $V(t)$ process is a close approximation to a one-dimensional Markov process [71,72,73,76], and it can be used to obtain estimates of the first-passage probability of oscillators with strong arbitrary nonlinear restoring forces [72,76].

Roberts [72] used a discrete random walk model of the energy envelope to obtain estimates of the first-passage probability of a Duffing oscillator subjected to white-noise excitation, and estimates of the mean time to first passage were determined. Results agreed well with the computer simulation results. In Ref. [76], Roberts applied the implicit finite difference scheme of the Crank-Nicolson type [85] to solve the diffusion equation of the energy envelope, and estimates of the mean time to failure of nonlinear oscillators under a stationary white noise were obtained. Results obtained by Roberts agreed closely with the results of a much more complex and time-consuming numerical finite element solution of the two-dimensional diffusion equation [9].

The random excitations considered by most studies reviewed above were limited to a stationary wide-band random process only, in which white noise was assumed frequently. Only the study by Goldberg, et al. [28] considered nonstationary random excitation of the earthquake type using a computer simulation method. In reality, white noise is physically unrealizable and dynamic loads in most practical problems are nonstationary in nature. The next section will review nonstationary random processes that have been used to represent earthquake ground motions.

2.3 Stochastic Models of Earthquake Excitations

The nature of excitations, in addition to the damping and nonlinearity of the system, is an important factor in selecting a suitable model for a structural or mechanical system. Two types of random excitations are known: parametric excitations which are time-dependent coefficients of the equation of motion, and non-parametric excitations which are nonhomogeneous parts of the equation of motion. Non-parametric excitations are considered in this study. According to the time duration of the random excitations, they can be classified into stationary and nonstationary random processes. When the duration of an excitation is relatively much longer than the oscillation period of the system, the excitation is stationary. On the other

hand, the excitation with relatively short duration compared to the period of the system is nonstationary. The random disturbances in nature that can be successfully described, on a stochastic basis, by the nonstationary random excitations are earthquake ground motions, severe turbulence [81], sea waves, and wind loads.

An earthquake ground motion is nonstationary, in which its autocorrelation function is variant with time [3]. In the past, selection of a realistic model of earthquake ground motions was based on past earthquake accelerograms, simple harmonic accelerations, a sequence of random impulses, and even stationary white noise. Several nonstationary models have been developed for representing the ground motions; among these are the simulation models of Bogdanoff, Goldberg, and Bernard [10], Shinozuka and Sato [81], and Amin and Ang [2]. However, in the strong motion part of an earthquake, which is primarily important to engineers, the ground motion may be assumed stationary. The so-called strong-motion earthquakes which are intense enough to cause structural damage are of main concern.

2.3.1 Response of Structures to Earthquake Excitations

The three approaches that have been used to determine structural responses due to earthquake ground motions are as follows: response spectra approach, time integration method, and theory of random vibrations [17]. For a nonlinear system, the time integration method is generally employed. The step-by-step integration procedure is probably the most powerful technique for nonlinear analysis. Chapter 6 of this study will use the time integration approach to obtain the probability of first snap-through of a shallow arch subjected to earthquake excitations.

The time integration approach involves step-by-step time integration of a governing equation of motion where the random loading function is based on an artificial earthquake ground motion generated by a computer [93]. This method is generally applicable for all problems, especially for complex nonlinear systems, but it is time-consuming and expensive.

In the numerical time integration procedure, the accuracy of this method depends on the time increment, Δt . The time increment must be sufficiently short, and can be selected by considering the following factors: the rate of variation of loading, the complexities of the non-linear damping and stiffness properties, and the period of free vibration of the structure, T. In general, $\Delta t/T \leq \frac{1}{10}$ is a good value for obtaining reliable results [17].

2.3.2 Artificial Earthquake Excitation

The properties of recorded earthquake ground motions are similar to a nonstationary random process, but so far there are not enough recorded ground motions to determine their precise statistical properties. Since the sample of recorded earthquakes is incomplete, some studies have used artificially generated accelerograms [2,36]. The artificial ground motions are generated by specified random processes. They have advantages that the statistical properties of the ground motions are known and that any duration of artificial accelerograms can be generated. Appropriate artificial earthquakes can be generated by a computer and used as an input process in the time integration of the equation of motion. Many simulation methods have been proposed, based on matching the spectral properties of response spectra of actual and artificial ground motions.

Housner [34] was the first to attempt to define analytically the random process of earthquake accelerations. He proposed to idealize the accelerograms as a series of random pulses occurring randomly in time. Some specific properties for frequency and amplitude of the earthquake excitations must be obeyed.

The ground motions caused by earthquakes occurring at some distance away might be considered as short-duration random pulses arriving randomly in time. Furthermore, the accelerograms usually have a phase of nearly constant intensity during the period of most severe shaking. As a result, the earlier researchers considered the possibility of modelling this phase of strong ground shaking with a white noise process of limited duration, and used

this to investigate the response of structures under earthquake loads. Bycroft [13] investigated the validity of using white noise and stated that the strong-motion earthquakes can be approximated by a white noise having a flat spectral density of 0.75 $ft^2/\sec^4/cps$ and a duration of 1/2 minute [13]. He also showed that this white noise representation yields velocity spectra that compare favorably with the average velocity spectra of Housner [35].

The possibility of describing the earthquake excitation as a white noise is apparently misleading due to the fact that white noise is a stationary random process with a constant power spectrum and the earthquakes are not stationary by nature. Therefore, a limited segment of white noise is considered for use in the period of strong-shaking motion where the input spectrum of an earthquake excitation is approximately constant. Furthermore, the nonstationary properties of an earthquake excitation can be approximately obtained by modulating a white noise where an artificial ground acceleration is represented by a product of an enveloped deterministic function of time and a stationary white-noise process. In some cases white noise representation of earthquake accelerations gave satisfactory results, especially for the design of buildings on firm rock.

It was suggested later that a stationary filtered white noise could represent more properly the actual ground motions, providing that the filter transfer characteristics are properly selected [7,17]. It appears in the existing strong-motion accelerograms that their Fourier amplitude spectra are not constant but oscillate with a frequency over a limited band. They may peak at one or several frequencies, and damp out with increasing frequency. One form of the filter transfer functions was suggested by Kanai and Tajimi [54,89]:

$$|H_1(i\bar{\omega})|^2 = \frac{1 + 4\xi_g^2(\bar{\omega}/\omega_g)^2}{[1 - (\bar{\omega}/\omega_g)^2]^2 + 4\xi_g^2(\bar{\omega}/\omega_g)^2} \tag{2.5}$$

where parameters ω_g and ξ_g may represent some characteristics of ground frequency and damping ratio, respectively. Kanai suggested 15.6 rad/s for ω_g and 0.6 for ξ_g as being representative for firm soil conditions. When the conditions of the soil are significantly different, other proper values of ω_g and ξ_g should be selected.

The nonstationary character of the actual earthquake accelerograms can be considered by representing the artificial ground motions by a nonstationary filtered white noise. The actual accelerograms frequently show a short phase of intensity buildup to some maximum level. The intensity of the real accelerograms then appears to be constant for a period of time. After that the intensity decays in an exponential fashion. Therefore, a nonstationary process, $n(t)$, can be given by

$$n(t) = g(t)f(t) \tag{2.6}$$

where $f(t)$ is the stationary filtered white noise or the stationary white noise and $g(t)$ is an intensity or deterministic function of time which is selected based on statistical properties of real accelerograms.

This study focuses on separable nonstationary stochastic models of seismic motions where the artificial earthquake accelerations are expressed in the form of Eq. (2.6). The stationary random process, $f(t)$, is assumed to be white noise, which was also investigated in Ref. [92].

Several forms of the deterministic function of time, $g(t)$, have been proposed. Some examples include:

(1). The function $g(t)$ is also called an envelope function, which is used to make $f(t)$ nonstationary. The envelope function is proportional to the variance of the amplitude of the ground acceleration. The envelope function usually takes the form [81]

$$g_1(t) = e^{-\beta_1 t} - e^{-\beta_2 t} \tag{2.7}$$

In Ref. [81], the variance of the amplitude of the ground acceleration was used to select the envelope function, and parameter values of $\beta_1 = 0.085$ and $\beta_2 = 0.170$ were obtained. Therefore, the function $g_1(t)$, given by Eq. (2.7), is a rational description of the variance of the earthquake motion [96].

The same form of this function was also used with different values of parameters, such as $\beta_1 = 0.025$ and $\beta_2 = 0.25$ [81,87,96]. Eq. (2.7) was also used in Ref. [51] for the function

$g(t)$, in which the values $\beta_1 = 0.5$ and $\beta_2 = 1.0$ were used in the generation of two earthquake accelerograms of 10-second duration.

(2). Another form of the function $g(t)$ is also based on Ref. [81] and given by

$$g_2(t) = k_1\left[e^{-\beta_1 t} - e^{-\beta_2 t}\right]; \quad t \geq 0, \beta_1 > 0, \beta_2 > 0. \tag{2.8}$$

where the values of $\beta_1 = 0.125$ and $\beta_2 = 0.25$ were used in Ref. [77], and k_1 is a normalization constant such that $g_{max} = 1$.

(3). The modulating function $g(t)$, which reflects the appearance of real accelerograms, is given by [2]

$$g_3(t) = \begin{cases} (t/t_1)^2, & t \leq t_1; \\ 1 & , t_1 < t \leq t_2; \\ e^{-c(t-t_2)}, & t \geq t_2. \end{cases} \tag{2.9}$$

Thus, the random processes of ground acceleration are assumed stationary in the interval (t_1, t_2). When direct data are not available, the following parameters can be assumed: $t_1 = 1.21\ sec.$, $t_2 = 11.5\ sec.$, and $c = 0.155\ sec.^{-1}$ for $d = 15 - 20\ sec.$, where d is the duration of the strong-motion earthquakes. Sometimes, $t_1 = 0$ is used.

(4). For a more realistic modulating function, $g(t)$, Ref. [86] used the following two envelopes [80]:

$$g_4(t) = 10.13\left[e^{(-0.25t)} - e^{(-0.50t)}\right] \tag{2.10}$$

$$g_5(t) = 5.934\left[e^{(-0.125t)} - e^{(-0.25t)}\right] \tag{2.11}$$

The first modulating function, $g_4(t)$, may represent an earthquake with a fast rise time, of approximately 2.7 seconds to maximum intensity, while the second, $g_5(t)$, is associated with a slow rise time of approximately 5.5 seconds. The natural period of the structure in Ref. [86] is 1 second. The constants 10.13 and 5.934 were selected in order to equalize approximately

the total energy received by the structure in a 20-sec. time interval [18], which is considered to represent the duration of the strong-motion earthquakes.

Chapter III

Formulation of Problem

3.1 Problem Statement

This study considers a two-pinned arch of span L and initial rise $Y_o(X)$ as shown in Fig. 1. It is assumed that the arch is in equilibrium with no initial static load. There is no initial thrust applied to the arch. At time $T \geq 0$, let the arch be subjected to a time-dependent random load of intensity $F(X,T)$. If the arch is sufficiently shallow, it is capable of failure by dynamic snap-through under loads. The deformed centerline of the arch at a subsequent time may be represented by $Y(X,T)$. The equation of motion for the shallow arch under time-dependent loadings has been derived, and it can be expressed as [24,27,37,38,66].

$$EI\frac{\partial^4}{\partial X^4}[Y(X,T) - Y_o(X)] + \mu\frac{\partial^2 Y(X,T)}{\partial T^2} + M\frac{\partial^2 Y(X,T)}{\partial X^2} + C\frac{\partial Y(X,T)}{\partial T} = -F(X,T) \qquad (3.1)$$

where E = modulus of elasticity, I = moment of inertia of the arch, μ = mass per unit length of the arch (i.e., $\mu = \rho A$ where ρ is the density of the arch), A = cross-section area of the arch, C = damping coefficient, L = span length of the arch, T = time, $F(X,T)$ = random force per unit length on the arch, and M = thrust induced in the arch. The thrust induced in the arch is given by

$$M = \frac{EA}{2L}\int_0^L \left[\left\{\frac{dY_o(X)}{dX}\right\}^2 - \left\{\frac{\partial Y(X,T)}{\partial X}\right\}^2\right] dX \tag{3.2}$$

The equation of motion, Eq. (3.1), is subjected to the following boundary conditions:

$$Y(X,T)\,|_{X=0,\,L} = 0, \quad and \tag{3.3}$$

$$EI\left[\frac{\partial^2 Y(X,T)}{\partial X^2} - \frac{d^2 Y_o(X)}{dX^2}\right]|_{X=0,\,L} = 0 \tag{3.4}$$

Introducing the following nondimensional quantities:

$$x = \frac{X}{L}, \quad y = \frac{Y}{2}\sqrt{\frac{A}{I}}, \quad y_o = \frac{Y_o}{2}\sqrt{\frac{A}{I}},$$

$$t = \frac{1}{L^2}\sqrt{\frac{EI}{\mu}}\,T, \quad \beta = \frac{L^2}{\sqrt{\mu EI}}\,C, \quad and$$

$$f(x,t) = \frac{L^4 F(X,T)}{2\pi^4 EI}\sqrt{\frac{A}{I}}$$

Eq. (3.1) then becomes

$$\frac{\partial^2 y(x,t)}{\partial t^2} + \frac{\partial^4}{\partial x^4}[y(x,t) - y_o(x)] + m\frac{\partial^2 y(x,t)}{\partial x^2} + \beta\frac{\partial y(x,t)}{\partial t} = -\pi^4 f(x,t) \tag{3.5}$$

where m is a nondimensional axial thrust, which is given by

$$m = 2\int_0^1 \left[\left\{ \frac{dy_o(x)}{dx} \right\}^2 - \left\{ \frac{\partial y(x,t)}{\partial x} \right\}^2 \right] dx \tag{3.6}$$

The boundary conditions for Eq. (3.5) are

$$y(x,t)\,|_{x=0,1} = 0, \text{ and} \tag{3.7}$$

$$\left[\frac{\partial^2 y(x.t)}{\partial x^2} - \frac{d^2 y_o(x)}{dx^2} \right] \Big|_{x=0,1} = 0 \tag{3.8}$$

Let $w(x,t)$ be the nondimensional downward deflection of the arch about the initial equilibrium state $y_o(x)$. $w(x,t)$ represents the dimensionless motion of the arch, under random loadings, vibrating relative to the unloaded position as shown in Figure 2. Then, $w(x,t)$ is defined as

$$w(x,t) = y_o(x) - y(x,t) \tag{3.9}$$

Let dots denote derivatives with respect to time, and primes denote derivatives with respect to spatial coordinate, x. Then, Eqs. (3.5) to (3.8) can be written as

$$\ddot{w}(x,t) + \beta \dot{w}(x,t) + w''''(x,t) + m[w''(x,t) - y_o(x)] = \pi^4 f(x,t) \tag{3.10}$$

where

$$m = 2\int_0^1 [2y_o'(x)w'(x,t) - \{w'(x,t)\}^2] dx \tag{3.11}$$

The boundary conditions for Eq. (3.10) are

$$w(x,t)|_{x=0,1} = 0, \text{ and} \tag{3.12}$$

$$w''(x,t)|_{x=0,1} = 0 \tag{3.13}$$

The governing equations, Eqs. (3.10), (3.11), (3.12), and (3.13), are valid for any initial shape of the pinned-pinned arch as long as the arch is shallow [24,66,67]. The arch with an initial sinusoidal shape is considered in this study. The initial shape of the arch can be described by

$$y_o(x) = \lambda \sin \pi x \tag{3.14}$$

λ is a dimensionless arch rise parameter, and it can be related to the initial shape of the arch $Y_o(X)$, by the factor of $2\sqrt{I/A}$; i.e., $\lambda = Y_o/2\sqrt{I/A}$ where Y_o is defined as

$$Y_o(X) = Y_o \sin \frac{\pi X}{L} \tag{3.15}$$

3.1.1 Galerkin's Method

For this type of equation of motion, Galerkin's method will be used to define the response. The motion of the arch will be expressed by

$$w(x,t) = \sum_{i=1}^{N} q_i(t)\sqrt{2} \sin i\pi x \tag{3.16}$$

where N is the number of modes, or degrees of freedom, and $q_i(t)$ are the generalized coordinates of the response of the arch at time t. The term $\sqrt{2} \sin(i\pi x)$ is the assumed shape function describing the deflected shape of the arch. This shape function is determined according to the boundary conditions given by Eqs. (3.12) and (3.13).

Substituting $w(x,t)$ in Eq. (3.16) and $y_o(x)$ in Eq. (3.14) into Eqs. (3.10) and (3.11), the equation of motion becomes

$$\sum_{i=1}^{N} \ddot{q}_i(t)\sqrt{2}\,\sin i\pi x + \beta \sum_{i=1}^{N} \dot{q}_i(t)\sqrt{2}\,\sin i\pi x + \sum_{i=1}^{N} q_i(t)\sqrt{2}\,i^4\pi^4 \sin i\pi x + m\left[\sum_{i=1}^{N} q_i(t)\left\{-\sqrt{2}\,i^2\pi^2 \sin i\pi x\right\} + \lambda\pi^2 \sin i\pi x\right] = \pi^4 f(x,t) \tag{3.17}$$

where m is expressed as

$$m = 2\left[\sqrt{2}\,\lambda\pi^2 q_1(t) - \sum_{i=1}^{N} i^2\pi^2 q_i^2(t)\right] \tag{3.18}$$

We make Eq. (3.17) orthogonal to $\sqrt{2}\,\sin(j\pi x)$ and integrate it over x from 0 to 1. For $j = 1, \ldots, N$, the equation of motion then becomes

$$\ddot{q}_j(t) + \beta\dot{q}_j(t) + \left[j^4\pi^4 - j^2\pi^2 m\right]q_j(t) + \frac{\sqrt{2}}{2}\lambda\pi^2 m\delta_{1j} = \sqrt{2}\,\pi^4 \int_0^1 f(x,t)\,\sin j\pi x\; dx \tag{3.19}$$

where m is given by Eq. (3.18) and

$$\delta_{ij} = \begin{cases} 1 & for\ \ i = j \\ 0 & for\ \ i \neq j \end{cases} \tag{3.20}$$

The natural frequencies of the system, ω_n, are given by [66]

$$\omega_1^2 = \pi^4(1 + 2\lambda^2),\ and$$
$$\omega_n^2 = \pi^4 n^4,\ for\ \ n = 2, 3, \ldots \tag{3.21}$$

Note that the ω_n^2 are given by the coefficient of the $q_j(t)$ term in the equation of motion.

3.1.2 Initial Conditions

In this study, the arch is assumed to start from rest in the case of one-mode analysis. Therefore, at time $t = 0$, the relative displacement is equal to zero. Then

$$\sum_{i=1}^{n} q_i(0)\sqrt{2}\,\sin i\pi x = w(x,0) = 0 \tag{3.22}$$

Making Eq. (3.22) orthogonal to $\sqrt{2}\,\sin(j\pi x)$ and integrating it over x from 0 to 1, it follows that

$$q_i(0) = 0 \tag{3.23}$$

Similarly, it can be determined that, since $w(x,0) = 0$,

$$\dot{q}_i(0) = 0 \tag{3.24}$$

3.1.3 Response Measurement

The displacement response of the arch at any time instant, for a given random load, can be measured by the quantity [24]

$$d = \left[\int_0^1 w^2(x,t)dx\right]^{\frac{1}{2}} \tag{3.25}$$

The quantity d also represents the root-mean-square (rms) of the displacement of the arch. Subsitituting $w(x,t)$ from Eq. (3.16) into Eq. (3.25)

$$d = \left[\sum_{i=1}^{n} q_i^2(t) \right]^{\frac{1}{2}} \tag{3.26}$$

The total inversion of the arch, after snap-through has occurred, is given approximately by $y(x,t) = -y_o(x)$. In other words, $w(x,t) = 2y_o(x)$, and then

$$d = \left[\int_0^1 \{2y_o(x)\}^2 dx \right]^{\frac{1}{2}} = \sqrt{2}\,\lambda \tag{3.27}$$

3.1.4 One-Mode Approximation

The one-mode approximation of the equation of motion, Eq. (3.19), is obtained by letting j = 1, and it is given by

$$\ddot{q}_1(t) + \beta\dot{q}_1(t) + (\pi^4 - \pi^2 m)q_1(t) + \frac{\sqrt{2}}{2}\lambda\pi^2 m = \sqrt{2}\,\pi^4 \int_0^1 f(x,t) \sin \pi x \; dx, \tag{3.28}$$

where

$$m = 2\left[\sqrt{2}\,\lambda\pi^2 q_1(t) - \pi^2 q_1^2(t)\right] \tag{3.29}$$

Substituting for m, Eq. (3.28) becomes

$$\begin{aligned} &\ddot{q}_1(t) + \beta\dot{q}_1(t) + \pi^4(1 + 2\lambda^2)q_1(t) - 3\sqrt{2}\,\pi^4\lambda q_1^2(t) \\ &+ 2\pi_4 q_1^3(t) = \sqrt{2}\,\pi^4 \int_0^1 f(x,t) \sin \pi x \; dx \end{aligned} \tag{3.30}$$

It can be seen in Eq. (3.30) that the natural frequency, ω_1 , of the one-mode approximation is given by $\omega_1^2 = \pi^4(1 + 2\lambda^2)$.

The equilibrium positions of the arch under no loading can be determined by setting

$$\ddot{q}_1(t) = \dot{q}_1(t) = f(x,t) = 0 \tag{3.31}$$

From Eqs. (3.30) and (3.31), the equilibrium equation is given by

$$q_1\pi^4\left[(1+2\lambda^2) - 3\sqrt{2}\,q_1 + 2q_1^2\right] = 0 \tag{3.32}$$

Solving Eq. (3.32), the three equilibrium positions of the arch are

$$\text{(1).} \quad q_1 = 0,$$

$$\text{(2).} \quad q_1 = \frac{3\sqrt{2}\,\lambda - \sqrt{2(\lambda^2-4)}}{4}, \quad \textit{and}$$

$$\text{(3).} \quad q_1 = \frac{3\sqrt{2}\,\lambda + \sqrt{2(\lambda^2-4)}}{4}$$

For instance, when the arch rise parameter λ is equal to 5.00, these three equilibrium positions are at $q_1 = 0$, $q_1 = 3.6833$, and $q_1 = 6.9235$, respectively. These equilibrium positions represent, respectively, a stable unbuckled state at the initial position, an unstable state just below the horizontal x-axis, and a stable buckled state below the horizontal x-axis.

3.1.5 Sinusoidal Time-Dependent Loadings

The simplest case of loading is when the random excitation $f(x,t)$ is represented by a time-dependent loading which is spatially sinusoidal, as shown in Fig. 4. In this case, $f(x,t)$ on the right-hand side of Eq. (3.30) can be written as

$$f(x,t) = f(t)\sin\pi x \tag{3.33}$$

Eq. (3.30) then becomes

$$\ddot{q}_1(t) + \beta\dot{q}_1(t) + \pi^4(1 + 2\lambda^2)q_1(t) - 3\sqrt{2}\,\pi^4\lambda q_1^2(t) + 2\pi^4 q_1^3(t) = \frac{\sqrt{2}}{2}\pi^4 f(t) \qquad (3.34)$$

where $f(t)$ is a time-dependent random process.

3.2 Failure Criterion of a Shallow Arch

For the dynamic instability of a shallow arch under deterministic time-dependent loadings, the critical loads are usually determined using the Budiansky-Roth Criterion [12]. The general idea of this criterion is that a sudden reversal of the shallow arch curvature toward another stable buckled state implies dynamic instability of the arch. At that instant of time, the response or displacement of the arch becomes large or increases to a much larger magnitude. This phenomenon may be called the dynamic snap-through of the shallow arch.

This study involves the dynamic response of a shallow arch under random excitations. For a low intensity of random excitations, which may be described by the power spectral density, the arch is expected to vibrate about its initial stable position. The arch is considered to be stable under this random load intensity if it continues to vibrate about its initial stable state for all time without snapping into an inverted state. However, it can be expected that the arch will snap back and forth about its horizontal x-axis for higher intensities of random excitation.

For a shallow arch responding to random excitation, the failure of the arch can be assumed to occur when the amplitude of its vibrations exceeds some critical level and the arch exhibits snap-through for the first time. After the arch crosses this critical level, the arch is assumed to exit from the safe region around the initial stable state and snap to an inverted state (below the horizontal axis). Therefore, failure of the arch is associated with the occurrence of the *first snap-through* [64,65,79]. The parameter to be determined is the time required to failure, which is also known as the *first-passage time*.

The first-passage time represents an essential characteristic of random processes concerning the safety or performance of a system. Therefore, it is necessary to establish the probability of first-passage time for reliability analysis and design of a system [63]. In this study, the stability and reliability of the shallow arch under stochastic loadings are investigated, and the probability of first-passage time (i.e., the probability of time of first snap-through) is determined.

3.3 Solutions of the First-Passage Time Problem

For a random process $q(t)$, the first-passage time, denoted by T_{fp} , can be defined as the time at which the process $q(t)$ crosses a level α for the first time as described in Fig. 3 [63]. T_{fp} is obviously a random variable associated with the random process q(t).

It is noted that an exact solution of the first-passage time problem is not yet available, except for the case of a first-order Markov random process [63]. However, several approximate solutions have been developed, such as the approximation to the Fokker-Planck equation using a Markov vector approach and numerical studies using a Monte Carlo simulation method. The probability of the first-passage time depends on the characteristics of the system, the nature of the excitation, the initial conditions, and the magnitude of the critical level.

The approximate methods based on the Markov vector approach are used to establish the probability distribution of the first-passage time in terms of the second-order statistics of the parent random process $q(t)$ and its derivative process $\dot{q}(t)$. The method of energy envelope approximation is discussed in detail in Chapter 4. The response of a shallow arch subjected to a stationary white-noise process is investigated. The approximate solution of the probability of the first-passage time is then estimated using the approximate solution of the Fokker-Planck equation.

In Chapter 5, the Monte Carlo method is used to solve the governing equation of motion of the system directly by a numerical step-by-step integration. The random load is assumed to be a stationary white-noise process. Statistical properties, such as the mean value and variance, of the time to first snap-through or the first-passage time are estimated from the collected data of simulation results. The probability distribution of the first-passage time can then be determined.

3.4 Critical Random Loading for the Snap-Through of a Shallow Arch

3.4.1 Problem Statement

The critical power spectral density parameter for snap-through of a shallow arch under white-noise excitation is studied in this section. The approach is similar to that presented in Ref. [79], in which the response of buckled clamped beams subjected to uniformly-distributed random loading was investigated, and the critical spectral density parameters of the random load for snap-through were estimated. The motion of the deflected arch is described by $w(x,t)$, which was previously given by Eq. (3.16).

For the one-mode approximation, in nondimensional variables, the equation of motion of the shallow arch subjected to sinusiodal random loading is given by Eq. (3.34) and may be rewritten, dropping the subscript 1, as

$$\ddot{q}(t) + \beta\dot{q}(t) + \omega_o^2\left[q(t) - \varepsilon_1 q^2(t) + \varepsilon_2 q^3(t)\right] = \varepsilon_3 f(t) \tag{3.35}$$

where $q(t)$ is the normalized central deflection of the arch, β is the damping coefficient, ω_o is the natural frequency of the corresponding linearized system, and $f(t)$ is the time-dependent random loading. The natural frequency, ω_o, is given by the relationship $\omega_o^2 = \pi^4(1 + 2\lambda^2)$, where λ is the dimensionless initial arch rise parameter. ε_1 and ε_2 are coefficients of the non-

linear terms and defined as follows: $\varepsilon_1 = 3\sqrt{2}\,\pi^4/\omega_o^2$, and $\varepsilon_2 = 2\pi^4/\omega_o^2$. ε_3 is a coefficient of the loading function and is equal to $\sqrt{2}\,\pi^4/2$.

The equation of motion, Eq. (3.35), describes the behavior of a mass-spring system with a nonlinear spring stiffness. The restoring spring force is given by

$$G(q) = \omega_o^2 q(1 - \varepsilon_1 q + \varepsilon_2 q^2) \tag{3.36}$$

Fig. 5 illustrates a plot of the restoring spring force , $G(q)/\omega_o^2$, as a function of the response q for $\lambda = 5.0$.

The spring resistance of the shallow arch is of the softening type as the response q increases from zero. The spring resistance is actually destabilizing when the arch becomes susceptible to snap-through from a stable unbuckled state at the initial position, $q = 0.0$, to a stable buckled state below the horizontal x-axis, $q = 6.9239$, as shown in Figs. 1 and 4. Therefore, the arch is expected to vibrate about its initial stable configuration under a low intensity of random loading, but to snap back and forth about the horizontal x-axis under a high intensity of random loading.

3.4.2 Dynamic Stability of a Shallow Arch

Two important considerations in the study of critical random loading for the snap-through of a shallow arch are the definition of dynamic instability of the arch and the method of calculating the critical spectral density parameter of the random load. If it is assumed that under a small magnitude of random excitations the arch will vibrate about its initially stable unbuckled position, while under a large magnitude of random excitations the arch will snap back and forth about the horizontal x-axis, it can then be assumed that there is a critical value or range of spectral density parameter of random excitations for which snap-through is initiated for the first time. The dynamic instability of the shallow arch can be defined as follows: the arch fails under some critical load when the motion of the arch changes from vibrating

about the initially stable unbuckled state to snapping across the horizontal axis for the first time. In other words, the arch fails when its deflection crosses the horizontal axis, i. e., the response q is greater than or equal to $\lambda/\sqrt{2}$.

The response of a shallow arch can be described by the time average of the response. Time histories of the response of the arch are obtained here by numerically integrating the nonlinear equation of motion, Eq. (3.35), using the IMSL subroutine DVERK [42]. Details of the subroutine DVERK are given in Section 5.2 and in Ref. [39,42].

The time-dependent random loading, $f(t)$, is assumed to be sufficiently modelled as a white-noise process. The statistics of $f(t)$, then, can be completely described by its mean value, $\bar{f}(t)$, and its autocorrelation function, $R_f(\tau)$, where

$$\bar{f}(t) = E[f(t)] = 0 \tag{3.37}$$

$$R_f(t) = E[f(t)f(t+\tau)] = 2\pi\Phi_o\delta(\tau) \tag{3.38}$$

where Φ_o is the intensity of the white noise, $\delta(\tau)$ is the Dirac delta function and $E[\ ]$ is the expectation.

A random loading function having a Gaussian distribution with a zero mean and a unit variance was first generated using the IMSL subroutine GNNML [43]. The loading function consists of steps, as shown in Fig. 6, which are constant over a given constant increment of time Δt. The intensity of the random loading function described previously is transformed to a white-noise process by multiplying each ordinate or constant step by the normalizing factor $\sqrt{2\pi\Phi_o/\Delta t}$ [17].

The primary objective of this study is the determination of the average frequency of zero crossing of the response of the arch, AF, which is defined as follows:

$$AF = \underset{T\to\infty}{LIMIT} \left[\frac{N(T)}{T}\right] \tag{3.39}$$

where $N(T)$ is the number of zero crossings of the central deflection of the arch during a time period T. The zero crossing of the central deflection of the arch is counted when the response q crosses the horizontal x-axis and snaps through to the other stable state below the horizontal axis.

For a single record of white-noise excitation applying on the arch, the equation of motion, Eq. (3.35), is numerically integrated and the time-dependent response of the arch is obtained. During the simulation procedure, the number of zero crossings of the central deflection, $q(t)$, both from above and below the horizontal x-axis, i. e., $q = \lambda/\sqrt{2}$, is counted. At each time interval, a time average of the crossing rate is calculated. Results from Ref. [79] showed that different loading sequences, i. e., different seed values for generating the random loading functions, led to essentially the same results, and that when the time duration, T, was sufficiently long the crossing rate was reasonably constant. Ref. [79] also suggests that the calculation of the critical spectral density parameter be based on the average frequency vanishing or becoming small, since for a sufficiently small intensity of random loads the number of zero crossings of the response is zero.

3.4.3 Numerical Results

In this study, the constant integration time step, Δt, is set equal to 0.02. $\Delta t = 0.02$ was also used by Seide [79]. This contant time increment is also used in the generation of the loading function. The maximum time period of $T_{max} = 400$ is considered to be sufficiently long since the average frequency of zero crossing seems to converge to a contant value as shown in Table 3.1. The time is nondimensional and can be expressed in terms of the number of cycles, N, where $N = T\omega_o/2\pi$. In this case, the maximum number of cycles of vibration needed for the integration is approximately equal to 4490. Table 3.1 gives the results for $\lambda = 5.0$ and $\beta = 0.20$, showing the effect of different loading sequences, various loading in-

tensities, and different time periods. It is found that the results obtained from this study are comparable to those of Ref. [79] and a similar conclusion to that of Ref. [79] can be made.

Seide indicated that beams of different initial amplitude, λ, having the same values of modified loading intensity, Φ_o/λ^4 , and a modified time, λT , should yield similar average responses [79]. Therefore, the results of this study are also expressed in terms of the modified loading function, Φ_o/λ^4, and modified time, λT, which will be used to estimate the critical spectral density parameter of random loadings.

Additional results are obtained for various combinations of values of λ, β, and Φ_o. Tables 3.2, 3.3, and 3.4 give the average frequency of the snap-through of a shallow arch under white-noise excitations of intensity Φ_o for $\lambda = 1.5$, 5.0, and 7.0, respectively. Table 3.5 contains the observed values of the critical spectral density parameter, Φ_{cr}, of the white noise, divided by λ^4, for $\lambda = 1.5$, 5.0, and 7.0 .

The modified average frequency of the snap-through, $N(T)/\lambda T$, for various values of initial arch rise parameters is plotted as a function of modified spectral density parameter, Φ_o/λ^4, of the random loads. The effect of different arch rise parameters is shown in Figs. 7 and 8 for $\beta = 0.1$, and 0.2, respectively. Figs. 9, 10, and 11 show, respectively, the effect of the damping coefficient on the spectral density parameter for $\lambda = 1.5$, 5.0, and 7.0. It can be observed that the average frequency of snap-through for various values of initial arch rise parameters and damping coefficients are vanishing or approaching zero nearly in the same vicinity ranging from Φ_o/λ^4 equal to $1.5x10^{-5}$ to $4.0x10^{-5}$.

3.4.4 Conclusion

The snap-through of a shallow arch subjected to white-noise excitation was investigated in this section. The primary objective is the determination of the average frequency of snap-through or zero crossing, which is the number of zero crossings, $N(T)$, of the maximum deflection divided by the time period, T. The vanishing or diminishing of the average frequency

of the snap-through can be used to estimate the critical spectral density parameter of the random loading. A precise or exact value of the critical random loading can not be obtained using this criterion since it is based on numerical integration of the nonlinear equation of motion and computer simulation which is expensive and time-consuming. However, the critical value of the spectral density parameter can be reasonably approximated with some degree of accuracy. The following conclusions can be drawn:

(1) An increase in the initial arch rise parameter increases the critical spectral density parameter of random loading.

(2) A decrease in the damping coefficient reduces the critical intensity of random loading.

(3) Arches of different initial rise parameters having the same value of Φ_o/λ^4 should yield similar average responses.

(4) After considering all that cases studied, an estimate of the critical power spectral density parameter for the snap-through of a shallow arch under white-noise excitation can be given by

$$\Phi_{cr} = (1.0 \times 10^{-5})\, \lambda^4, \tag{3.40}$$

which can be regarded as a lower bound. The shallow arch subjected to white-noise excitation of intensity less than the critical value, given by Eq. (3.40), should not fail due to dynamic snap-through.

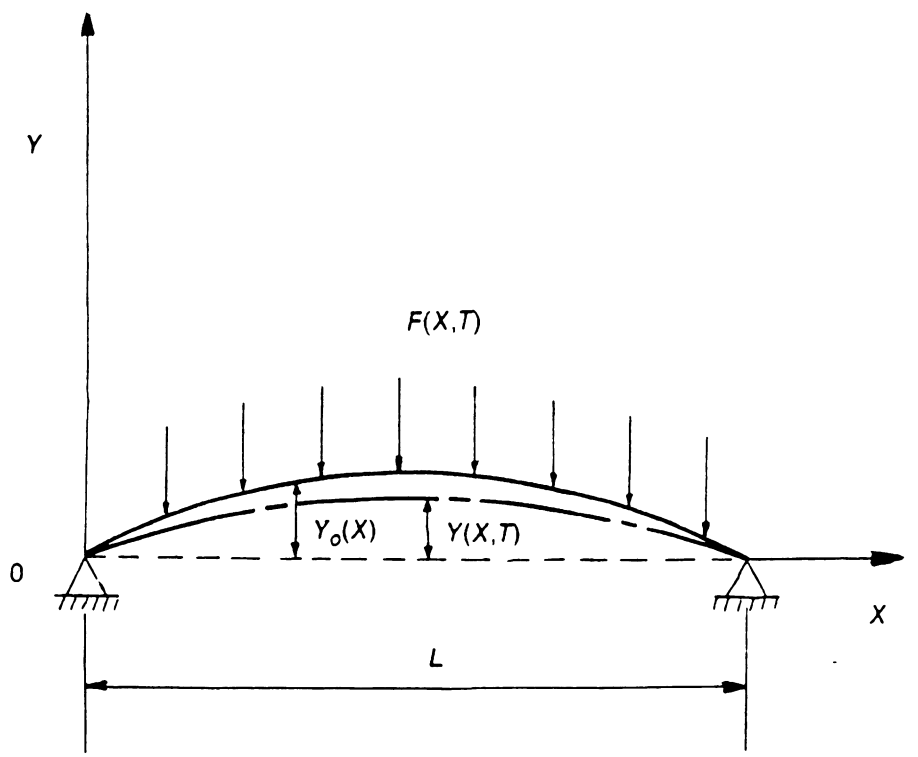

Figure 1. Configuration of the arch

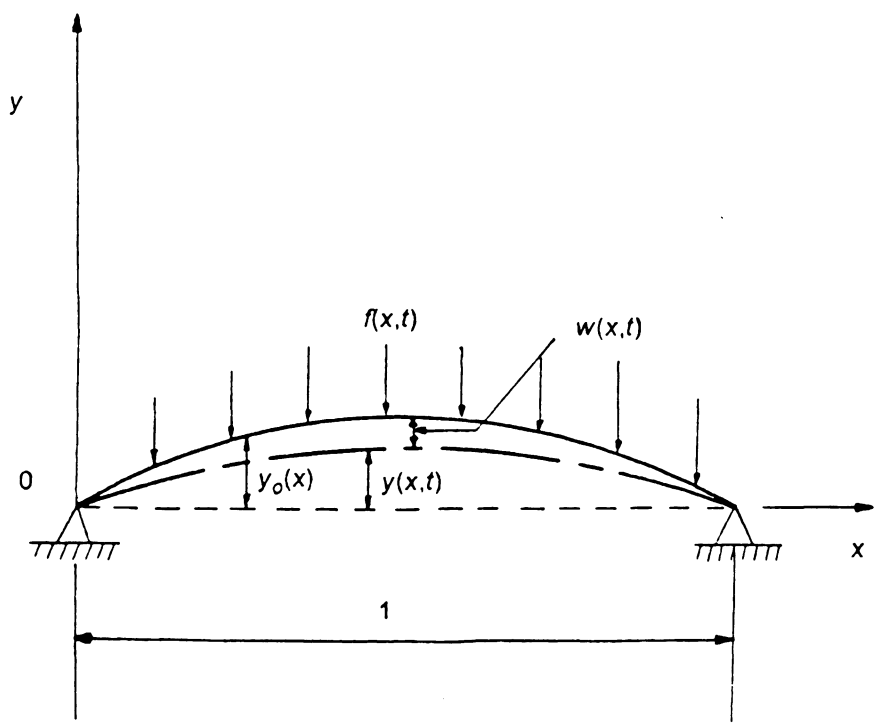

Figure 2. Configuration of the arch in dimensionless form

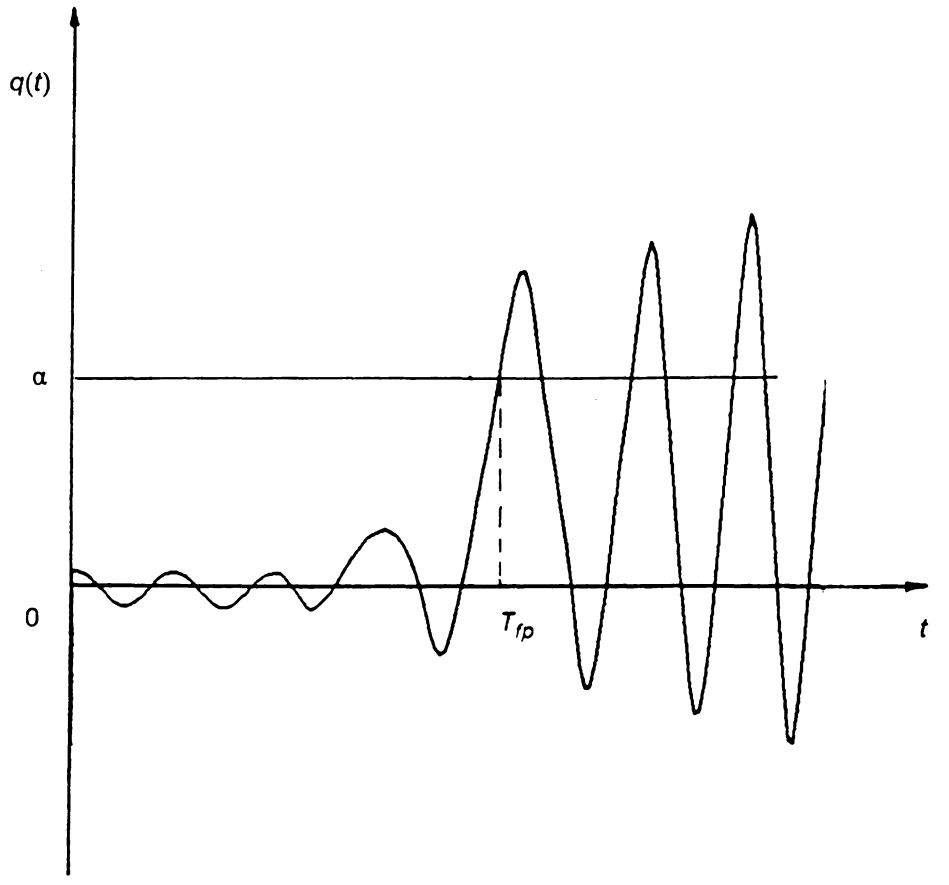

Figure 3. Description of the first-passage time of a random process.

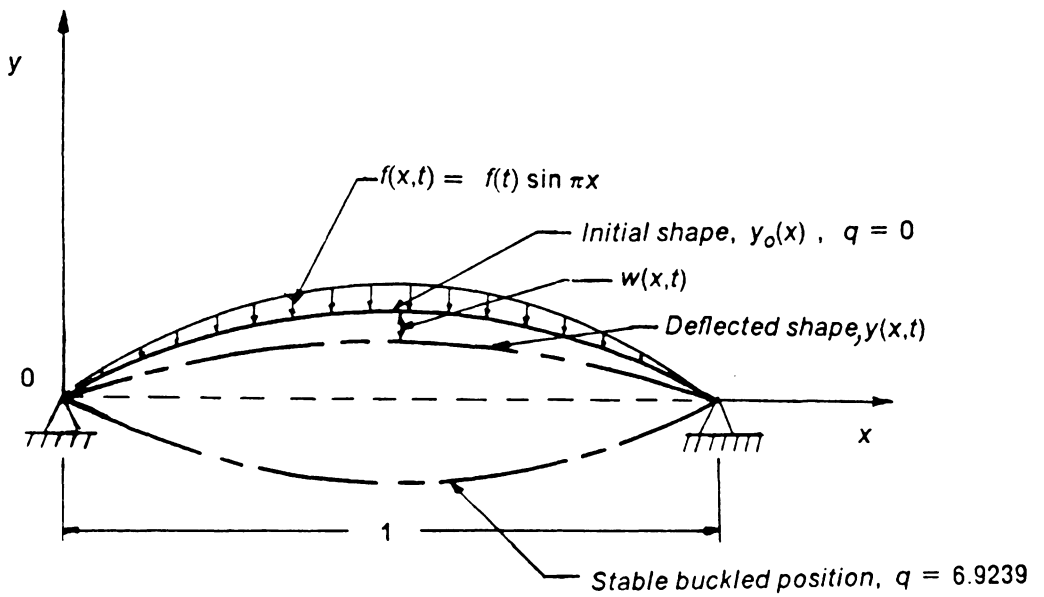

Figure 4. Shallow arch subjected to sinusoidal random loading

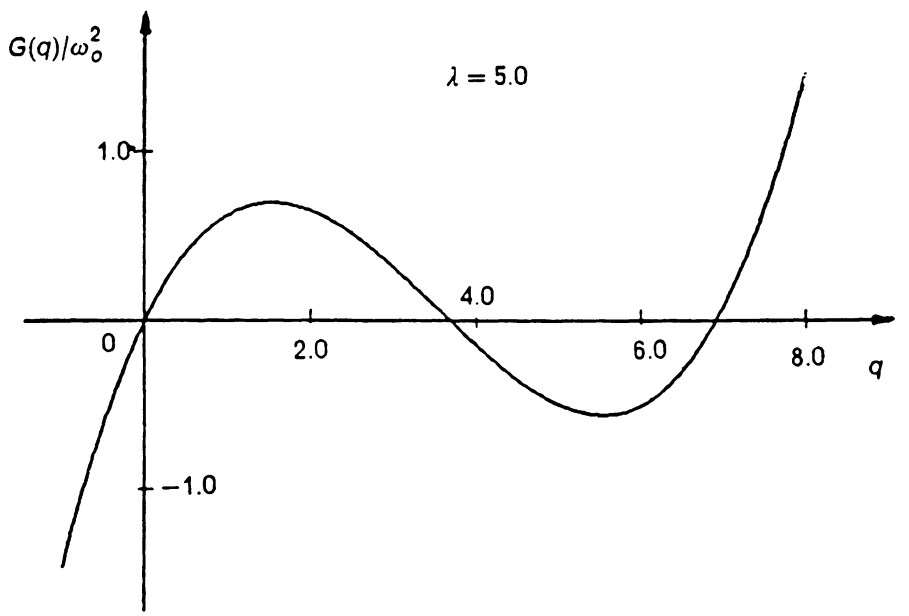

Figure 5. One mode approximation to shallow arch restoring force

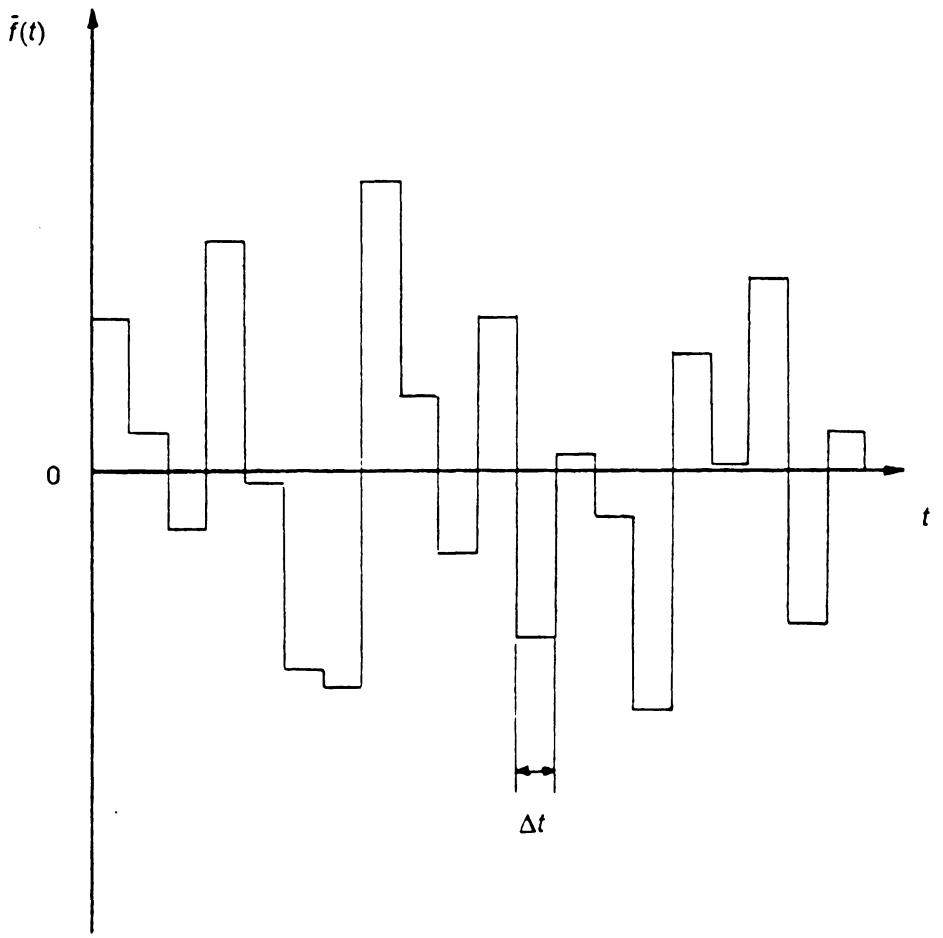

Figure 6. Typical generated random pulses as a function of time

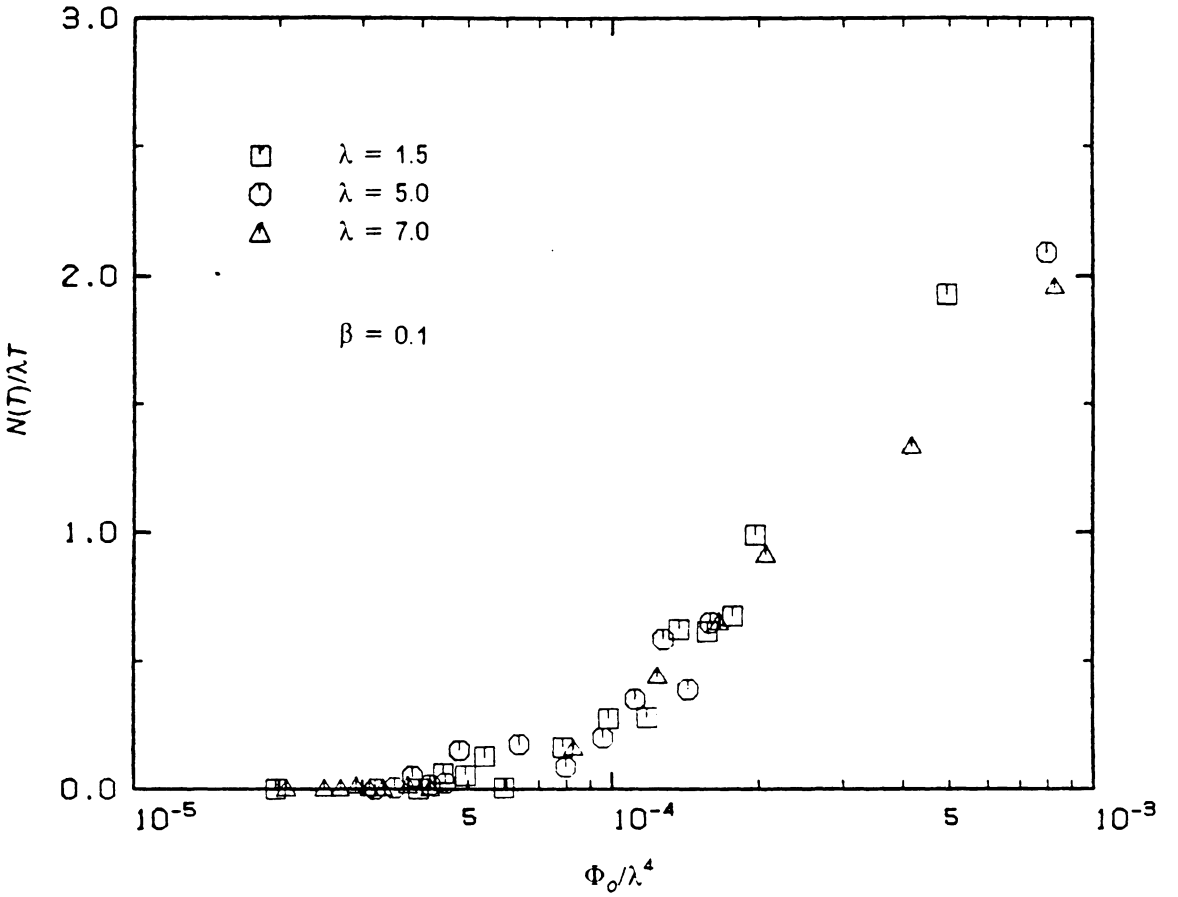

Figure 7. Variation of modified average frequency of snap-through with modified spectral density parameter of random loading

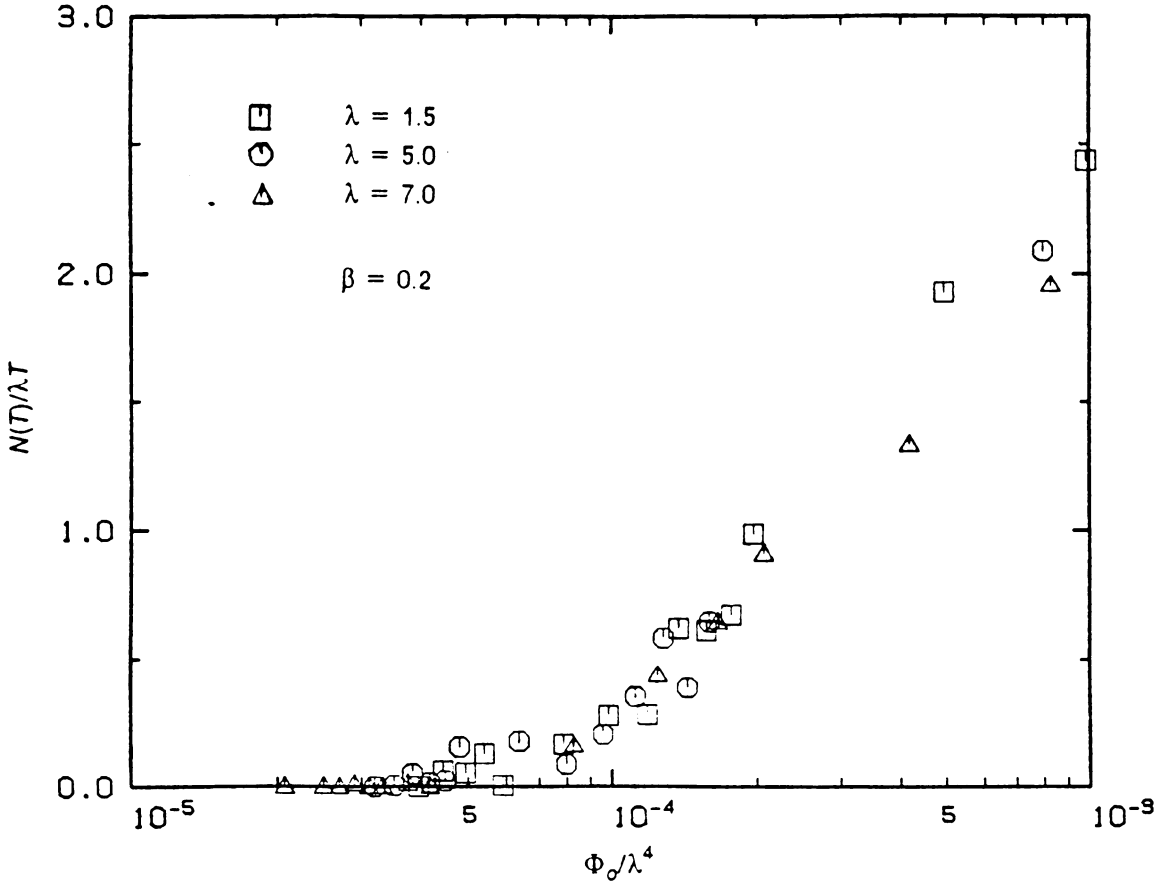

Figure 8. Variation of modified average frequency of snap-through with modified spectral density parameter of random loading

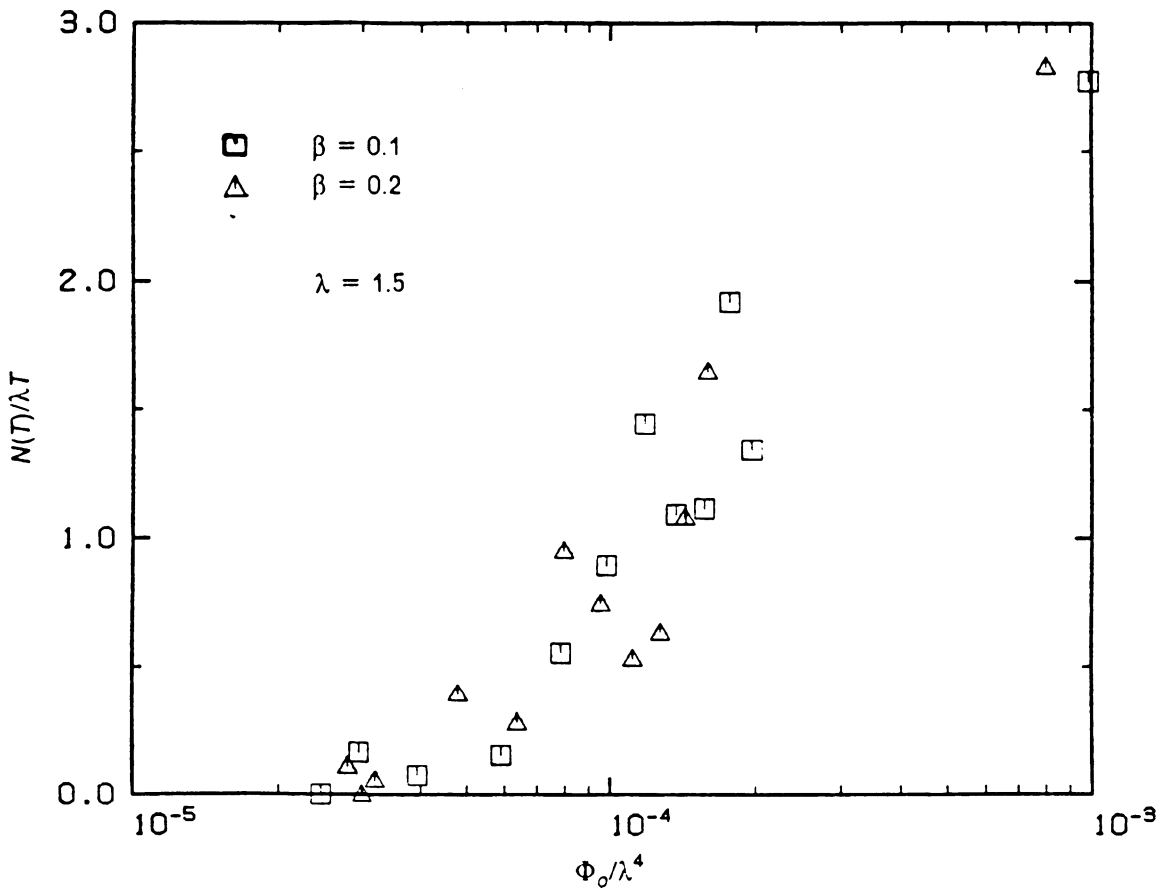

Figure 9. Variation of modified average frequency of snap-through with modified spectral density parameter of random loading

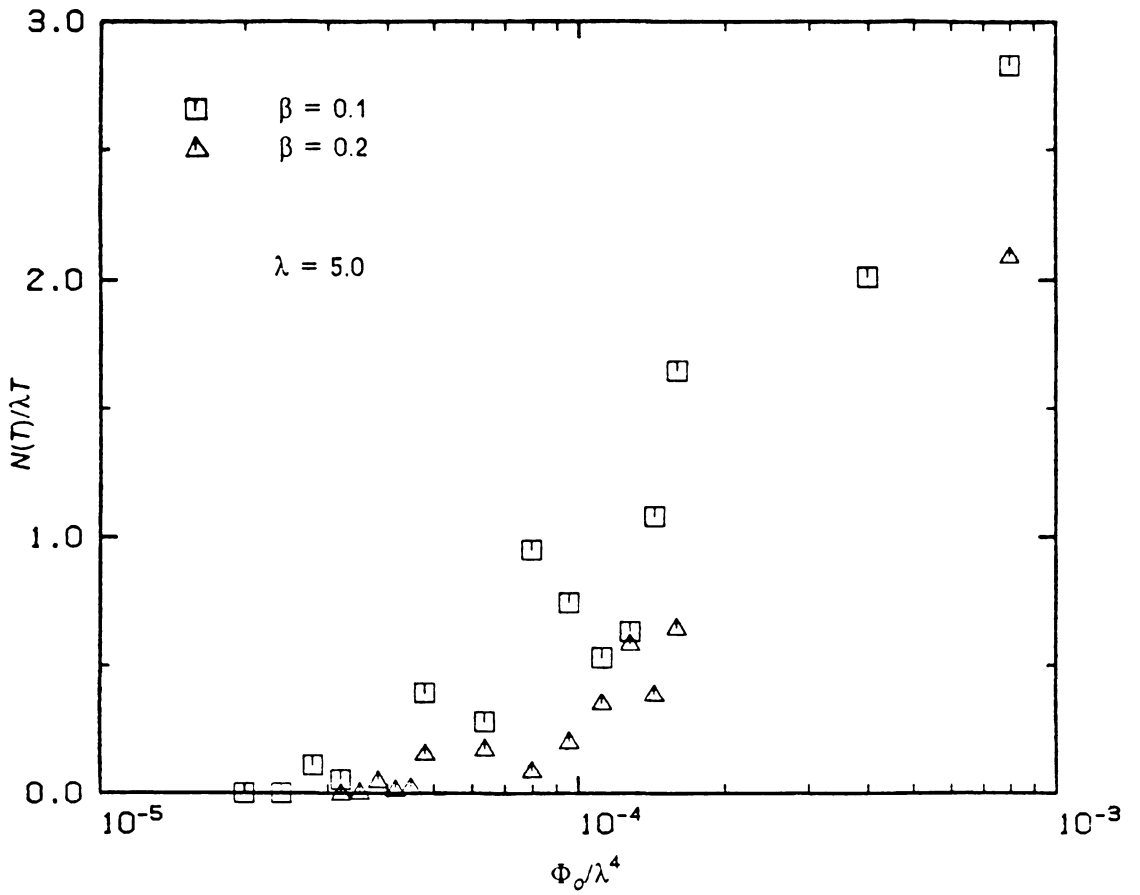

Figure 10. Variation of modified average frequency of snap-through with modified spectral density parameter of random loading

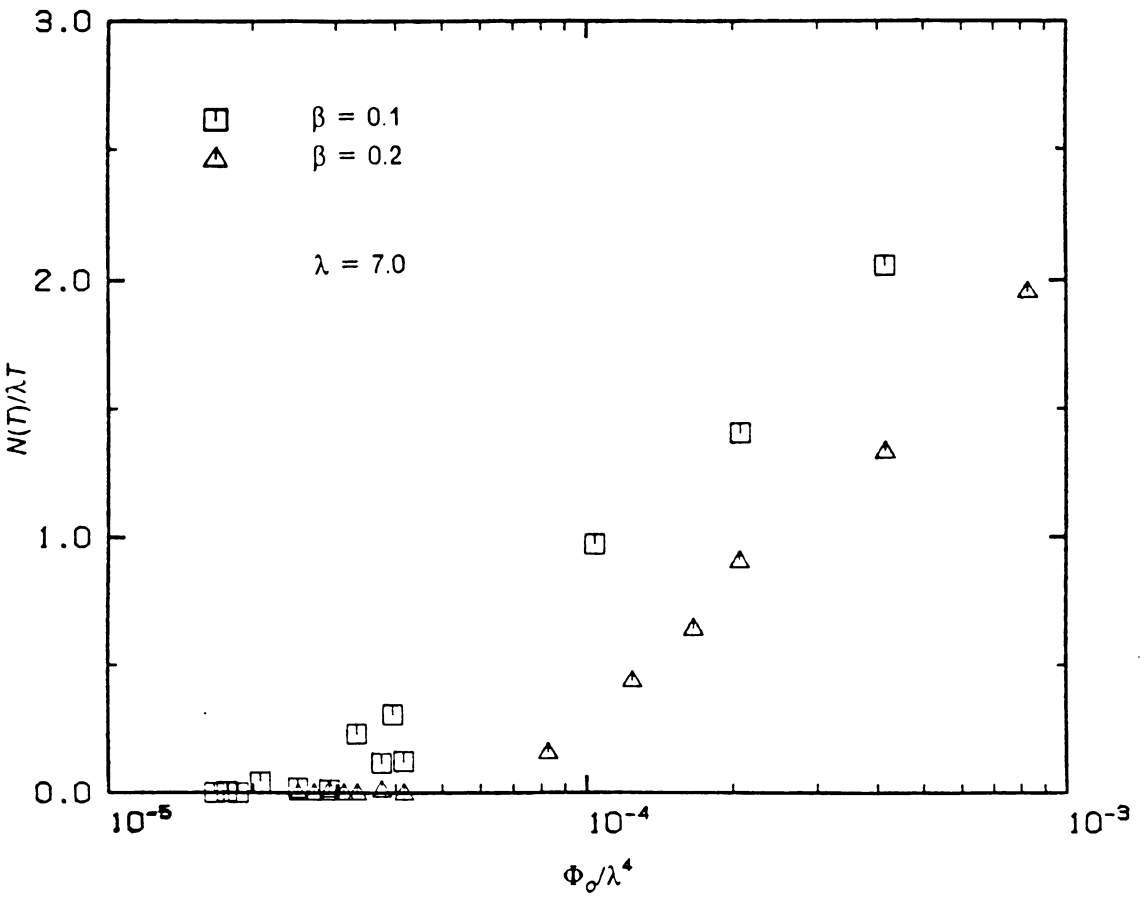

Figure 11. Variation of modified average frequency of snap-through with modified spectral density parameter of random loading.

Table 3.1

Effect of Seed Value and Load Intensity, Φ_o, on Average Crossing Frequency, $N(T)/T$
($\lambda = 5.0$, $\beta = 0.20$, $\Delta t = 0.02$)

Seed Value	123457.0			999999999.0		
Φ_o	0.5	0.1	0.01	0.5	0.1	0.01
Time	N(T)/T	N(T)/T	N(T)/T	N(T)/T	N(T)/T	N(T)/T
40	11.5500	0.5500	0.0	9.1000	3.4000	0.0
80	11.0250	0.8125	0.0	12.2500	2.5375	0.0
120	10.5000	2.3333	0.0	12.3583	3.3833	0.0
160	10.6500	2.9000	0.0	11.8312	3.4375	0.0
200	10.9250	2.5950	0.0	11.6900	3.0500	0.0
240	10.9958	2.7667	0.0	10.9625	2.8458	0.0
280	10.8821	2.8714	0.0	10.2643	3.5143	0.0
320	10.7625	2.8469	0.0	10.9219	3.4688	0.0
360	10.4056	3.1333	0.0	10.4611	3.7917	0.0
400	10.4500	3.2400	0.0	10.3725	3.4075	0.0

Table 3.2

Average Frequency of Zero Crossing, $N(T)/\lambda T$, of a Shallow Arch Under White-Noise Excitation of Intensity Φ_o ($\lambda = 1.5$, $\Delta t = 0.02$)

β		0.1	0.2
Φ_o	Φ_o/λ^4	$N(T)/\lambda T$	$N(T)/\lambda T$
5.0	0.9876	19.7300	17.1617
1.0	0.1976	13.8067	11.8033
0.5	0.09876	11.6967	10.0383
0.1	0.01976	7.6433	6.4500
0.05	0.009876	7.0150	5.4500
0.01	0.001976	4.3017	3.6233
0.005	0.0009876	2.7767	2.4417
0.001	0.0001976	1.3467	0.9900
0.0005	0.00009876	0.8967	0.2767
0.000225	0.0000444	0.3767	0.0600
0.0002	0.00003951	0.0733	0.0
0.000150	0.00002963	0.1633	0.0
0.000125	0.00002469	0.0	0.0
0.0001	0.00001976	0.0	0.0

Table 3.3

Average Frequency of Zero Crossing, $N(T)/\lambda T$, of a Shallow Arch Under White-Noise Excitation of Intensity Φ_o ($\lambda = 5.0$, $\Delta t = 0.02$)

β		0.1	0.2
Φ_o	Φ_o/λ^4	$N(T)/\lambda T$	$N(T)/\lambda T$
10.0	0.016	6.4600	5.9995
5.0	0.008	4.9685	4.6440
1.0	0.0016	3.4800	2.6520
0.5	0.0008	2.8300	2.0900
0.1	0.00016	1.6490	0.6480
0.05	0.00008	0.9515	0.0880
0.022	0.0000352	0.0760	0.0035
0.02	0.000032	0.0535	0.0
0.0175	0.000028	0.1070	0.0
0.0150	0.000024	0.0	0.0
0.01	0.000016	0.0	0.0

Table 3.4

Average Frequency of Zero Crossing, $N(T)/\lambda T$, of a Shallow Arch Under White-Noise Excitation of Intensity Φ_o ($\lambda = 7.0$, $\Delta t = 0.02$)

β		0.1	0.2
Φ_o	Φ_o/λ^4	$N(T)/\lambda T$	$N(T)/\lambda T$
10.0	0.004165	4.4546	3.8118
5.0	0.002080	3.4561	2.8154
1.0	0.0004165	2.0532	1.3354
0.5	0.0002080	1.4068	0.9107
0.1	0.00004165	0.1221	0.0
0.07	0.00002915	0.0107	0.0086
0.065	0.0000271	0.0	0.0
0.06	0.00002499	0.0178	0.0
0.05	0.00002082	0.0407	0.0
0.0425	0.00001770	0.0021	0.0
0.04	0.00001667	0.0	0.0

Table 3.5

Observed Critical Spectral Density Parameter, Φ_{cr}, of White-Noise Excitation for Snap-Through of a Shallow Arch ($\Delta T = 0.02$)

β	0.1	0.2
λ	Φ_{cr}/λ^4	Φ_{cr}/λ^4
1.5	2.469×10^{-5}	3.951×10^{-5}
5.0	2.400×10^{-5}	3.200×10^{-5}
7.0	1.667×10^{-5}	2.710×10^{-5}

Chapter IV

Energy Envelope Approximation of Diffusion Process

The snap-through of a shallow arch subjected to white noise excitation is presented in this chapter. Solutions are obtained in terms of curves of the survival probability or the reliability function, $P_s(T)$, at time T as a function of T. The mean time to first snap-through, $\bar{T}$, which is the single most important statistic, is also determined. The time of first snap-through will depend on the vibratory system (i.e., on the values of a damping coefficient, β , and the natural frequency, ω_o), the excitation level, Φ_o, the critical barrier level, b, and the initial conditions and the type of critical barrier [20].

The purpose of this study is to obtain probabilistic information on the time T when a prescribed response process, $q(t)$, of the shallow arch first passes outside the domain of safe operation. It is assumed that low response levels of $q(t)$ are safe. The parameter of interest is the time at which the response first exceeds a prescribed threshold or passage level which corresponds to the physical failure of a structure, i.e., due to the displacement becoming so large as to cause "' bottoming or snap-through'" [20].

The nature of the safe domain associated with the type of critical barrier must be precisely specified for first-passage failure problems. There are several cases of safe domains which can be described by a critical barrier. In most practical cases, the following two barriers are important and widely used.

(1). A single-sided barrier or type-B barrier: In this type, the passage level is $q(t) = b$, as shown in Figures 12 and 13(a). Failure occurs when the response, $q(t)$, first exceeds the critical barrier, $q(t) = b$. The quantity of interest is the probability distribution of time T at which $q(t)$ first takes on a value of $q(t) \geq b$.

(2). A double-sided barrier or type-D barrier: In this type, the passage level is $q(t) = \pm b$, as shown in Figure 13(b). Failure occurs when the absolute value of the response, $|q(t)|$, first exceeds the critical barrier, $q(t) = \pm b$. The quantity of interest is the probability distribution of time T at which $q(t)$ first takes on a value of $|q(t)| \geq b$.

First-passage failure is one important type of failure for which a precise mathematical model can be formulated [76]. First-passage failure occurs when the response first exceeds a prescribed critical level. For a system subjected to white noise excitation, the response process whose state variables are the velocity and the displacement may be modelled as a two-dimensional Markov process, governed by a diffusion or Fokker-Planck-Kolmogorov (FPK) equation. Then, the backward Kolmogorov (BK) equation governing the probability of the first-passage failure can be derived from the FPK equation. If only the moments of the first-passage time are required, they can be obtained from a set of generalized Pontriagin-Vitt (GPV) equations which can be derived from the BK equation. However, analytical solutions of the probability of first-passage failure obtained from the GPV and BK equations are not yet available for most practical cases. As a result, most solutions rely on numerical approximation techniques.

In this study, a numerical technique proposed by Roberts [76] is used. Roberts approximated the FPK equation of the response process by an energy envelope process. This is based on the fact that, for sufficiently light damping, the energy envelope process, $V(t)$, as given by Eqs. (2.3) and (2.4), may be modelled, to a close approximation, as a one-dimensional Markov process [71,72,73,76].

The derived diffusion equation of $V(t)$, with suitable boundary conditions, can be solved numerically for estimates of the probability of first-passage failure associated with the dis-

placement response of the oscillators [71,72,76]. A system with nonlinear restoring forces can be solved using this technique [72,76].

An implicit finite difference method, of the Crank-Nicolson type, was used to approximate the diffusion process of the energy envelope process [76,85]. The proposed method can be used to obtain full information on the probability distribution of first-passage failure, as a function of a time interval. The mean time to failure related to first-passage problems can also be obtained.

4.1 Description of the Problem

For the response of a nonlinear system, the equation of motion is generally of the form

$$\ddot{q} + \beta H(q, \dot{q}) + G(q) = F(t) \tag{4.1}$$

where $q(t)$ is the displacement response, β is a damping coefficient, $H(q, \dot{q})$ and $G(q)$ are nonlinear functions, and $F(t)$ is a zero-mean, wide-band stationary random process.

This study focuses on the single-sided barrier, as shown in Figures 12 and 13(a). The first-passage failure, $P_f(t)$, is defined as the probability that the response $q(t)$ exceeds the critical barrier b, at least once, in some interval of time, from $0 - t$. The reliability function, $P_s(t)$, associated with $P_f(t)$, is defined as the probability that $q(t)$ is less than the critical level b throughout the time interval $0 - t$. Obviously,

$$P_s(t) = 1 - P_f(t) \tag{4.2}$$

The probability density function, $p_f(t)$, of the time to first-passage failure, T, is given by

$$p_f(t) = \frac{dP_f(t)}{dt} = -\frac{dP_s(t)}{dt}, \tag{4.3}$$

and the moments of time to first-passage failure are given by

$$M_n = E[T^n] = \int_0^\infty t^n p_f(t)\, dt \tag{4.4}$$

4.2 Energy Envelope Approximation

For snap-through of a shallow arch subjected to a white noise excitation, the one-mode approximation of the equation of motion is given by Eq. (3.34) and rewritten here as

$$\ddot{q} + \beta\dot{q} + \omega_o^2 q\left[1 + \varepsilon_1 q + \varepsilon_2 q^2\right] = \varepsilon_3 F(t) \tag{4.5}$$

where $q(t)$ is the displacement response of the shallow arch, β is a small damping parameter, ε_1 and ε_2 are coefficients of nonlinear terms, ε_3 is the constant coefficient of the loading function, and ω_o is the natural frequency of a corresponding linearlized system. Eq. (4.5) describes the system with linear damping and nonlinear restoring forces.

The parameters are defined as follows:

$$\begin{aligned} \omega_o^2 &= \pi^4(1 + 2\lambda^2) \\ \varepsilon_1 &= -3\sqrt{2}\,\pi^4\lambda/\omega_o^2 \\ \varepsilon_2 &= 2\pi^4/\omega_o^2 \\ \varepsilon_3 &= \sqrt{2}\,\pi^4/2 \end{aligned} \tag{4.6}$$

where λ is a nondimensional arch rise parameter.

$F(t)$ is assumed to be sufficiently modelled as a white noise process. Therefore, $F(t)$ is completely described by

$$E[F(t)] = 0, \text{ and} \tag{4.7}$$

$$R_F(\tau) = E[F(t)F(t+\tau)] = I\delta(\tau) \tag{4.8}$$

where $R_F(\tau)$ is the autocorrelation function, $\delta(\tau)$ is the Dirac delta function, and E[.] is the expectation or ensemble average. I is the intensity of the random force and, in this study, defined as $2\pi\Phi_o$, where Φ_o is the constant power spectrum of the white noise.

For convenience, the following scaled parameter is introduced:

$$Q = \frac{q}{\varepsilon_3} \tag{4.9}$$

The equation of motion, Eq. (4.5), then becomes

$$\ddot{Q} + \beta\dot{Q} + \omega_o^2 Q\left[1 + \gamma_1 Q + \gamma_2 Q^2\right] = F(t) \tag{4.10}$$

where $\gamma_1 = \varepsilon_1 \varepsilon_3$, and $\gamma_2 = \varepsilon_2 \varepsilon_3^2$. The scaled critical barrier for the displacement response of Eq. (4.10) is now taken to be $Q(t) = \eta$, where $\eta = b/\varepsilon_3$.

The energy envelope process, $V(t)$, of Eq. (4.10), may be expressed as

$$V(t) = \frac{\dot{Q}^2}{2} + U(Q) \tag{4.11}$$

where $U(Q)$ is the potential energy function, and it is defined as

$$U(Q) = \int_0^Q G(\xi)d\xi \tag{4.12}$$

In this study, the function $U(Q)$ is given by

$$U(Q) = \omega_o^2\left[\frac{Q^2}{2} + \gamma_1\frac{Q^3}{3} + \gamma_2\frac{Q^4}{4}\right] \tag{4.13}$$

The transition density function is denoted by $p(V;t|V_0)$, which is defined as the probability that $V(t)$ lies in the range $V, V + dV$ at time t, for a given initial condition of $V(t) = V_0$ at $t = 0$. The corresponding FPK equation, governing $p(V;t|V_0)$, is given by [71,72,73,76].

$$\frac{\partial p}{\partial t} = \frac{\partial}{\partial V}\left\{\left[\beta B(V) - \frac{I}{2}\right]p\right\} + \frac{I}{2}\frac{\partial^2}{\partial V^2}[C(V)p] \tag{4.14}$$

where $B(V)$ and $C(V)$ are defined as follows [76]:

$$B(V) = \frac{1}{\sqrt{2}\,A(V)}\int_R H(Q, \dot{Q})dQ, \tag{4.15}$$

$$C(V) = \frac{1}{A(V)}\int_R \sqrt{(V-U)}\,dQ, \tag{4.16}$$

and

$$A(V) = \frac{1}{2}\int_R \frac{dQ}{\sqrt{V-U}} \tag{4.17}$$

The integration range, R, is such that $U(Q) < V$. Since the system in this case is linear in damping, then

$$H(Q, \dot{Q}) = \dot{Q} = \sqrt{2(V-U)} \tag{4.18}$$

Hence, Eqs. (4.15) and (4.16) become

$$B(V) = C(V) = \frac{2\int_R \sqrt{V-U(\xi)}\,d\xi}{\int_R \frac{d\xi}{\sqrt{V-U(\xi)}}} \tag{4.19}$$

The FPK equation, as given by Eq. (4.14), describes the diffusion process of the response probability mass in the phase plane. The probability mass diffused with time is considered

as the ensemble of the response process. The probability mass absorbed or lost at any time instant represents conceptually the response ensemble which failed at that time. Thus, the probability mass that remained in the safe domain can be used to determine the reliability of the system [91].

4.3 Boundary Conditions

In order to use Eq. (4.14) to obtain the evolution of probability "mass" during a diffusion process of $V(t)$, as a function of time, suitable boundary conditions must be established. These boundary conditions may be introduced in the form of absorbing and reflecting barriers. After the evolution process of probability mass is obtained, it can be modified to yield estimates of the probability that the response $Q(t)$ stays within the safe domain, i.e., $Q(t) < \eta$, throughout the time interval $0 - t$.

In this study, the single-sided barrier at $Q(t) = \eta$, as shown in Figure 14, is used as an absorbing barrier in the diffusion processs of $V(t)$. At the absorbing barrier, probability mass is lost when it diffuses past this barrier and does not diffuse back into the safe domain [76]. Figure 14(a) shows a trajectory in the phase plane of the response as it exits from the safe domain. When the damping is light, the energy level, $V(t)$, will be changing slowly with time. Therefore, a trajectory exitting from the safe domain will almost certainly cross the Q-axis shortly afterwards at some value of $Q(t) > \eta$, as shown in Figure 14(a). As a result, the single-sided barrier for the displacement response can be modified by folding back the barrier, as indicated in Figure 14(b), until it lies entirely along the Q-axis, as shown in Figure 14(c) [72,76].

When the energy envelope approximation is used, the modification of the single-sided barrier, as described above, greatly simplifies the first-passage problem associated with the displacement response. The condition for the first-passage failure can now be approximately stated as follows: failure occurs when $V(t)$ exceeds the critical level of energy, $h = U(\eta)$, for the

first time and the velocity, $\dot{Q}(t)$, is, simultaneously, equal to zero [76]. Therefore, the appropriate absorbing barrier for $V(t)$ will appear as a sequence of vertical lines, as shown in Figure 15(a), which occur each time the velocity is equal to zero. Failure occurs when $V(t)$ intersects one of these vertical lines for the first time. These absorbing vertical lines reach minimum value at $h = U(\eta)$, which is a constant energy level.

The times at which these vertical lines occur, say t_i, are random. However, in the case of light damping, these lines are almost equi-spaced when the energy level is close to the value $h = U(\eta)$. As a result, an average interval, Δt, between these equi-spaced lines can be, in the case of light damping, approximately taken as the value of the natural period of oscillation of the system, evaluated at $h = U(\eta)$.

It is shown that the natural period of oscillation can be given by [63,72,73,76].

$$T(V) = 4\int_0^{\eta} \frac{d\xi}{\sqrt{V - U(\xi)}}, \tag{4.20}$$

where $V = h = U(\eta)$. Hence

$$\Delta t = T(V) = 2\sqrt{2}\, A(V) \tag{4.21}$$

where $A(V)$, defined by Eq. (4.17), now becomes

$$A(V) = \frac{1}{2}\int_0^{\eta} \frac{d(\xi)}{\sqrt{V - U(\xi)}} \tag{4.22}$$

In summary, the absorbing barrier is represented by the vertical lines, as shown in figure 15(b), with a minimum value at $h = U(\eta)$. These vertical lines occur at equi-spaced time intervals of Δt , which is given by Eq. (4.21).

The diffusion process with the modified absorbing barrier can then be described as follows. From a given initial condition of $V(t) = V_0$ at $t = 0$, the evolution of probability mass is computed using Eq. (4.14) up to the time of the first absorbing barrier line, $t = \Delta t$. At this time, probability mass is lost or absorbed, for $V > h$, i.e., $p(V; \Delta t|V_0)$ is set equal to zero for $V > h$. The evolution of probability mass is allowed to diffuse freely between any two consecutive absorbing lines. The procedure is repeated at each absorbing line, so that the "lost or absorbed" probability mass does not diffuse back into the safe domain. The reliability function, $P_s(t)$, is computed at each absorbing barrier of time t_j, where $t_j = j\Delta t$, using the following expression:

$$P_s(t_j|V_0) = \int_0^h p(V;t_j|V_0)\, dV \tag{4.23}$$

where the quantity $p(V;t_j|V_0)dV$, for $V < h$, represents the probability that $V(t)$ reaches the interval ΔV , centered at V, at time t_j, without intersecting the barrier line. $P_s(t_j|V_0)$ can be used to estimate the reliability function for the process $Q(t)$ with the single-sided barrier. The first-passage probability density function can be estimated at each time interval as

$$p_f(t) = -\frac{[P_s(t) - P_s(t - \Delta t)]}{\Delta t} \tag{4.24}$$

In addition to the absorbing barrier, a reflecting barrier must be specified at $V = 0$. The reflecting barrier describes the boundary condition that the process cannot diffuse into the region where $V < 0$. Since probability mass is conserved for the diffusion process between each absorbing line, the reflecting barrier can be given by the condition [76]

$$\int_0^\infty p(V;t_j|V_0)dV = k_j \tag{4.25}$$

The first value of k, between time $t = 0$ and the first absorbing barrier at time $t = \Delta t$, is equal to unity. Due to absorption at the barrier lines, other values of k_j will be less than unity.

The values of k_j are constant between consecutive barriers with a value which undergoes a step decrease at every absorbing line.

4.4 Mean First-Passage Time

The approximate method of solving the first-passage problem for the displacement response, $Q(t)$, outlined earlier, gives estimates of the reliability function, $P_s(t)$, as a function of time at equi-spaced intervals of time Δt . The mean time to first-passage failure, $\bar{T}$, can be expressed directly in terms of $P_s(t)$, and is given by [76]

$$\bar{T} = \int_0^\infty P_s(t)dt \tag{4.26}$$

In the calculation of $\bar{T}$, Eq. (4.26) can be separated into two parts, as follows:

$$\bar{T} = \bar{T}_A + \bar{T}_B, \tag{4.27}$$

where

$$\bar{T}_A = \int_0^{\hat{t}} P_s(t)dt, \tag{4.28}$$

$$\bar{T}_B = \int_{\hat{t}}^\infty P_s(t)dt \tag{4.29}$$

Due to the fact that $P_s(t)$ approaches the exponential form, $e^{-\alpha t}$, as t becomes large, $\bar{T}_B$ can be approximated as

$$\bar{T}_B = \frac{1}{\alpha} e^{-\alpha \hat{t}} \tag{4.30}$$

where α is a constant parameter, which is also known as "the limiting decay rate." Therefore, $\bar{T}$ can be estimated by evaluating $P_s(t)$ up to $t = \hat{t}$, where convergence is achieved. From Eq. (4.28), $\bar{T}_A$ can be estimated using a simple discrete summation approximation of the integral, as follows:

$$\bar{T}_A = \Delta t \left[0.5 + \sum_{i=1}^{j} P_s(i\Delta t) \right] \tag{4.31}$$

where $j\Delta t = \hat{t}$ and the fact that $P_s(0) = 1$ has been used. Using Eq. (4.30), $\bar{T}_B$ can be approximated, asymptotically, as

$$\bar{T}_B = \frac{\Delta t \, P_s[(j+1)\Delta t]}{1 - r} \tag{4.32}$$

where r is a constant and given by

$$r = \frac{P_s(t_{i+1})}{P_s(t_i)} \tag{4.33}$$

Therefore, the mean time to failure can be estimated using Eqs. (4.27), (4.31), and (4.32).

4.5 Numerical Solutions-Finite Difference Approximation

The equation of motion for a shallow arch subjected to a white noise excitation, $F(t)$, is given by Eq. (4.10), as described in Section 4.2. The FPK equation governing the transition density function, $p(V;t|V_0)$, of the energy envelope process, $V(t)$, is given by Eq. (4.14). From Eq. (4.19), the functions $B(V)$ and $C(V)$ can be numerically evaluated as follows:

$$B(V) = C(V) = \frac{2\int_R \sqrt{V - \omega_o^2\left[\frac{1}{2}\xi^2 + \frac{1}{3}\gamma_1\xi^3 + \frac{1}{4}\gamma_2\xi^4\right]}\, d\xi}{\int_R \frac{d\xi}{\sqrt{V - \omega_o^2\left[\frac{1}{2}\xi^2 + \frac{1}{3}\gamma_1\xi^3 + \frac{1}{4}\gamma_2\xi^4\right]}}} \tag{4.34}$$

With the change of variables

$$V = \omega_o^2\left[\frac{1}{2}a^2 + \frac{1}{3}\gamma_1 a^3 + \frac{1}{4}\gamma_2 a^4\right]; \quad \xi = a\sin\theta.$$

in Eq. (4.34), $B(V)$ and $C(V)$ can be expressed simply as

$$B(V) = C(V) = \frac{\omega_o^2 a^2 K(m, u_1, u_2)}{L(m, u_1, u_2)} \tag{4.35}$$

where

$$K(m, u_1, u_2) = \int_0^{\pi/2}\left[m - (1 + u_1\sin\theta + u_2\sin^2\theta)\sin^2\theta\right]^{1/2}\cos\theta d\theta, \tag{4.36}$$

$$L(m, u_1, u_2) = \int_0^{\pi/2}\left[m - (1 + u_1\sin\theta + u_2\sin^2\theta)\sin^2\theta\right]^{-1/2}\cos\theta d\theta, \tag{4.37}$$

and $u_1 = \frac{2}{3}\gamma_1 a$, $u_2 = \frac{1}{2}\gamma_2 a^2$, and $m = 1 + u_1 + u_2$. Note that $B(V)$ and $C(V)$ can only be determined numerically.

Let

$$F(V) = \beta B(V) - \frac{I}{2}, \text{ and } G(V) = I\frac{C(V)}{2}$$

Then, Eq. (4.14) becomes

$$\frac{\partial p}{\partial t} = \frac{\partial}{\partial V}[F(V)p] + \frac{\partial^2}{\partial V^2}[G(V)p] \tag{4.38}$$

The initial condition of the system of Eq. (4.38), in terms of $V(t)$, is $V(t) = V_0$ at $t = 0$. This can be expressed in terms of the transition density function as

$$\underset{t \to 0}{LIMIT}\; p(V; t|V_0) = \delta(V - V_0) \tag{4.39}$$

The function $\delta(V - V_0)$ is defined as

$$\delta(V - V_0) \begin{cases} = 0 & for \quad V \neq V_0 \\ \to \infty & for \quad V = V_0 \end{cases} \tag{4.40}$$

and, for any $\varepsilon > 0$,

$$\int_{V_0 - \varepsilon}^{V_0 + \varepsilon} \delta(V - V_0)\, dZ = 1 \tag{4.41}$$

A finite difference approximation to Eq. (4.38) is obtained by considering $V(t)$ at discrete values, $V_i = i\delta v$ for $i = 0, 1, ...$, and time at discrete values, $t_j = j\delta\tau$ for $j = 0, 1, ...$. A rectangular mesh of points in the $V - t$ plane is shown in Figure 16.

At $i = 0$, where $V = 0$, there is a reflecting barrier as given by Eq. (4.25). The upper limit to the value of V_i must also be provided by introducing an artificial absorbing barrier at $i = N$. V_N must be high enough for its effect on the diffusion process to be negligible. For a Duffing oscillator, studied in Ref. [76], a value of $V_{max} = V_N = 3h$, where $h = U(\eta)$, was found to be generally satisfactory. Note that $\eta = b/\varepsilon_3$, which is a scaled critical barrier. Obviously, it is convenient to select δv and $\delta\tau$ such that $L = h/\delta v$ and $M = \Delta t/\delta\tau$ are integer quantities.

A suitable implicit finite difference approximation to Eq. (4.38), of the Crank-Nicolson type, is used in this study [76,85]. The derivative terms on the right-hand side of Eq. (4.38) are re-

placed by the mean of their finite difference representations at the $(j+1)th$ time step and jth time step. $\partial p/\partial t$ is replaced by a simple, forward difference approximation. The following notation is used:

$$\begin{aligned} p(i\delta v, j\delta\tau) &= p_{i,j}, \\ F(i\delta v) &= F_i, \text{ and} \\ G(i\delta v) &= G_i. \end{aligned}$$

For $i = 1, 2, \ldots, N-1$, Eq. (4.38) becomes

$$\begin{aligned} \left[\frac{p_{i,j+1} - p_{i,j}}{\delta\tau}\right] = \frac{1}{2}\left[\frac{F_{i+1}p_{i+1,j+1} - F_{i-1}p_{i-1,j+1}}{2\delta v} + \frac{F_{i+1}p_{i+1,j} - F_{i-1}p_{i-1,j}}{2\delta v}\right] \\ + \frac{1}{2}\left[\frac{G_{i+1}p_{i+1,j+1} - 2G_ip_{i,j+1} + G_{i-1}p_{i-1,j+1}}{(\delta v)^2}\right] \\ + \frac{1}{2}\left[\frac{G_{i+1}p_{i+1,j} - 2G_ip_{i,j} + G_{i-1}p_{i-1,j}}{(\delta v)^2}\right] \end{aligned} \tag{4.42}$$

The above difference equation can be simplified by putting all quantities related to the $(j+1)th$ time step on the left-hand side of the equation and all quantities relating to the jth time step on the right-hand side. Now, the $(j+1)$ and j subscripts can be dropped and the difference equations can be written in the form [76]

$$-a_ip_{i-1} + b_ip_i - c_ip_{i+1} = d_i, \text{ for } i = 1, 2, \ldots, N-1, \tag{4.43}$$

where

$$\begin{aligned} a_i &= -(s'/4)\,F_{i-1} + (r'/2)\,G_{i-1}, \\ b_i &= 1 + r'G_i, \\ c_i &= (s'/4)\,F_{i+1} + (r'/2)\,G_{i+1}, \\ d_i &= a_ip_{i-1} + e_ip_i + c_ip_{i+1}, \\ e_i &= 1 - r'G_i, \\ s' &= \frac{\delta\tau}{\delta v}, \\ r' &= \frac{\delta\tau}{(\delta v)^2}, \end{aligned}$$

The boundary conditions must be introduced, in addition to the above equations, so that at each time step the number of equations equals the number of unknowns. First, at $i = N$, the artificial absorbing barrier may be expressed, in a finite difference approximation, as

$$p_{Nj} = 0, \quad \text{for } j = 0, 1, \ldots \tag{4.44}$$

The absorbing barrier is given by a sequence of vertical lines occurring at equi-spaced intervals, Δt, as given by Eq. (4.21). For the reflecting barrier, a discrete summation of Eq. (4.25), in terms of a finite difference approximation, is given by

$$\delta v\left[0.5p_{0j} + p_{1j} + \cdots + p_{N-1j}\right] = k_j \tag{4.45}$$

At each time step, t_j, $j = 1, 2, \ldots$, the complete set of equations can now be written as

$$\begin{aligned} 0.5p_0 + p_1 + p_2 + \cdots + p_{N-1} &= d_0, \\ -a_1p_0 + b_1p_1 - c_1p_2 &= d_1, \\ &\cdots, \\ -a_ip_{i-1} + b_ip_i - c_ip_{i+1} &= d_i, \\ &\cdots, \\ -a_{N-1}p_{N-2} + b_{N-1}p_{N-1} &= d_{N-1} \end{aligned} \tag{4.46}$$

where $d_0 = k_j/\delta v$. The variables a_i, b_i, c_i, and e_i, for $i = 1, 2, \ldots, N-1$, are determined only once, before the marching process begins.

At each time step, the d_i's on the right-hand side of Eqs. (4.46) are known, and the p_i's on the left-hand side are the unknowns. With the exception of the first equation, Eqs. (4.46) are of tri-diagonal form. The modified procedure for solving the set of these equations using the standard Thomas algorithm was described by Roberts [76]. This procedure involves elimination and back-substitution techniques. This procedure is briefly presented here, as follows.

First, the parameters α_i and S_i, for $i = 1, 2, \ldots, N-1$, are recursively calculated from the following expressions:

$$\alpha_{N-1} = b_{N-1}, \quad S_{N-1} = d_{N-1}; \tag{4.47}$$

and for $i = 1, 2, \ldots, N-2$,

$$\alpha_{N-i-1} = b_{N-i-1} - \frac{a_{N-i}c_{N-i-1}}{\alpha_{N-i}}, \text{ and} \tag{4.48}$$

$$S_{N-i-1} = d_{N-i-1} + \frac{c_{N-i-1}S_{N-i}}{\alpha_{N-i}} \tag{4.49}$$

After the parameters α_i and S_i are determined, a set of equations for the p_i's, for $i = 1, 2, \ldots, N-1$, can be given as follows:

$$-a_i p_{i-1} + \alpha_i p_i = S_i \tag{4.50}$$

or

$$p_i = \rho_i + \lambda_i p_{i-1}, \tag{4.51}$$

where

$$\rho_i = S_i/\alpha_i, \text{ and } \lambda_i = a_i/\alpha_i \tag{4.52}$$

Repeated use of Eq. (4.51), for $i = 1, 2, \ldots$, shows that

$$p_i = \theta_i + \psi_i p_0 \tag{4.53}$$

where θ_i and ψ_i are calculated recursively from

$$\theta_{i+1} = \rho_{i+1} + \lambda_{i+1}\theta_i, \tag{4.54}$$

and

$$\psi_{i+1} = \lambda_{i+1}\psi_i \tag{4.55}$$

where

$$\theta_1 = \rho_1, \text{ and } \psi_1 = \lambda_1 \tag{4.56}$$

A substitution from Eq. (4.53) into the first of Eqs. (4.46) gives the following explicit expression for p_0:

$$p_0 = \frac{d_0 - \beta_1}{0.5 + \beta_2} \tag{4.57}$$

where

$$\beta_1 = \sum_{i=1}^{N-1} \theta_i, \quad \text{and} \quad \beta_2 = \sum_{i=1}^{N-1} \psi_i \tag{4.58}$$

Once p_0 is obtained, p_i's for $i = 1, 2, \ldots, N-1$ can be evaluated successively using Eq. (4.51). Note that α_i's are also time-independent; thus, they need be calculated only once.

In this study, the arch is assumed to start from rest. Then, at $t = 0$, $Q(0) = 0$, and $\dot{Q}(0) = 0$; thus, $V(t) = 0$ at $t = 0$. Therefore, at $t = 0$, the initial condition for the diffusion process may be expressed, in a finite difference approximation, as [76]

$$p_{0,0} = \frac{2}{\delta v} \tag{4.59}$$

At $j = 0$, k_0 is evaluated using Eq. (4.45); then

$$k_0 = \delta v\left[0.5p_{0,0} + p_{1,0} + \cdots + p_{N-1,0}\right]$$

Since $p_{i,0}$, for $i = 1, 2, \ldots, N-1$, are equal to zero, $k_0 = 1$ is obtained for the first reflecting barrier between time $t = 0$ and the first absorbing barrier line at time $t = \Delta t$. The other values of k_j for the reflecting barrier can be evaluated at each absorbing barrier using Eq. (4.45).

As previously described in Section 4.3, the absorbing barrier appears as vertical lines which occur at equi-spaced intervals, Δt . The minimum value of these absorbing vertical lines is equal to $h = U(\eta)$, as shown in Figure 16. This study considers a single-sided barrier, and Δt, as given by Eq. (4.21), can be expressed as follows:

$$\Delta t = \sqrt{2}\int_0^{\eta} \frac{d\xi}{\sqrt{U(\eta) - U(\xi)}} = \frac{2L(m, u_1, u_2)}{\omega_o} \tag{4.60}$$

$L(m, u_1, u_2)$ is given by Eq. (4.37), where $u_1 = \frac{2}{3}\gamma_1\eta$, $u_2 = \frac{1}{2}\gamma_2\eta^2$, and $m = 1 + u_1 + u_2$. The constant energy level h is given by

$$h(\eta) = \frac{\eta^2}{2}\left[1 + \frac{2}{3}\gamma_1\eta + \frac{1}{2}\gamma_2\eta^2\right] \tag{4.61}$$

The boundary conditions are now completely established for the diffusion process; so the finite difference approximation is used to obtain the transition density function, $p(V; t_j | V_0)$, at each time step t_j, for $j = 1, 2, \ldots, \Delta t, \ldots, 2\Delta t, \ldots$. At each absorbing line, probability mass is absorbed for $V > h$ (i.e., probability mass is lost when it diffuses past the absorbing barrier) ; this can be put in the form of a finite difference approximation as follows:

$$p_{i,j\Delta t} = 0, \quad \text{for } i = L + 1, L + 2, \ldots, N - 1. \tag{4.62}$$

where L is an integer quantity defined as $L = h/\delta v$.

At each absorbing line, say at time t_j where $t_j = j\Delta t$, the reliability function, $P_s(t_j)$, as a function of time interval Δt , can be determined using Eq. (4.23). A discrete approximation to Eq. (4.23) is given by

$$P_s(t_j) = \delta v\left[0.5p_{0j} + p_{1j} + p_{2j} + \cdots + p_{Lj}\right] \tag{4.63}$$

The probability of first-passage failure in an interval $0 - T$ is evaluated using the following expression:

$$P_f(T) = 1 - P_s(T) \tag{4.64}$$

where $T = j\Delta t$. The mean time to first-passage failure is determined using the known values of $P_s(j\Delta t)$ and the procedure described in Section 4.4.

4.6 Numerical Results

A shallow arch subjected to a white noise excitation is considered here. The initial rise of the arch, λ, is 5.0. The parameters are calculated and are as follows:

$$\omega_o = 70.48307$$
$$\varepsilon_1 = -0.41594$$
$$\varepsilon_2 = 0.03921$$
$$\varepsilon_3 = 68.87863$$
$$\gamma_1 = -28.64973$$
$$\gamma_2 = 186.04963$$

A single-sided barrier is considered, and the passage level is $q(t) = b$. In this case, b is assumed to be $\lambda/\sqrt{2}$, where the arch will fail by dynamic snap-through if the response, $q(t)$, exceeds this critical level. The quantity $\lambda/\sqrt{2}$ is the distance between the central deflection of the arch, $q(t)$, at $t = 0$ and the horizontal axis. It is assumed that the arch will snap to the other side of the horizontal axis at a subsequent time t if the central deflection of the arch $q(t)$ is equal to or greater than the quantity $\lambda/\sqrt{2}$. Hence

$$b = \lambda/\sqrt{2} = 3.53553$$

The scaled parameter of the critical passage level is given by

$$\eta = \frac{b}{\varepsilon_3} = 0.05133$$

The minimum value of the absorbing barrier is given by h, which is defined by Eq. (4.61), and it is equal to 1.73238.

The absorbing barrier appears as a sequence of vertical lines occurring at equi-spaced intervals of time, Δt. Δt is evaluated using Eq. (4.60), and the results are as follows:

$$u_1 = -0.98039, \quad u_2 = 0.24510, \quad m = 0.26471, \quad \text{and} \quad L(m, u_1, u_2) = 5.89637$$

Hence,

$$\Delta t = 0.16731$$

Before the implicit finite difference approximation can begin, suitable values of $\delta\tau$ and δv must be selected. The values of $\delta\tau$ and δv must be sufficiently small for the discretization error to be negligible. In each case, trial values of $\delta\tau$ and δv were chosen and successively reduced until a fully converged solution is obtained. The selection of V_{max} for the artificial absorbing barrier is also significant. A sufficiently high value of V_{max} may be necessary for its effect on the diffusion process to be negligible.

Table 4.1 shows the effect of the value of V_{max} on the mean time to first snap-through for the case of $\lambda = 5.0$, $\beta = 0.20$, and $\Phi_o = 5.0$. Trial values of $\delta\tau = 0.001673$, and $\delta v = 0.0866$ and 0.0433 were used. Results indicate that the value of V_{max} as an artificial absorbing barrier actually has a significant effect on the diffusion process. Since a high value of V_{max} results in increased computation time, the decision on the selection of V_{max} is a compromise between negligible error and computer effort. Therefore, $V_{max} = 7h$ is considered to be sufficient in this study.

Table 4.2 shows the effect of δv and $\delta\tau$ on the mean time to first snap-through for the same values of λ, β, and Φ_o. The value of $V_{max} = 5h$ is used in this table. Results show that full convergence can be obtained for small values of $\delta\tau$ and δv. Convergence is achieved as $\delta\tau$ is reduced, and the value of $\delta\tau = 0.001673$ is sufficiently small. Smaller values of $\delta\tau$ do not improve the results. It is also observed that the value of $\delta v = 0.0433$ gives satisfactory results and does not require too much computational effort. Smaller values of δv do not give a faster rate of convergence. Therefore, $\delta\tau = 0.001673$ and $\delta v = 0.0433$ will be used for the rest of this study.

Additional results are presented in Table 4.3. This table gives the mean time to first snap-through of a shallow arch with $\lambda = 5.0$ subjected to various values of β and Φ_o. The following parameters are used: $V_{max} = 7h$, $\delta\tau = 0.001673$, and $\delta v = 0.0433$. The mean time to failure increases as the intensity of the random load is reduced. An increase in the damping parameter also increases the mean time to failure. At a high value of damping, the mean time to first snap-through is extremely high and the calculation is costly. Hence, some results are not available.

The approximation technique also gives full information on the probability distribution of the first-passage time failure, as shown in Figs. 17 and 18. Fig. 17(a) illustrates the reliability function $P_s(t)$ for the case of $\lambda = 5$ and $\beta = 0.2$, for various values of Φ_o. Probability density function of the time to first snap-through for the same problem is given in Fig. 17(b). Fig. 18 shows the first-passage probability distribution for $\lambda = 5.0$ and $\Phi_o = 5.0$, for various values of β.

Fig. 19 shows the variation of the mean time to first snap-through, $\overline{N}$, in cycles, where $\overline{N} = \omega_o \overline{T}/2\pi$, for various values of Φ_o and β. The mean time to failure tends to increase rapidly when the damping coefficient is greater than 2.0. A small value of the damping coefficient, i.e., $\beta \leq 2.0$, has an insignificant effect on the value of the mean time.

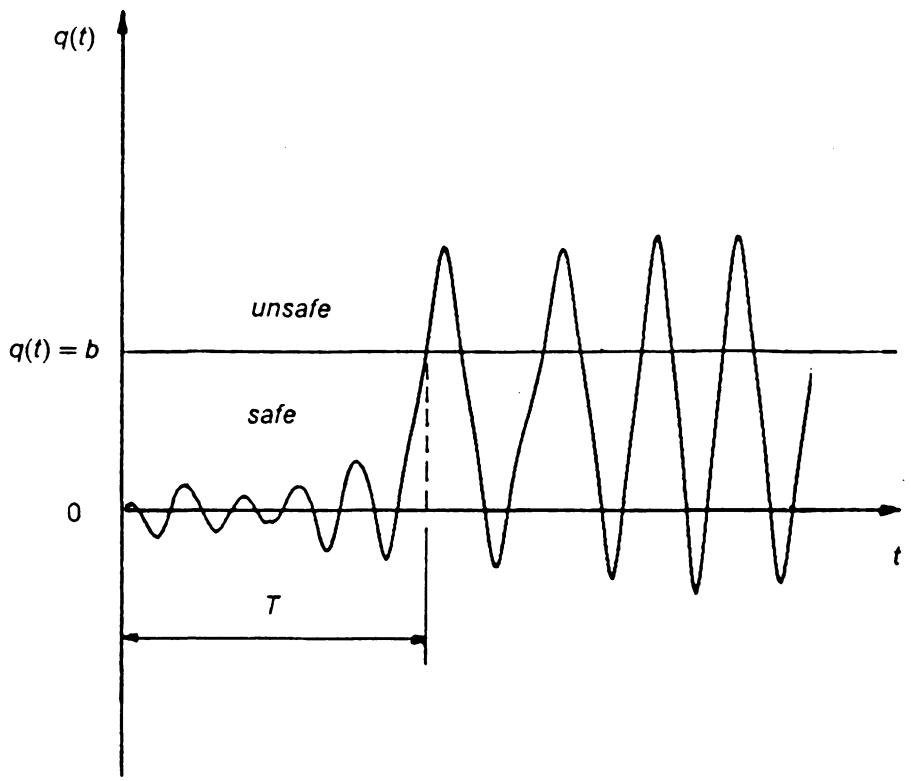

Figure 12. Typical response q(t) and time to first-passage failure: A single-sided barrier, at a barrier level $q(t) = b$.

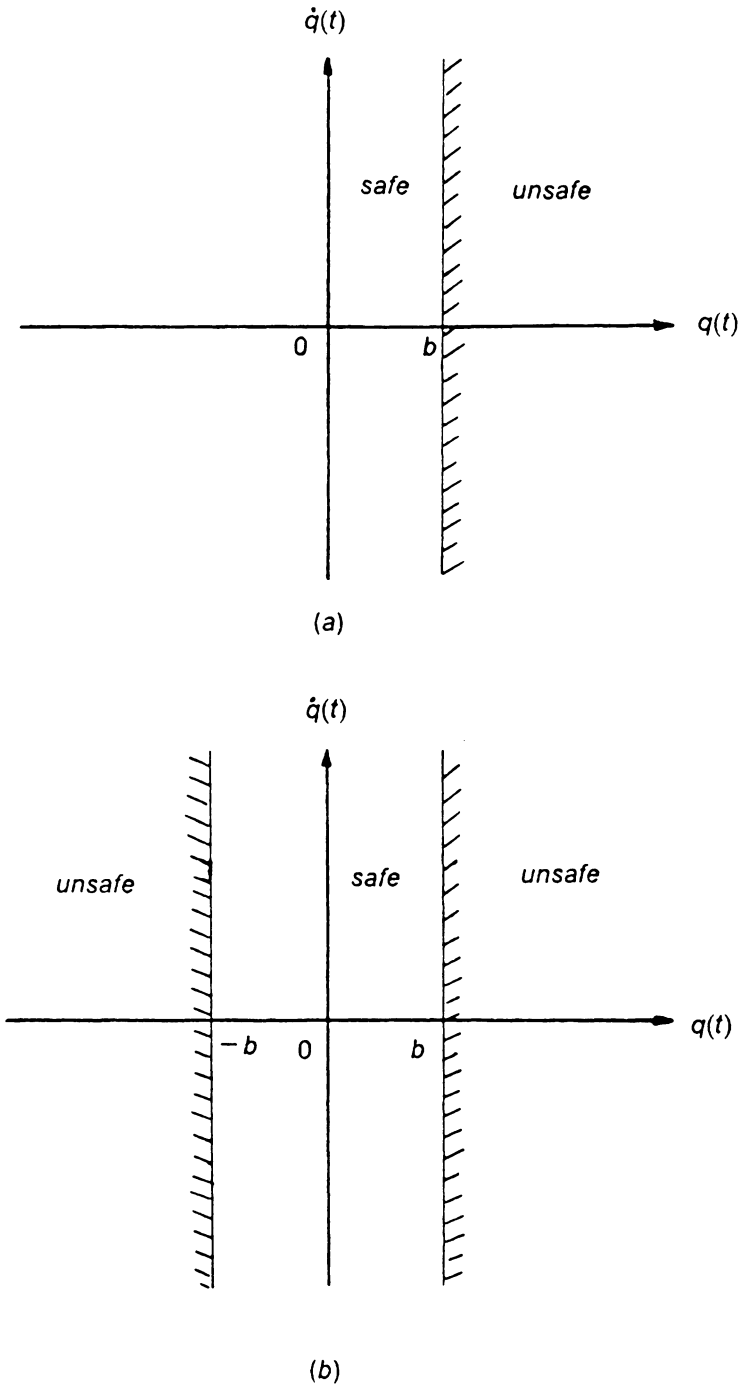

Figure 13. **Domains of safe operation in the phase plane:** (a) a single-sided barrier, (b) a double-sided barrier.

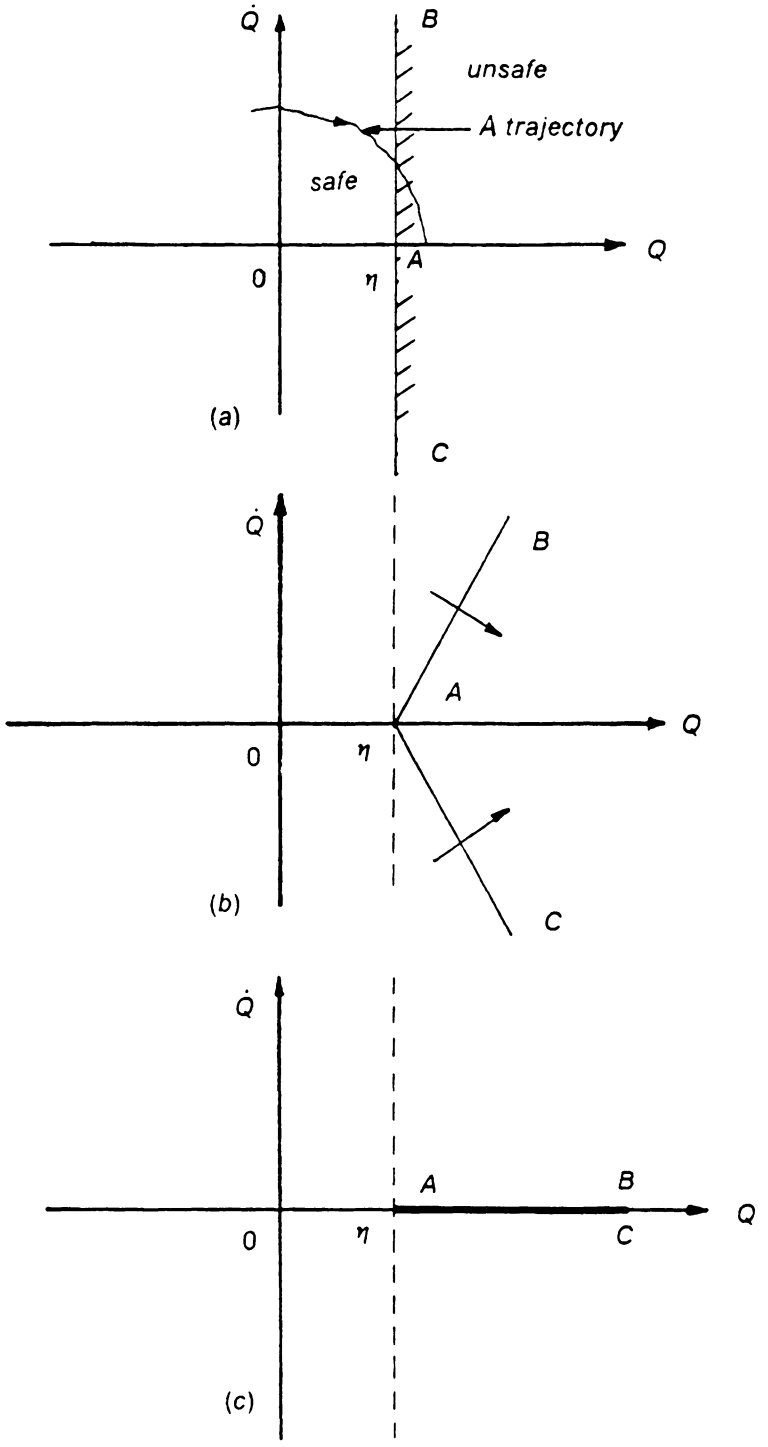

Figure 14. Modification of a single-sided barrier: (a) a trajectory in the phase plane, (b) folding-back the barrier, (c) a modified absorbing barrier.

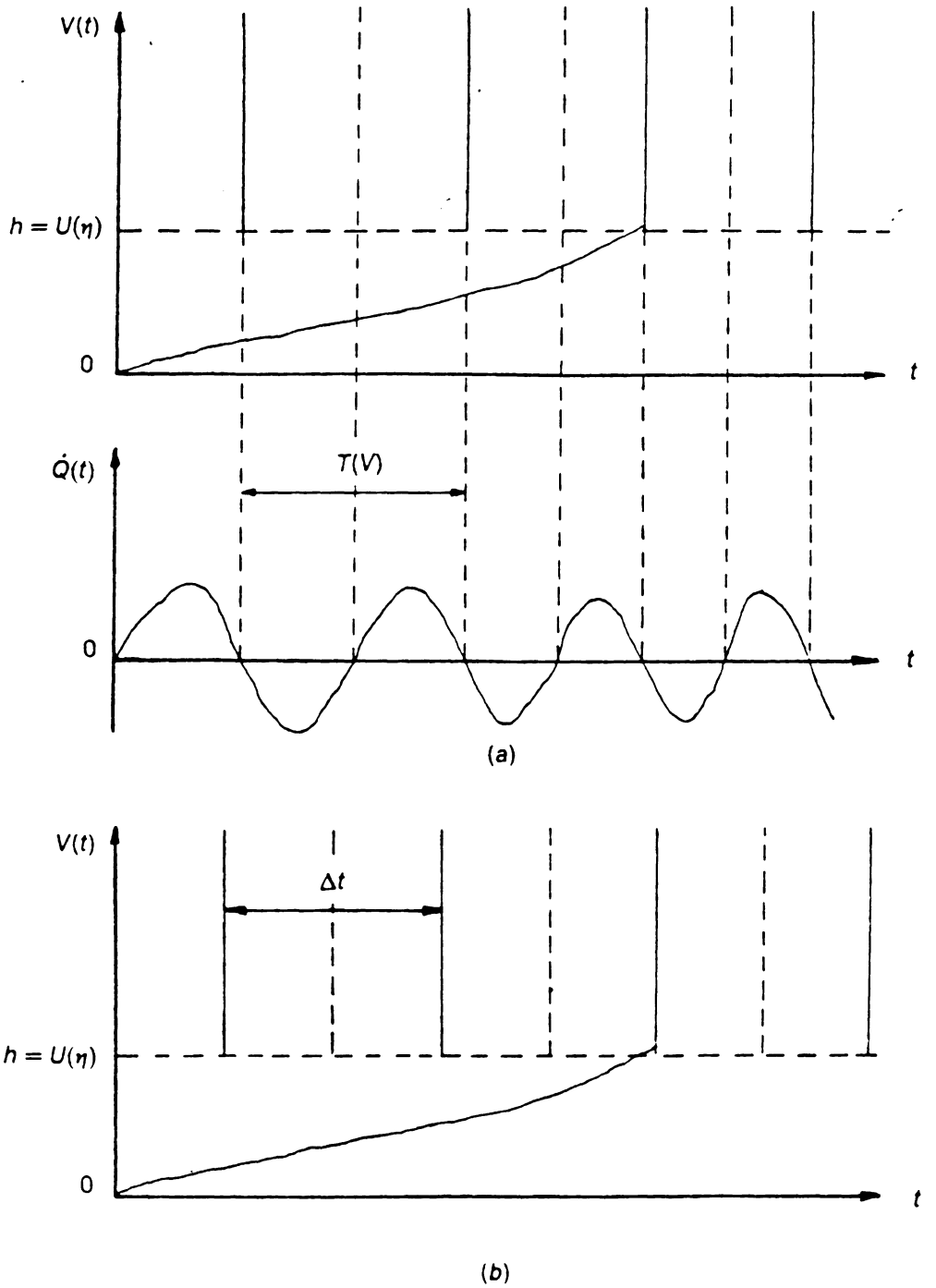

Figure 15. Absorbing barrier for the V(t) process: (a) Typical V(t) and $\dot{Q}(t)$ realizations (b) the approximately equi-spaced barrier line configuration.

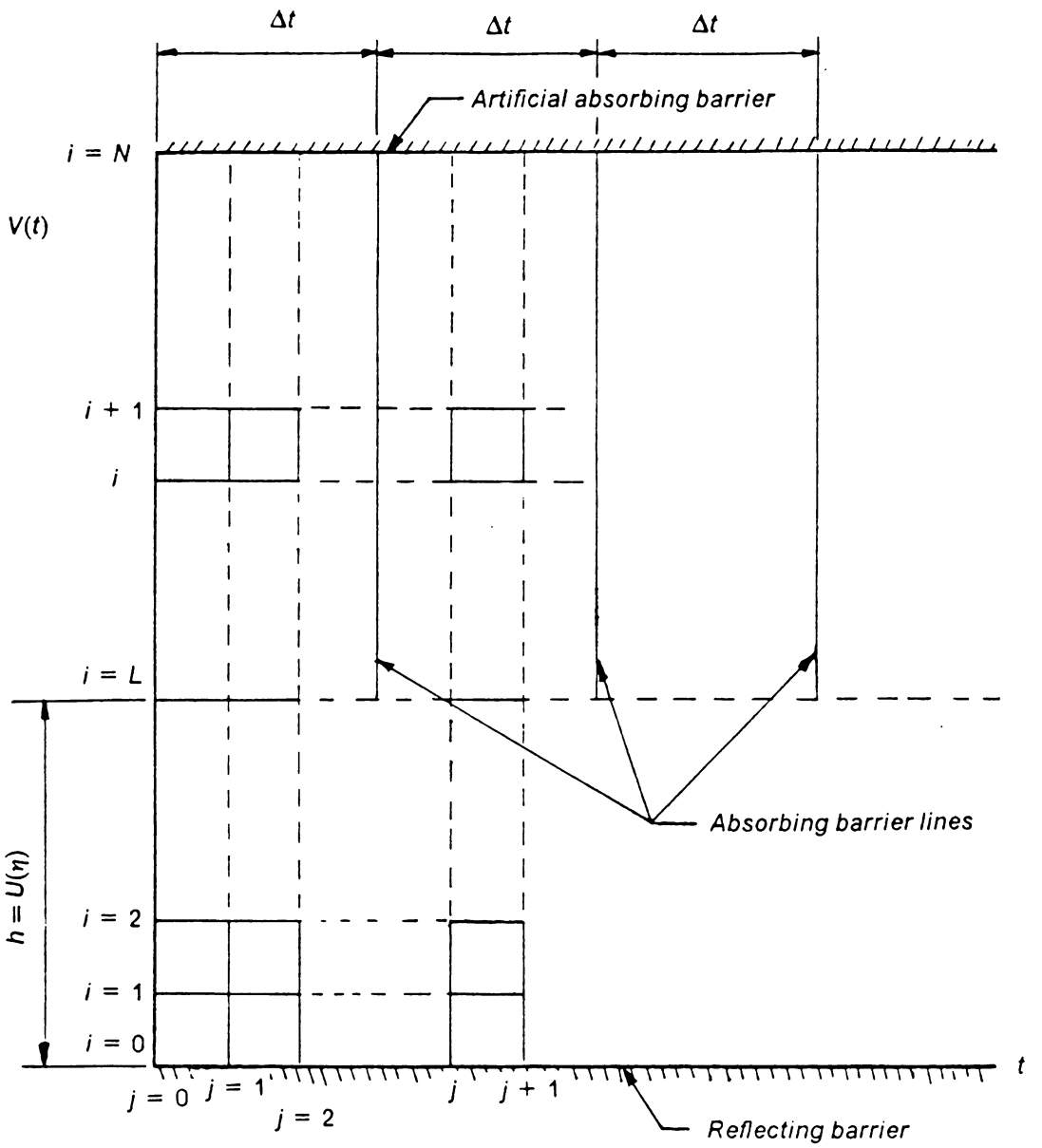

Figure 16. Rectangular mesh of points for the finite difference method.

Table 4.1

Effect of V_{max} on the Mean Time to First Snap-Through
($\lambda = 5.0$, $\beta = 0.20$, $\Phi_o = 5.0$, $\Delta t = 0.1673$, $\delta\tau = 0.001673$)

δv	0.0866	0.0433
V_{max}/h	$\bar{T}$	$\bar{T}$
3	0.4702	0.4543
4	0.3431	0.3337
5	0.2884	0.2814
6	0.2603	0.2547
7	0.2447	0.2398

Table 4.2

Effect of $\delta\tau$ and δv on the Mean Time to First Snap-Through
($\lambda = 5.0,\ \beta = 0.20,\ \Phi_o = 5.0, \Delta t = 0.1673,\ V_{max} = 5h$)

δv	0.0866	0.0433	0.02165
$\delta\tau$	$\bar{T}$	$\bar{T}$	$\bar{T}$
0.01673	0.2943	0.2916	0.2908
0.003346	0.2895	0.2816	0.2799
0.001673	0.2883	0.2814	0.2777
0.0011153	0.2883	0.2814	0.2777

Table 4.3

Effect of Φ_o and β on the Mean Time to First Snap-Through
($\lambda = 5.0$, $\Delta t = 0.1673$, $V_{max} = 7h$, $\delta v = 0.0433$, $\delta\tau = 0.001673$)

β	0.2	1.0	2.0	5.0	10.0	20.0
Φ_o	$\bar{T}$	$\bar{T}$	$\bar{T}$	$\bar{T}$	$\bar{T}$	$\bar{T}$
0.5	1.5002	2.0423	3.3311	31.3570		
1.0	0.7944	0.9343	1.1770	2.9214	25.9491	
3.0	0.3207	0.3422	0.3738	0.5089	0.9485	4.3174
5.0	0.2398	0.2479	0.2601	0.3118	0.4598	1.1311

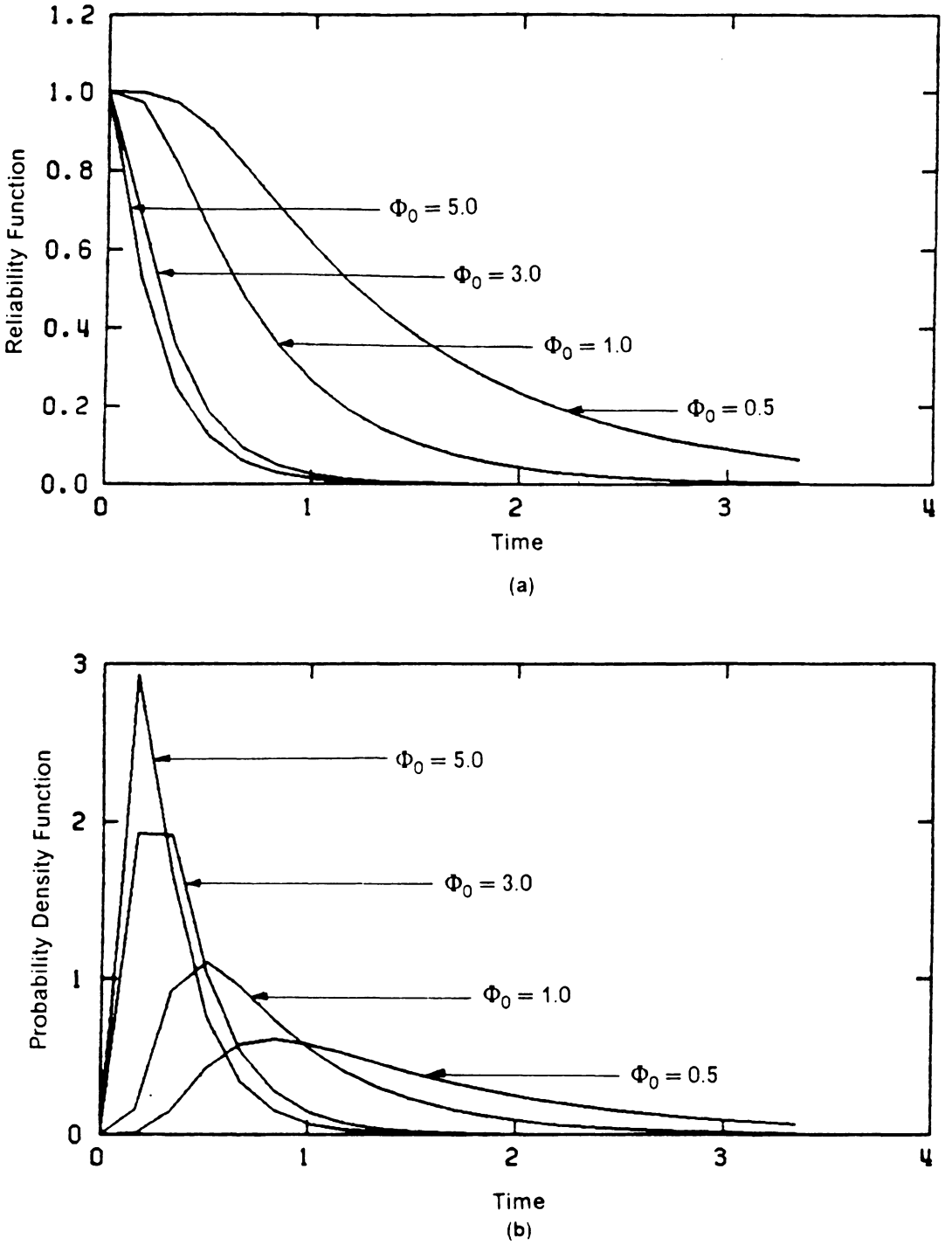

Figure 17. **Probability distribution of the first-passage failure for various values of load intensity:** $\lambda = 5.0$, $\beta = 0.2$ (a). reliability function, (b). probability density function

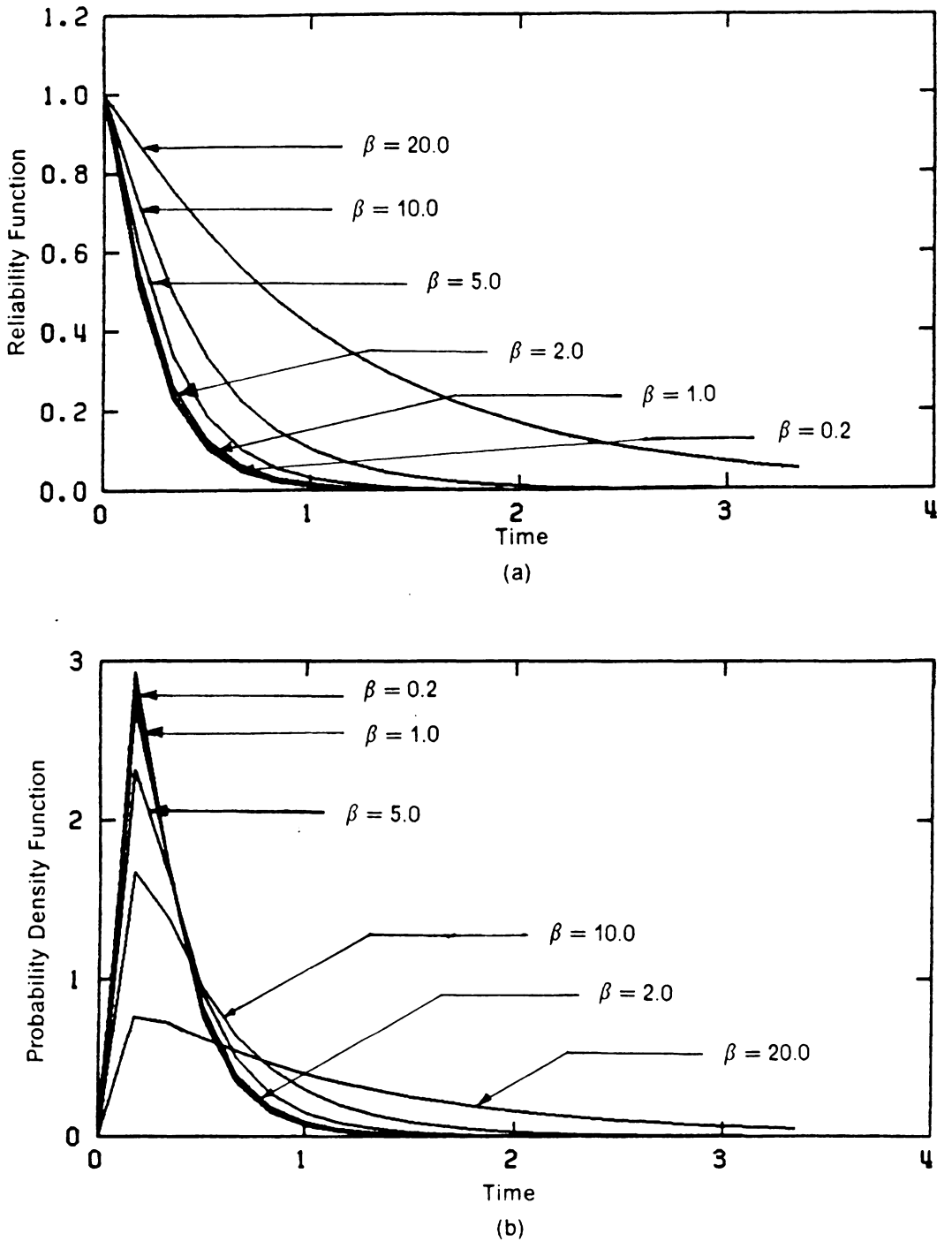

Figure 18. Probability distribution of the first-passage failure for various values of damping coefficient: $\lambda = 5.0$, $\Phi_o = 5.0$ (a). reliability function, (b). probability density function

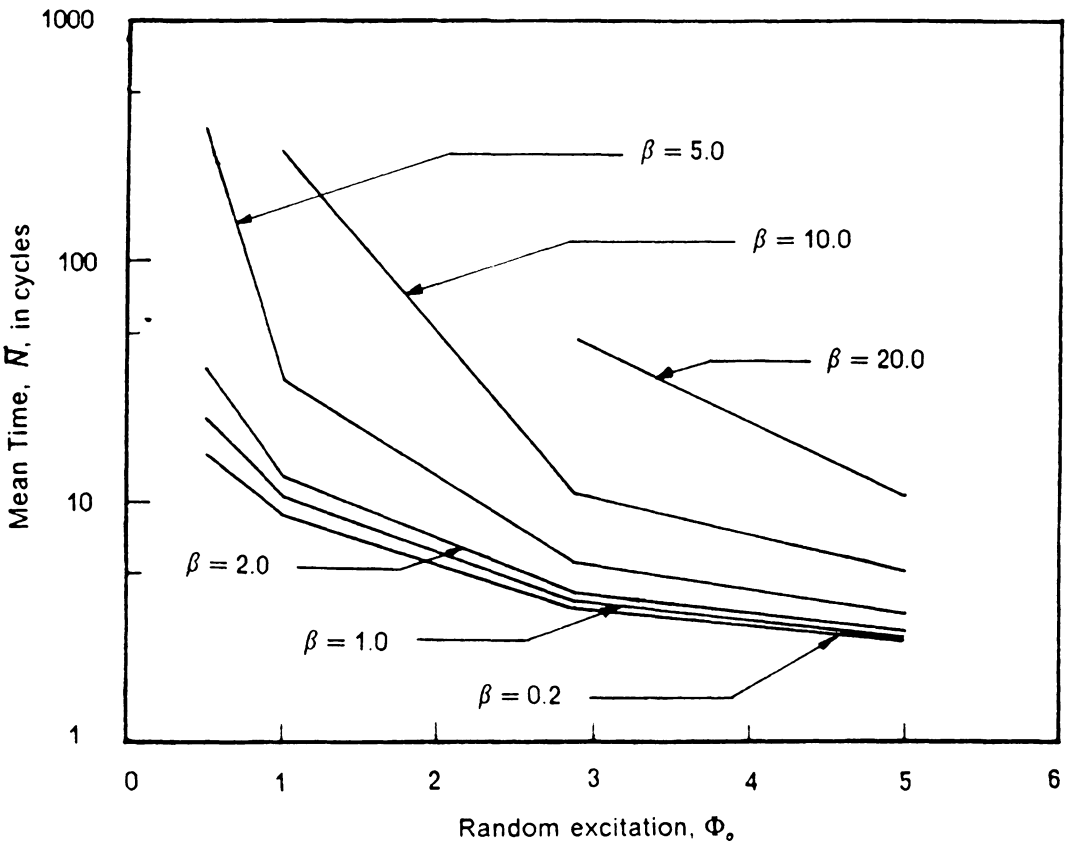

Figure 19. Variation of the mean time to first snap-through

Chapter V

Monte Carlo Simulation Method

5.1 General

Due to the recent development of fast digital computers, simulation methods have been extensively applied to various engineering problems, including nonlinear random vibrations. One advantage of the simulation methods is that they are generally applicable for all problems. In structural engineering problems where some parameters are random variables, analytical solution procedures are usually either inefficient or unavailable. Mostly, these problems are nonlinear problems involving dynamic analyses and damage accumulation. Furthermore, analytical solutions to these problems are difficult to obtain due to the fact that in many cases there is insufficient statistical information from physical experiments, and there is also considerable uncertainty in the parameters. As a result, the use of simulation techniques has been widely accepted. In many cases, simulation is used to compare and verify the results of proposed analytical approximation techniques.

The simulation methods involve a repeated sampling of the random quantities, and the problems are solved numerically many times to obtain a statistical sample of responses. A large number of observations of the event of interest must be collected for the simulation results to be reliable. Therefore, simulation techniques are sometimes very expensive and time-consuming.

In nonlinear random vibrations of a structure, parameters in a governing equation of motion are random variables. The corresponding response of the structure is also characterized by a random process. The random parameters cannot be represented by analytical functions of time, but they are usually described by their mean values and autocorrelation functions or equivalently by their spectral density functions [39,63]. The response of a structure cannot be expressed by an analytical function of time, but its statistical properties can be determined using a Monte Carlo simulation method.

The response of a shallow arch subjected to random excitations is investigated in this study. All parameters in the governing equation of motion are assumed to be deterministic, except that the loadings are random processes. These random loading processes may include various natural excitations such as earthquakes, sea waves, traffic loads, and winds. The simulation procedure can be summarized as follows:

1. An appropriate distribution model for random excitations must first be selected. The random excitations are assumed to act on an arch for a finite-time duration. This is reasonable for earthquake excitations, since it was shown that the durations of strong-motion earthquakes, obtained from 92 past earthquake records, are finite and range from 2.16 seconds to 66.54 seconds [52]. A mean value of the durations of those strong motions is also reported to be 20.8 seconds [52]. After the model of random excitations is selected, the simulation then proceeds by applying a large number of records of random excitations to the arch.

2. For each record of random excitation, the equation of motion becomes deterministic, and it can be solved numerically using known differential equation methods such as the Runge-Kutta method.

3. For each record of excitations, the response of a structure solved in step 2 is monitored. At the first time for which the amplitude of structural response exceeds a certain level, the structure is assumed to exit from the safe region and it becomes unstable. The simulation for this single record is terminated and the time is recorded. The time just described is called the *first-passage time* or the *time of first snap-through* of the arch under random excitations.

4. The simulation is carried out for a large number of excitation records, say 500. The number of occurrences of the first snap-through and the *time of first snap-through* are recorded. It is noted that for some records of excitations, snap-through may not occur during a given period, denoted by T. The period T also represents the time length of integration of step 2, and it is taken to be greater than the duration of the applied excitations. Time histories of the response process, or the length of integration, must be sufficiently long to prevent the overlooking of delayed snap-through that may occur after the applied loadings on the structure have been terminated.

5. From a large number of realizations of time of first snap-through, the statistical properties of the first-passage time can be estimated. These statistical properties may include mean value, variance, and higher moments.

6. Using the estimated statistics of the observed data from step 5, appropriate distribution models for the probability distribution of first-passage time may be selected. The selection procedure of the distribution model is described in Section 5.3.

5.2 Monte Carlo Simulation

The response of a shallow arch under random excitations is described by the system of Eq. (3.1). For the single-degree-of-freedom system, the equation of motion, expressed in dimensionless variables, is rewritten as

$$\begin{aligned} &\ddot{q}_1(t) + \beta\dot{q}_1(t) + \pi^4(1 + 2\lambda^2)q_1(t) - 3\sqrt{2}\,\pi^4\lambda q_1^2(t) \\ &\quad + 2\pi_4 q_1^3(t) = \sqrt{2}\,\pi^4\int_0^1 f(x,t)\sin\pi x\; dx \end{aligned} \tag{5.1}$$

where $q_1(t)$ is the generalized coordinate of the displacement of the arch and $\dot{q}_1(t)$ and $\ddot{q}_1(t)$ are its generalized velocity and acceleration, respectively. λ and β are, respectively, the initial arch rise parameter and the damping coefficient. The right-hand side of Eq. (5.1) is the random generalized force to be simulated. Let $f_1(t)$ be defined as

$$f_1(t) = \sqrt{2}\,\pi^4 \int_0^1 f(x,t) \sin \pi x \; dx \tag{5.2}$$

For simplicity, this study considers sinusoidal loading where $f(x,t)$ is represented by Eq. (3.33). The random generalized force then becomes independent of the spatial coordinate and is time-dependent only, and $f_1(t)$ becomes

$$f_1(t) = \frac{\sqrt{2}}{2}\pi^4 f(t) \tag{5.3}$$

The equation of motion becomes, as previously given by Eq. (3.34),

$$\ddot{q}_1(t) + \beta\dot{q}_1(t) + \pi^4(1 + 2\lambda^2)q_1(t) - 3\sqrt{2}\,\pi^4\lambda q_1^2(t) + 2\pi_4 q_1^3(t) = \frac{\sqrt{2}}{2}\pi^4 f(t) \tag{5.4}$$

The Monte Carlo simulation method is used to solve the nonlinear system described by Eq. (5.4). In this case, the time-dependent excitation $f(t)$ is assumed to be a stationary white-noise process. The white noise with constant spectral density was used earlier to represent strong-motion earthquakes [13]. The random load $f(t)$ is assumed to have a mean value of zero, and it is completely described by its autocorrelation function

$$R_f(\tau) = E[f(t)f(t+\tau)] = 2\pi\Phi_o\delta(\tau) \tag{5.5}$$

where Φ_o is the intensity of white noise, δ is the Dirac delta function, and $E[.]$ is the expectation.

5.2.1 Method of Simulating the Stationary White Noise

The random excitation $f(t)$ is to be simulated by the random function $\bar{f}(t)$. The procedure used to generate the random excitation, $\bar{f}(t)$, having a stationary white-noise process is described in the literature [7,17]. The following procedure is used in this study. First, a series

of psuedo random numbers, $r_1, \ldots, r_n$, having a Gaussian distribution with a mean of zero and variance of unity is generated using IMSL subroutine GGNML [43]. The random numbers, $r_i, \ldots, r_n$, are statistically independent random variables. A record of sample functions is then established by assigning the values of $r_1, \ldots, r_n$ to n successive ordinates spaced at equal intervals Δt along a time abscissa as shown in Fig. 20. The time interval Δt must be sufficiently short. A linear variation of ordinates is assumed over each interval, and the initial ordinates are taken to be zero at time $t = 0$.

The intensity of the random process described above is transformed to a white-noise process $\bar{f}(t)$ by multiplying each ordinate r_i by the normalizing factor $(2\pi\Phi_o/\Delta t)^{1/2}$. It is reported that this function $\bar{f}(t)$ is flat to within 5 percent error for $\omega_o \Delta t < 0.57$, where ω_o is the natural frequency of the corresponding linear system of Eq. (5.4) [7,17]. It is also shown that as Δt approaches zero, the autocorrelation function of the simulated process $\bar{f}(t)$ approaches the autocorrelation function of the white noise [7,17], as described below:

$$\underset{\Delta t \to 0}{LIMIT} \; R_{\bar{f}}(\tau) = R_f(\tau) = 2\pi\Phi_o\delta(\tau) \tag{5.6}$$

Therefore, the random process $\bar{f}(t)$ becomes a stationary white-noise process of intensity Φ_o over the infinite frequency range $-\infty < \omega_o < \infty$.

5.2.2 The Time Step

For convenience of computation, the interval Δt for each independently arriving Gaussian pulse is assumed to be equally spaced and is taken to be equal to the time step of the numerical integration of the equation of motion in step 2 of the simulation procedure.

The equation of motion is solved numerically for each excitation record using the IMSL subroutine DVERK [39,42]. DVERK solves a system of first order ordinary differential equations of the form $dy/dx = f(x,y)$. It calculates approximate solutions of the system by both

fifth and sixth order Runge-Kutta method and then compares the answers to determine the step size, Δt. It is very accurate and easy to use, but it is expensive. In order to obtain reliable results, the time step Δt must be considerably smaller than the natural period of vibration of the structure. The time step Δt equal to $\tau/20$, where τ is the natural period of vibration of the structure, is found to give reliable results for the case of nonlinear vibration of a shallow arch [65].

5.2.3 Numerical Results

Numerical results are obtained for the case of $\lambda = 5.00$ and $\beta = 0.20$. In this case the natural period of vibration of the arch is approximately 0.089. Consequently, the time step of integration $\Delta t = 0.0045$ will be used.

Five hundred records of simulated input process $\bar{f}(t)$ are generated for use in simulations. The time duration of the simulated random process is finite and is taken to be 1.35 or $300\Delta t$. However, the time length of integration of Eq. (5.4) is carried out to 1.8 or $400\Delta t$, to insure that the response $q_1(t)$ of the arch does not get larger and to prevent the overlooking of delayed snap-through. Complete time histories of the response $q_1(t)$ for the system of Eq. (5.4) when subjected separately to each of the 500 input records are determined. For a single random input, time histories of the generalized random force and the displacement of the arch are illustrated in Figs. 21 and 22, respectively.

The vibration of the arch is assumed to start from rest. At time zero, the initial response of the arch is also zero, as given by Eqs. (3.23) and (3.24). The random loads are applied to the arch starting from time equal to zero, and the arch begins to vibrate about its initial stable position. The amplitude of vibration tends to increase with increasing time if the intensity of the random loads is sufficiently high. The arch is assumed to fail when the amplitude of the response $q_1(t)$ reaches and passes a critical threshold level. The critical level is taken to be $\lambda/\sqrt{2}$. The time at which the amplitude of the response is equal to or greater than the critical

level is noted in each input. The time just described, denoted by t, is called the *time of first snap-through* of a shallow arch. The ranked data of the time of first snap-through, for example, is given in Table 5.1 for the white noise intensity of 0.50.

5.2.4 Estimation of Statistical Properties of the Time, t

The time of first snap-through, t, recorded for each input simulation is a random variable. The probability distribution of a random variable t can be established from its statistical properties. The statistical properties of interest may include the mean value, variance, skewness coefficient, and higher moments. These properties can be used to select the appropriate distribution model for the probability distribution of the time of first snap-through. The selection of the distribution models is discussed in Section 5.3.

The mean and variance of a random sample of size n, namely $t_1, \ldots, t_n$, can be, respectively, determined as follows [4]:

$$\bar{t} = \frac{1}{n}\sum_{i=1}^{n} t_i, \tag{5.7}$$

$$s^2 = \frac{1}{n-1}\left[\sum_{i=1}^{n} t_i^2 - n\bar{t}^2\right] \tag{5.8}$$

The higher moments can be obtained using the following expressions [32]:

$$m_2 = \frac{\sum_{i=1}^{n}(t_i - \bar{t})^2}{n}, \tag{5.9}$$

$$m_3 = \frac{\sum_{i=1}^{n}(t_i - \bar{t})^3}{n}, \tag{5.10}$$

$$m_4 = \frac{\sum_{i=1}^{n}(t_i - \bar{t})^4}{n} \tag{5.11}$$

For a given set of samples for which the estimated moments are represented by m_2, m_3, and m_4, as given by Eqs. (5.9), (5.10), and (5.11), the skewness coefficient and the relative measure of the forth moment about the mean, also called kurtosis, of a random variable are estimated by $\sqrt{b_1}$ and b_2, respectively, and they are

$$\sqrt{b_1} = \frac{m_3}{(m_2)^{3/2}}, \tag{5.12}$$

$$b_2 = \frac{m_4}{(m_2)^2} \tag{5.13}$$

Numerical results of Monte Carlo simulation are obtained for the cases of white noise intensity equal to 0.5, 1.0, 3.0, and 5.0, and are given in Table 5.2.

5.3 Selection of Probability Models

This section deals with probability distributions for continuous random variables which represent engineering phenomena. The random variable of interest is the time of first snap-through of a shallow arch under random excitations, which is denoted by t. t is a continuous random variable, and a set of t samples of size n is obtained from the method of Monte Carlo simulation. From these samples, a probability model is selected to describe the distribution

of t. The probability models considered are the gamma distribution, the lognormal distribution, the Weibull distribution, and the beta distribution.

The choice of a probability distribution to describe a physical system is generally motivated by an understanding of the nature of the underlying phenomenon and is verified by the available data. First, a model is selected, and then its parameters are evaluated. These parameters are related to the location, scale, and shape of the distribution. Finally, the adequacy of the selected model is tested and it is verified that the model can appropriately represent and predict the behavior of the system.

The initial selection of a statistical model based on the given data, which is the time of the first snap-through of a shallow arch, is performed by visually inspecting histograms of the given data. Two types of histogram may be used: a frequency histogram and a cumulative histogram. The shape of the histogram is used to choose a few trial probability models that have similar shapes and may fit the histogram. After parameters of these statistical models are estimated, other techniques such as statistical tests must be used to assess the accuracy of the selected models. These assessments are important, especially in this case when the model is to be used for prediction. Two statistical tests are used in this study: the Chi-Square goodness-of-fit test and the Kolmogorov-Smirnov goodness-of-fit test. These statistical tests are used to select the valid model and to disregard the ones that fail the tests. The statistical tests provide a probability framework which is used to evaluate the adequacy of the selected model. Although many models may appear appropriate within the range of the given data, they may provide incorrect results in the range for which predictions are desired.

5.3.1 Estimation of Parameters

Given a set of sample values or observed data, two classical methods for estimating parameters for an assumed theoretical probability distribution are the method of moments and the method of maximum likelihood [4].

5.3.1.1 The Method of Moments

It will be shown later that the parameters of a probability distribution are related to the mean and variance of a random variable. For example, the parameters of the gamma distribution, γ and β , are related to the mean and variance as follows:

$$E[t] = \mu_t = \beta\gamma \tag{5.14}$$

$$VAR[t] = \sigma_t^2 = \beta^2\gamma \tag{5.15}$$

Therefore, an estimate of the parameters of the distribution can be obtained by estimating the mean and variance (or higher moments if necessary) of the given data and then relating them to the parameters of the distributions of interest.

Define $\sqrt{\beta_1}$ and β_2 as a skewness coefficient and kurtosis of a distribution, respectively. $\sqrt{\beta_1}$ and β_2 of a distribution are related to the second, third, and fourth moments, which are denoted by μ_2, μ_3, and μ_4 , respectively, as follows:

$$\sqrt{\beta_1} = \frac{\mu_3}{(\mu_2)^{3/2}} \tag{5.16}$$

$$\beta_2 = \frac{\mu_4}{(\mu_2)^2} \tag{5.17}$$

The desired parameters of a probability distribution can be determined from the above relationships.

5.3.1.2 The Method of Maximum Likelihood

A procedure for estimating parameters of a distribution is the maximum likelihood method [4], in which the likelihood function of observed data is established according to the

probability distribution. For a probability distribution of two or more parameters, the likelihood function can be expressed as

$$L(t_1, \ldots, t_n; \theta_1, \ldots, \theta_m) = \prod_{i=1}^{n} f(t_i; \theta_1, \ldots, \theta_m) \tag{5.18}$$

where $\theta_1, \ldots, \theta_m$ are m parameters of a distribution to be determined and t is a random variable. The maximum likelihood estimators can be obtained by solving simultaneously the following set of equations:

$$\frac{\partial L(t_1, \ldots, t_n; \theta_1, \ldots, \theta_m)}{\partial \theta_j} = 0, \quad j = 1, \ldots, m. \tag{5.19}$$

It is noted that the maximum likelihood method is often considered to be the best estimate for parameters of a distribution when the sample size n is large [4,33].

5.3.2 The Gamma Distribution

The gamma distribution of a random variable t is described by the probability density function

$$f(t; \gamma, \beta) = \frac{t^{\gamma-1} e^{-t/\beta}}{\beta^{\gamma} \Gamma(\gamma)}, \quad \text{for } t \geq 0, \quad \gamma > 0, \quad \text{and } \beta > 0. \tag{5.20}$$

where $\Gamma(\gamma)$ is the gamma function and is defined as

$$\Gamma(\gamma) = \int_0^{\infty} t^{\gamma-1} e^{-t} dt \tag{5.21}$$

and $\Gamma(\gamma) = (\gamma-1)!$ when γ is a positive integer.

A wide variety of shapes can be obtained for the gamma distribution. In particular, the distribution is a reversed J curve for $\gamma \leq 1$, and it is single peaked, with the peak at $t = (\gamma - 1)/\beta$, for $\gamma > 1$. Consequently, γ and β are shape and scale parameters, respectively.

The gamma distribution is considered to be the natural candidate for a time-to-failure model since it can diversely represent random variables with values from zero to infinity [32]. Many phenomena that cannot be justified theoretically as gamma variates have been found to be empirically well approximated by this model [32]. The distribution of family income and the time-to-failure for capacitors are two examples. This model is also used often in Bayesian analyses as a prior model to describe initial uncertainty concerning the rate of occurrence of some process, such as the failure rate of a system.

The cumulative gamma distribution is given by

$$F(t; \gamma, \beta) = \begin{cases} \dfrac{1}{\beta^{\gamma}\Gamma(\gamma)} \displaystyle\int_0^t t^{\gamma-1} e^{-t/\beta}\, dt, & \text{for } t > 0 \\ 0 \text{ for } t \leq 0 \end{cases} \tag{5.22}$$

which is also known as the incomplete gamma function. The probability associated with the gamma distribution can be determined conveniently using the IMSL subroutine MDGAM [45].

The gamma distribution approaches a normal distribution as γ increases [32], which can be proved by a central limit theorem. The skewness of the gamma distribution also goes to zero with increasing γ , indicating that this model becomes symmetrical for large γ.

Estimation of the Parameters of the Gamma Distribution

(a) The Method of Moments: This method is simpler but gives less precise estimates. The statistical properties of the gamma distribution, i.e., the mean value and the variance, are given by Eqs. (5.14) and (5.15). The skewness coefficient is described by [32]

$$\sqrt{\beta_1} = \frac{2}{\sqrt{\gamma}} \tag{5.23}$$

To estimate the parameters of a gamma distribution, $\tilde{\gamma}$ and $\tilde{\beta}$, the following equations are solved:

$$\tilde{\beta}\,\tilde{\gamma} = \bar{t} \tag{5.24}$$

$$\tilde{\beta}^2\,\tilde{\gamma} = s^2 \tag{5.25}$$

where $\bar{t}$ and s^2 are, respectively, the sample mean and sample variance of the observed data as defined by Eqs. (5.7) and (5.8).

(b) The Method of Maximum Likelihood : For a set of observed data t_i , i = 1 ,..., n , and the probability density function of the gamma distribution in the form of Eq. (5.20), the maximum likelihood estimators, $\tilde{\gamma}$ and $\tilde{\beta}$, are given by [53]

$$\frac{1}{n}\sum_{i=1}^{n}\log t_i = \log\tilde{\beta} + \Psi(\tilde{\gamma}) \tag{5.26}$$

$$\bar{t} = \tilde{\beta}\,\tilde{\gamma} \tag{5.27}$$

$\psi(\gamma)$ is called the Digamma function and is defined as [1]

$$\Psi(\gamma) = \frac{d}{d\gamma}[\ln\Gamma(\gamma)] \tag{5.28}$$

Eqs. (5.26) and (5.27) can be used to estimate $\tilde{\gamma}$ and $\tilde{\beta}$. This study uses the approximate solution suggested by Greenwood and Durand [29,53]. The error from this solution is very small.

5.3.3 The Lognormal Distribution

The lognormal distribution is the model for a random variable whose logarithm follows the normal distribution with parameters μ and ζ . The probability density function of the lognormal variate t is

$$f(t;\mu,\zeta) = \frac{1}{\zeta t\sqrt{2\pi}} \exp\left[-\frac{1}{2\zeta^2}(\ln t-\mu)^2\right]; \quad \text{for } t>0, -\infty<\mu<\infty, \text{ and } \zeta>0 \tag{5.29}$$

The lognormal distribution possesses many different shapes for non-negative variates: it is skewed to the right, and the degree of skewness increases with increasing ζ. For this distribution, μ and ζ are scale and shape parameters, respectively.

The lognormal distribution has been used in many applications for processes in which the observed value is a random proportion of the previous value. This model has random variables from zero to infinity, like the gamma distribution, so it is a natural candidate for the time-to-failure model.

Estimation of the Parameters of the Lognormal Distribution

(a) The Method of Moments: The parameters of the lognormal distribution are related to its mean value and variance as follows [4]:

$$E[t] = \mu_t = \exp\left[\mu+\frac{1}{2}\zeta^2\right] \tag{5.30}$$

$$\begin{aligned} VAR[t] &= \ln\mu-\frac{1}{2}\zeta^2 \\ &= E^2[t]\left[e^{\zeta^2}-1\right] \end{aligned} \tag{5.31}$$

The estimators, $\tilde{\mu}$ and $\tilde{\zeta}$, of parameters of the lognormal distribution, μ and ζ , are evaluated by solving the following equations:

$$\bar{t} = \exp\left[\tilde{\mu} + \frac{1}{2}\tilde{\zeta}^2\right], \tag{5.32}$$

$$\frac{s^2}{\bar{t}^2} = e^{\tilde{\zeta}^2} - 1 \tag{5.33}$$

where $\bar{t}$ and s^2 are defined for the random variable t by Eqs. (5.7) and (5.8), respectively.

(b) The Method of Maximum Likelihood: Define $y_i = \log t_i$, where t_i, i = 1 ,..., n , are random samples of size n. The maximum likelihood estimators, $\tilde{\mu}$ and $\tilde{\zeta}$, of parameters of the lognormal distribution, μ and ζ , respectively, are [53]

$$\tilde{\mu} = \bar{y} = \frac{1}{n}\sum_{i=1}^{n} y_i, \tag{5.34}$$

$$\tilde{\zeta} = \left[\frac{1}{(n-1)}\sum_{i=1}^{n}(y_i - \bar{y})^2\right]^{\frac{1}{2}} \tag{5.35}$$

5.3.4 The Weibull Distribution

The probability density function of the Weibull distribution of a random variable t is

$$f(t; \alpha, \eta) = \begin{cases} \frac{\alpha}{\eta}\left(\frac{t}{\eta}\right)^{\alpha-1} \exp\left[-\left(\frac{t}{\eta}\right)^{\alpha}\right]; & t \geq 0, \alpha > 0, \eta > 0, \\ 0 & \textit{elsewhere.} \end{cases} \tag{5.36}$$

where η and α are scale and shape parameters, respectively.

The mean, variance, and skewness coefficient of the Weibull distribution are defined as follows:

$$E[t] = \eta\,\Gamma(1 + \frac{1}{\alpha}) \tag{5.37}$$

$$VAR[t] = \eta^2\left[\Gamma(1+2/\alpha) - \Gamma^2(1+1/\alpha)\right], \tag{5.38}$$

$$\sqrt{\beta_1} = \frac{\Gamma(1+3/\alpha) + 3\Gamma(1+2/\alpha)\,\Gamma(1+1/\alpha) + 2\Gamma^2(1+1/\alpha)}{\left[\Gamma(1+2/\alpha) - \Gamma^2(1+1/\alpha)\right]^{3/2}} \tag{5.39}$$

The probability associated with the Weibull distribution is easily evaluated from the cumulative distribution function

$$F(t;\alpha,\eta) = 1 - \exp\left[-\left(\frac{t}{\eta}\right)^{\alpha}\right];\quad t \geq 0 \tag{5.40}$$

The Weibull distribution has been frequently suggested as a time-to-failure model on empirical grounds and some satisfactory results have been obtained [32].

Estimation of Parameters of Weibull Distribution: Estimation of parameters of the Weibull distribution from given random data generally involves the solution of nonlinear equations [31,55]. Only the method of maximum likelihood is discussed and used in this study. Given a set of independent random variables of size n, say t_i, i = 1 ,...., n , the maximum likelihood estimators, $\tilde{\alpha}$ and $\tilde{\eta}$, of the parameters α and η , respectively, of the Weibull distribution can be obtained by simultaneously solving the following equations:

$$\tilde{\eta} = \left[\frac{1}{n}\sum_{i=1}^{n} t_i^{\tilde{\alpha}}\right]^{1/\tilde{\alpha}}, \tag{5.41}$$

$$\tilde{\alpha} = \left[\frac{\sum_{i=1}^{n} t_i^{\tilde{\alpha}} \log t_i}{\sum_{i=1}^{n} t_i^{\tilde{\alpha}}} - \frac{1}{n}\sum_{i=1}^{n} \log t_i\right]^{-1} \tag{5.42}$$

$\tilde{\alpha}$ is estimated from Eq. (5.42) and is then used in Eq. (5.41) to determine $\tilde{\eta}$. Eq. (5.42) can be solved iteratively.

5.3.5 The Beta Distribution

A random variate t having the beta distribution is described by the probability density function [4]

$$f(t; q, r) = \frac{1}{B(q,r)} \frac{(t-A)^{q-1} (B-t)^{r-1}}{(B-A)^{q+r+1}}; \quad A \le t \le B \tag{5.43}$$

in which q and r are parameters of the beta distribution. B(q,r) is the beta function and is defined as

$$B(q,r) = \int_0^1 t^{q-1} (1-t)^{r-1} \, dt \tag{5.44}$$

B(q,r) is related to the gamma function as follows:

$$B(q,r) = \frac{\Gamma(q) \, \Gamma(r)}{\Gamma(q+r)} \tag{5.45}$$

A and B are the lower and upper bounds of the distribution, respectively.

The mean, variance, and skewness coefficient of the beta distribution are related to its parameters as follows:

$$E[t] = A + \frac{q}{q+r} (B-A), \tag{5.46}$$

$$VAR[t] = \frac{qr}{(q+r)^2 (q+r+1)} (B-A)^2, \tag{5.47}$$

$$\sqrt{\beta_1} = \frac{2(r-q)}{(q+r)(q+r+2)\sqrt{VAR[t]}} \tag{5.48}$$

The beta distribution is a useful model for random variables whose values are limited to a finite range. Both parameters of the beta distribution, q and r, are considered to be shape parameters [32], and various shapes of the beta distribution are observed for different choices of q and r. It is noted that when q and r are less than 1, the distribution is single peaked with the peak at $t = (q-1)/(q+r-2)$; when q and $r < 1$, the distribution is U shaped; when $q < 1$ and $r \geq 1$, the distribution is reversed J shaped; and finally when $q = r = 1$, the distribution is symmetric and uniformly distributed [32].

The standard beta distribution, with t limited to a finite interval from 0 to 1 (or A = 0, and B = 1) is given by [4]

$$f(t;q,r) = \frac{1}{B(q,r)} t^{q-1}(1-t)^{r-1}; \quad 0 \leq t \leq 1 \tag{5.49}$$

The probability associated with the beta distribution can be evaluated in terms of the incomplete beta function defined by Eq. (5.45). For instance, the probability between $T = t_1$ and $T = t_2$ can be evaluated by

$$P(t_1 \leq T \leq t_2) = \frac{1}{B(q,r)} [B_u(q,r) - B_v(q,r)] \tag{5.50}$$

$B_u(q,r)$ and $B_v(q,r)$ are the incomplete beta functions, where $u = (t_1 - A)/(B-A)$ and $v = (t_2 - A)/(B-A)$. The probability associated with the beta distribution can be evaluated using the IMSL subroutine MDBETA [44].

Estimation of Parameters of Beta Distribution: The estimation of the parameters of the beta distribution by the method of maximum likelihood is complicated and somewhat difficult. However, the method of moments is simpler and the error is small when the sample size is

large [32]. Therefore, the estimated parameters, $\tilde{q}$ and $\tilde{r}$, of the beta distribution can be obtained using the following expressions:

$$\tilde{r} = \frac{q(1-y)}{y}, \tag{5.51}$$

$$\tilde{q} = \frac{y[y(1-y)-z]}{z} \tag{5.52}$$

where $y = (\bar{t} - A)/(B - A)$ and $z = (s^2)/(B - A)^2$, and $\bar{t}$ and s^2, respectively, are the sample mean and variance as defined by Eqs. (5.7) and (5.8).

5.3.6 Testing the Validity of the Assumed Distribution

After a theoretical distribution has been assumed to represent random data of a physical system, perhaps determined on the basis of the general shape of the histogram or on the basis of the data plotted on the probability paper, the validity of the assumed distribution must then be verified statistically by goodness-of fit tests. Two types of goodness-of-fit tests are used in this study: the chi-square test and the Kolmogorov-Smirnov test.

There are four sets of sample data for four study cases. The sample data are random variables t_i, $i = 1, \ldots, n$, where the random variable t is the time of first snap-through of a shallow arch subjected to stationary white-noise excitations. The white noise intensity, denoted by Φ_o, for the four cases is 0.5, 1.0, 3.0, and 5.0.

Histograms of the observed data are presented in Figs. 23 to 26. These histograms show the general shapes of the distribution. The histograms for the first case, where $\Phi_o = 0.5$, compared with plots of the probability density function of the gamma distribution, the lognormal distribution, the Weibull distribution, and the beta distribution are shown in Figs. 23(a), 23(b), 23(c), and 23(d), respectively. The histograms for the second case, the third case,

and the fourth case, where $\Phi_o = 1.0,\ 3.0,$ and 5.0, respectively, compared with plots of the same probability density functions are shown in Figs. 24, 25, and 26.

Tables 5.3, 5.4, 5.5, and 5.6 present the results for the four cases considered in the simulation study. These tables also summarize results of the selection of the probability distribution model for the random variate t. Results include the statistical tests (the chi-square value and the Kolmogorov-Smirnov value) and the statistical properties of each assumed theoretical distribution (mean value, variance, skewness, and kurtosis). These are compared to the estimated statistical properties of the observed data.

5.3.6.1 The Chi-Square Goodness-of-Fit Test

The general procedure of the chi-square goodness-of-fit test is as follows: The observed data are first grouped into frequency intervals and compared to the expected number of observations based on the proposed theoretical distribution. If the proposed model is not correct, the test statistic will tend to exceed a chi-square variate. Therefore, the percentiles of the chi-square distribution may be used to verify whether the assumed model is appropriate for the observed data. Details of the chi-square test and procedure are available in Ref. [32].

The test statistic, χ^2, is computed using

$$\chi^2 = \sum_{i=1}^{k} \frac{(M_i - e_i)^2}{e_i} \tag{5.53}$$

where k is the number of intervals used to divide the whole data, and M_i and e_i are, respectively, the observed frequencies from the data and the expected frequencies from the proposed distribution in each interval. After the chi-square value is obtained , it is compared with the tabulated percentiles of a chi-square variate such as the ones given in Table A.3 of Ref. [4], using f = k-r-1 degrees of freedom where r is the number of parameters that were esti-

mated for the proposed model. A high value of χ^2 implies that the observed data contradicts the proposed probability model.

Results of the chi-square test are summarized as follows:

(a) Case 1 : The beta distribution is the best model in this case and is an acceptable model at the significance level of $\alpha - 1 = 0.1$. The lognormal distribution must be rejected. The Weibull distribution and the gamma distribution do not represent the data well, especially at the tail of the largest value; however, both models are acceptable at the significance level of 0.025 and 0.001, respectively.

(b) Case 2 : The beta distribution must be rejected since it does poorly in each interval. The lognormal and Weibull distributions represent the data better than the beta distribution; however, they are especially poor at the tail of the largest value. The gamma distribution is the best model for this case and is acceptable at the significance level of 0.1.

(c) Case 3 : The lognormal and gamma distribution fit the data very well, and both are acceptable at the significance level of 0.05 and 0.1, respectively. The gamma distribution deviates from the data a little at the tail, but the deviation is insignificant. The Weibull and beta distributions yield unacceptable results.

(d) Case 4 : The lognormal and gamma distributions fit the data very well, and both are acceptable at the significance level of 0.1 and 0.025, respectively. The Weibull and beta distributions yield unacceptable results.

5.3.6.2 The Kolmogorov-Smirnov Goodness-of-Fit Test

The test statistic obtained from the Kolmogorov-Smirnov test is denoted by D_n, or the KS value. The procedure for the calculation of the KS statistic is well known [30], and is summarized as follows: Given a random sample of n observations, $t_1, \ldots, t_n$, the KS value is determined using

$$D_n = \max_t \left| F^*(t) - S_n(t) \right| \tag{5.54}$$

where $S_n(t)$ is the sample cumulative distribution function and $F^*(t)$ is the cumulative distribution function computed with parameters estimated from the sample.

For a specified significant level α, the Kolmogorov-Smirnov test compares the value of D_n with the critical value D_n^α, which is defined as follows [4]:

$$Probability\,(D_n < D_n^\alpha) \;=\; 1 - \alpha$$

If the value of D_n exceeds the critical value D_n^α given in the table, such as Table A.4 in Ref. [4], one rejects the hypothesis that the observations are from the proposed distribution; otherwise, the proposed distribution is acceptable at the specified significant level α. It is noted in Ref. [30] that if parameters of a proposed distribution are estimated from the sample to provide a control distribution against which to test the sample, then the KS test using standard tables is no longer applicable. That is, standard tables for the non-parametric test available in the text, such as the one mentioned previously, should not be used when parameters are estimated from the data.

The critical values of D_n^α in the Kolmogorov-Smirnov test, taken from Table A.4 of Ref. [4], for large n and for $\alpha =$ 0.20, 0.10, 0.05, and 0.01, are $1.07/\sqrt{n}$, $1.22/\sqrt{n}$, $1.36/\sqrt{n}$, and $1.63/\sqrt{n}$, respectively.

Results of the Kolmogorov-Smirnov test are summarized as follows:

(a) Case 1 : The size of the data, n, is equal to 284 for this case, and the shape parameter for the gamma distribution is estimated to be 7.83. The critical values of D_n^α are listed in Table 5.8. According to the computed KS values as given in Table 5.3, the beta and Weibull distributions are suitable in this case. The gamma and lognormal distributions are not acceptable at any significance level, except when the standard tables for critical KS value are used. Note that an asterisk in Table 5.8 indicates the acceptable significance level of the model.

(b) Case 2 : For this case, n = 435, and the shape parameter for the gamma distribution is estimated to be 4.73. The critical values of D_n^α are listed in Table 5.8. According to the computed KS values as given in Table 5.4, all proposed models except the Weibull distribution are acceptable.

(b) Case 3 : For this case, n = 496, and the shape parameter for the gamma distribution is estimated to be 2.95. The values of D_n^* are listed in Table 5.8. According to the computed KS values as given in Table 5.5, all proposed models except the Weibull distribution are acceptable. However, lognormal and gamma distributions are the best models, and the beta distribution is questionable.

(b) Case 4 : For this case, n = 500, and the shape parameter for the gamma distribution is estimated to be 2.94. The values of D_n^* are listed in Table 5.8. According to the computed KS values as given in Table 5.6, the lognormal distribution is acceptable at the significance level of 0.10. The other models yield unacceptable results.

5.3.7 Summary

This section dealt with the selection of the distribution model for use in describing the time of the first snap-through of a shallow arch under random excitations. First, the proposed models, which are the lognormal distribution, the gamma distribution, the Weibull distribution, and the beta distribution, were selected based on a visual comparison of their shapes to the shapes of histograms constructed for each data set. The chi-square goodness-of-fit test and the Kolmogorov-Smirnov goodness-of-fit test were then used to test the validity of the proposed distributions. Results are summarized as follows.

It is found that for a high level of load intensity, say $\Phi_o > 3.0$, when the mean time of the first snap-through tends to be low, the lognormal distribution fits the observed data very well. For an intermediate level of load intensity, say $1.0 \leq \Phi_o \leq 3.0$, the gamma distribution is the best model for the data. For a low load intensity, say $\Phi_o \leq 0.5$, where the mean time of the first snap-through tends to be high , the data is fitted best by the beta distribution. The Weibull and beta distributions are found to fit the data well only at a low load intensity, as indicated by the Kolmogorov-Smirnov test.

The lognormal distribution does not fit the data well in the case of low load intensity, while the beta and Weibull distributions do poorly in the case of high load intensity. The gamma distribution is observed to represent the data sufficiently well for all ranges of load intensity. However, the gamma distribution contradicts the data at the tail of the largest value, but the deviation is small and the gamma model is acceptable at a lower significance level of test statistics. Table 5.9 summarizes results of the chi-square test and the Kolmogorov-Smirnov test. The validity of the assumed distribution for the time to first snap-through is determined for all cases using both tests. The terms best, good, and poor for the assumed distribution are determined according to the significant level at which the model is acceptable. If only one model is to be used for all ranges of load intensity, then the gamma distribution is the appropriate model.

Figures 27 to 29 compare the plots of probability distribution for the first-passage time, for case No. 2, using the proposed distribution models as mentioned above. The probability density function is shown in Fig. 27, while Figs. 28 and 29 illustrate the first-passage probability and the reliability function, respectively. Tables 5.3 to 5.6 show the comparisons of the statistical properties of the observed data and the proposed distribution models in consideration. These statistical parameters are the mean value, variance, skewness coefficient, and kurtosis. Results of these comparisons can be used to supplement the process of selecting the best probability distribution. It is found that the statistical properties for all cases estimated by the gamma distribution are reasonably close to those values calculated from the observed data. Therefore, the gamma distribution is recommended as the probability model for the probability density function of the time to first snap-through of a shallow arch under random excitations.

Fig. 30 compares the plots of the survival probability using the gamma distribution and the probability distribution computed directly from data. The effect of the intensity of the white noise excitation on the solutions of the probability distribution is illustrated in Figs. 31, 32, and 33. These curves of probability distribution of the first snap-through are plotted using the gamma distribution. The density function, the first-passage probability, and the survival probability are given in Figs. 31, 32, and 33, respectively. It is observed from these figures that

the gamma model may be used to represent the probability distribution of the first-passage failure.

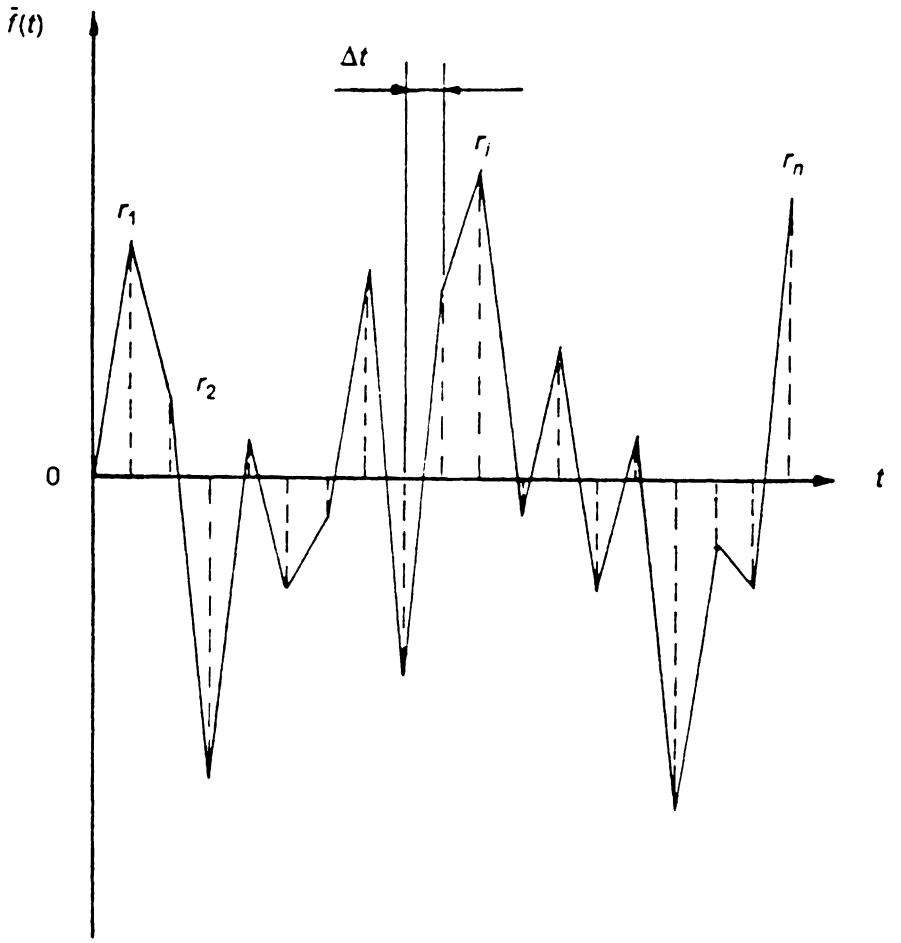

Figure 20. Random ordinates of stationary Gaussian process.

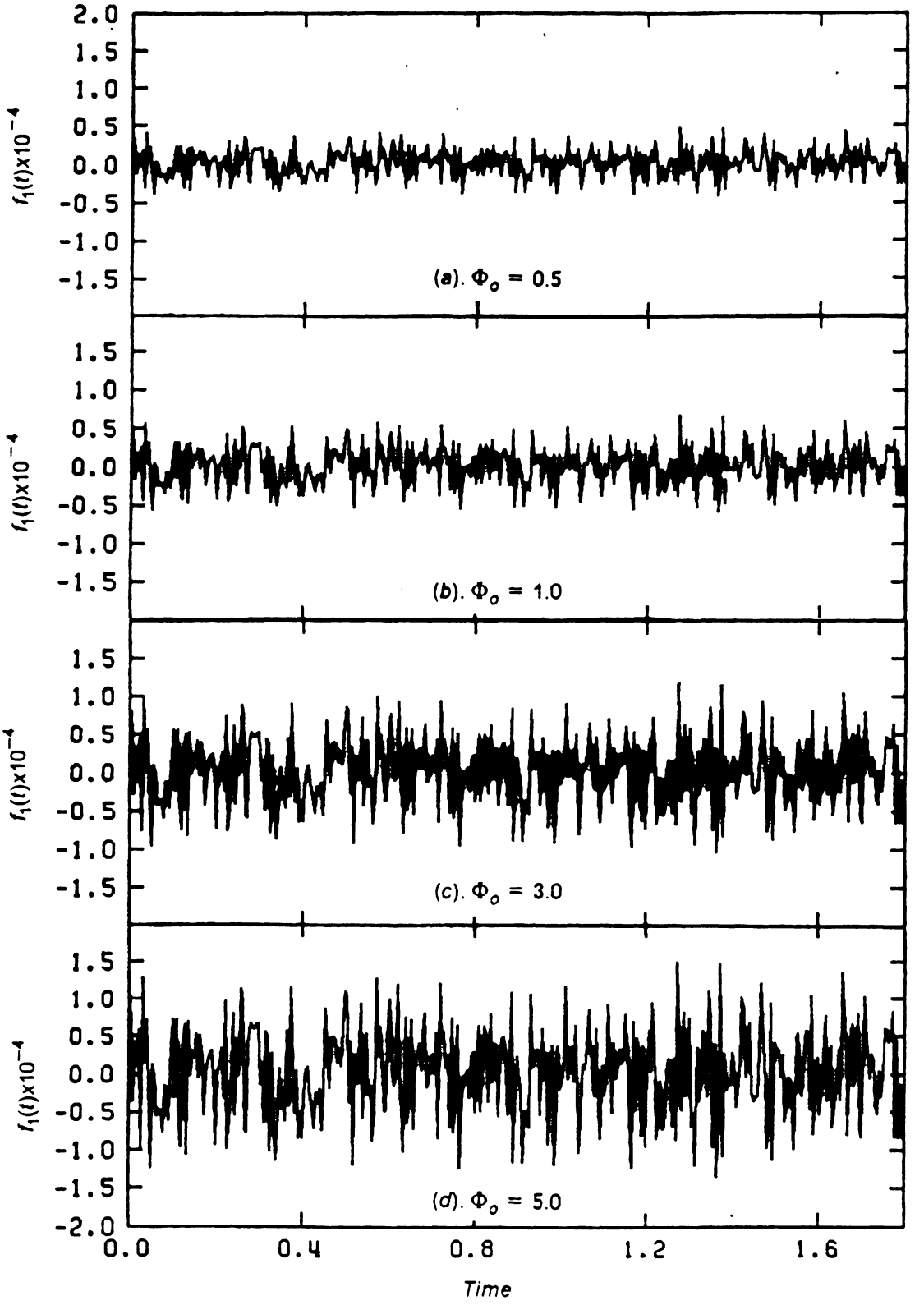

Figure 21. Time history of random generalized force $f_1(t)$.

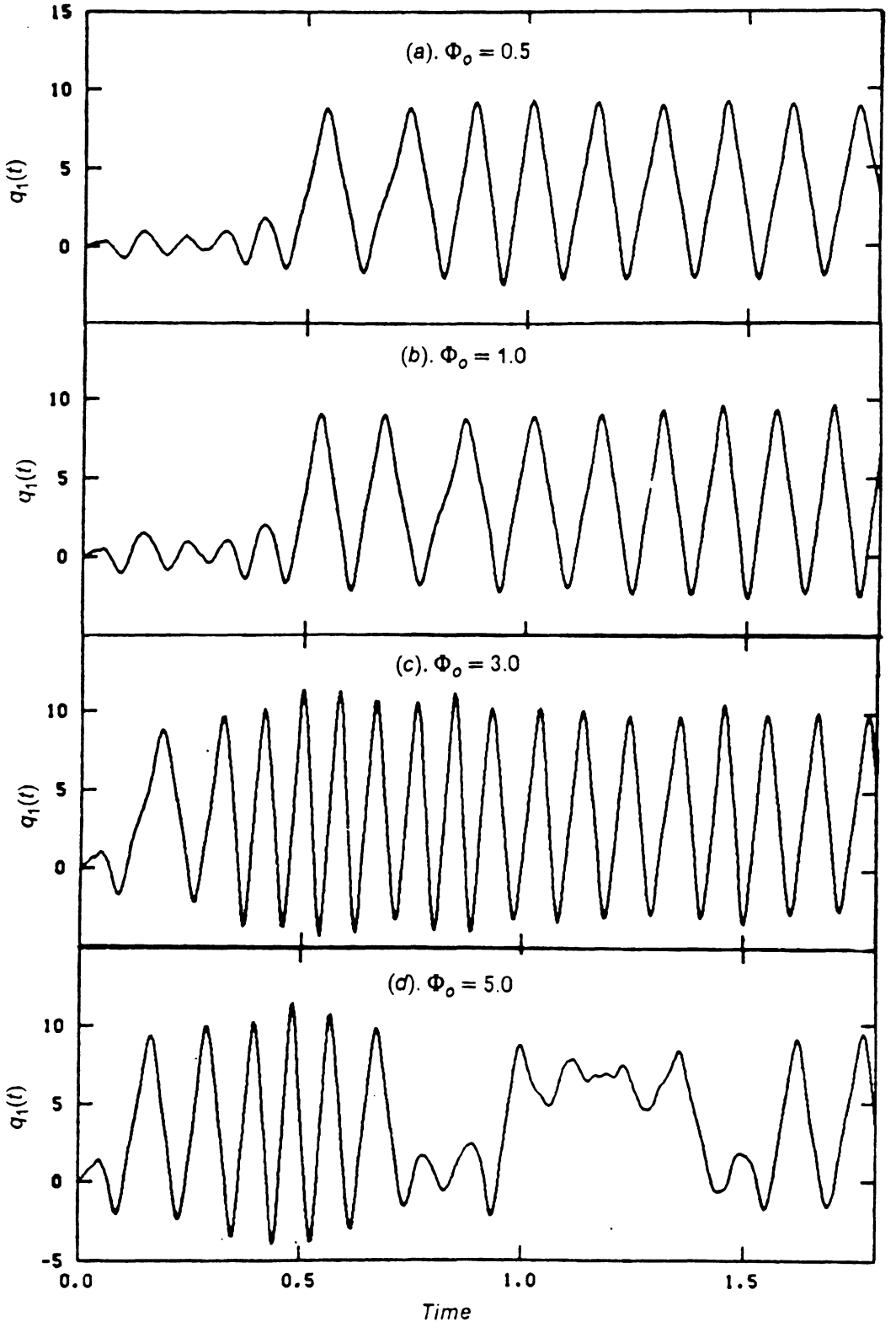

Figure 22. Time history of generalized displacement $q_1(t)$.

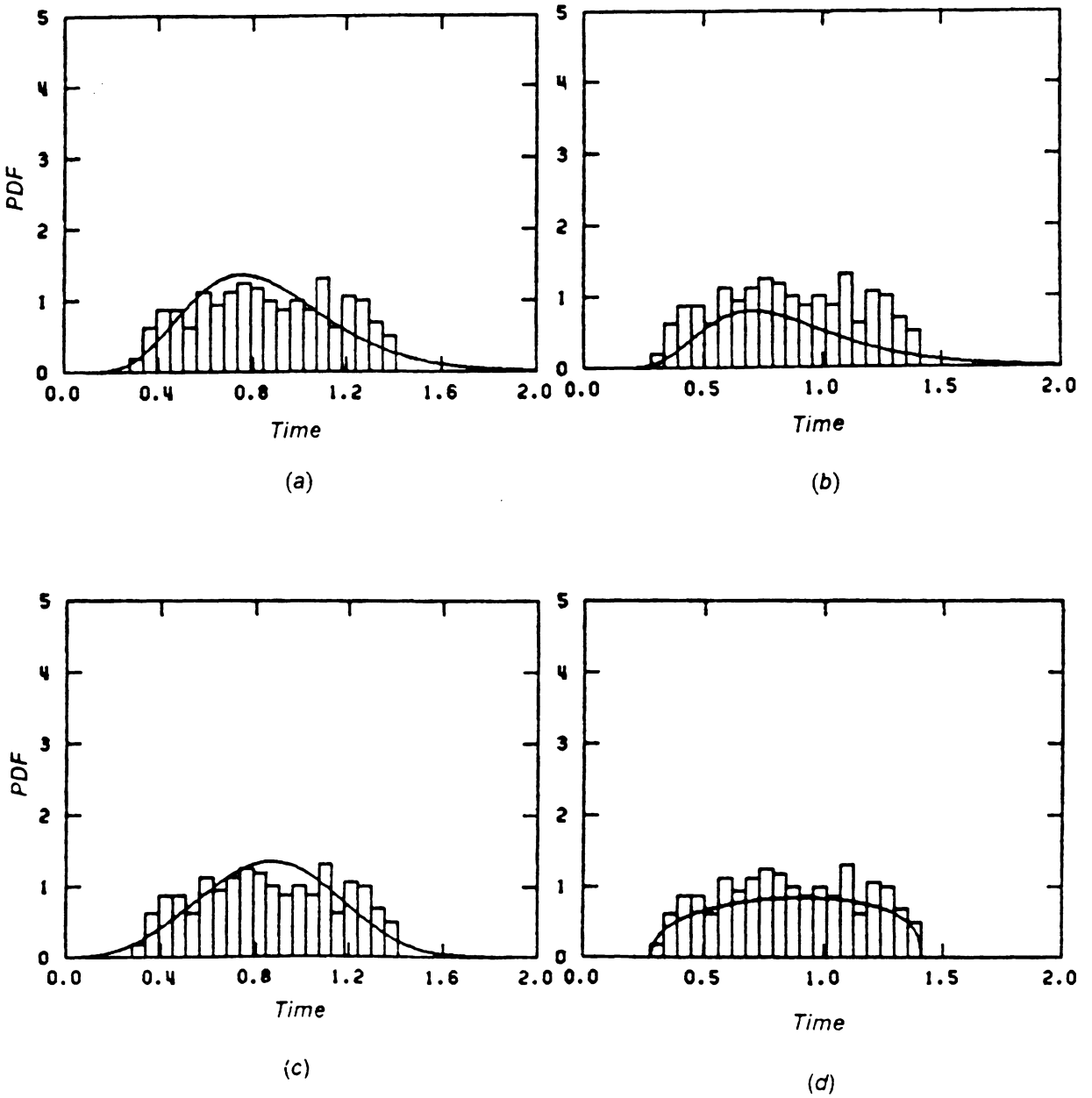

Figure 23. Histogram of time to first snap-through for Case 1: (a) the gamma distribution, (b) the lognormal distribution, (c) the Weibull distribution, and (d) the beta distribution

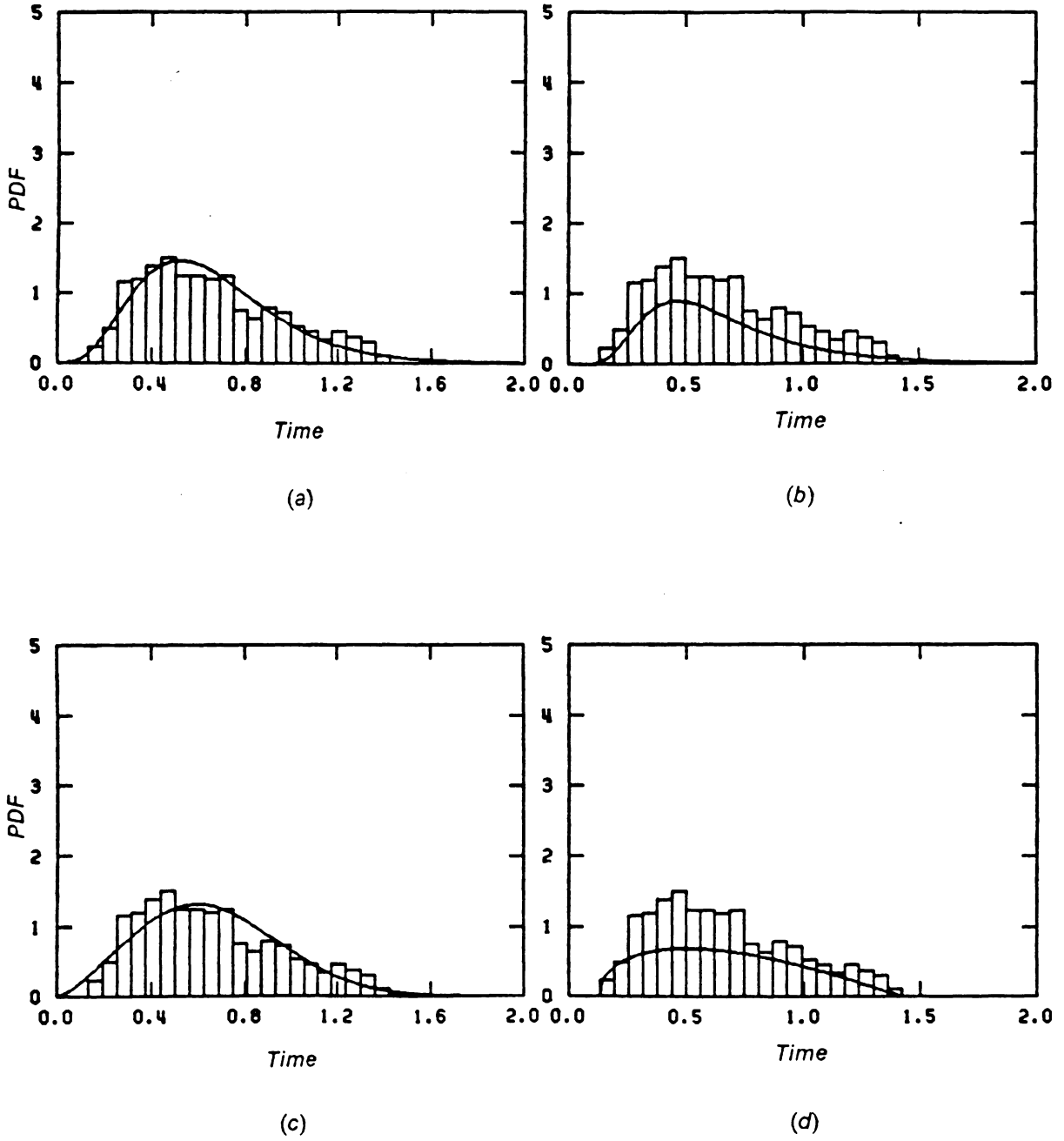

Figure 24. Histogram of time to first snap-through for Case 2: (a) the gamma distribution, (b) the lognormal distribution, (c) the Weibull distribution, and (d) the beta distribution

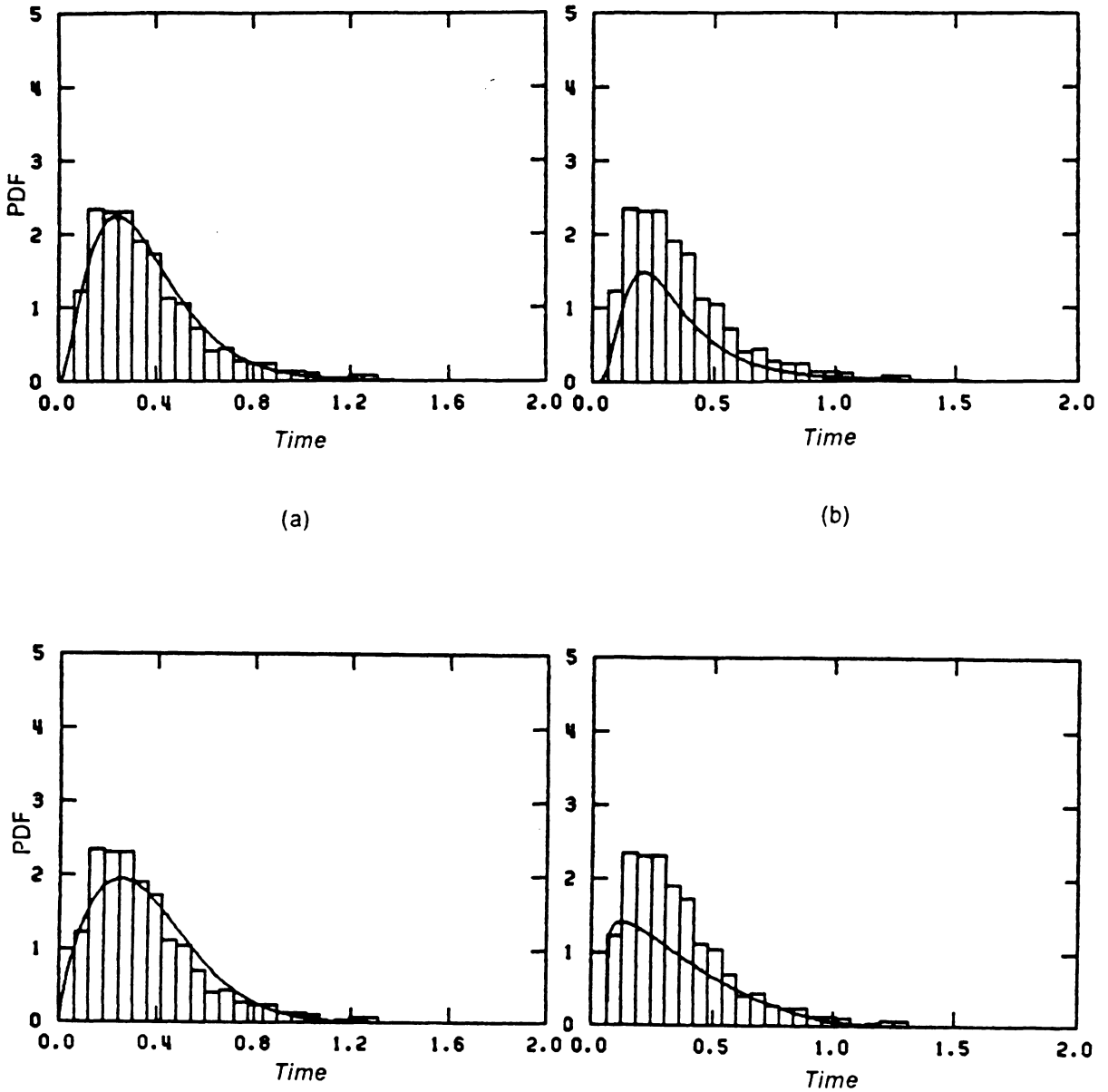

Figure 25. **Histogram of time to first snap-through for Case 3:** (a) the gamma distribution, (b) the lognormal distribution, (c) the Weibull distribution, and (d) the beta distribution

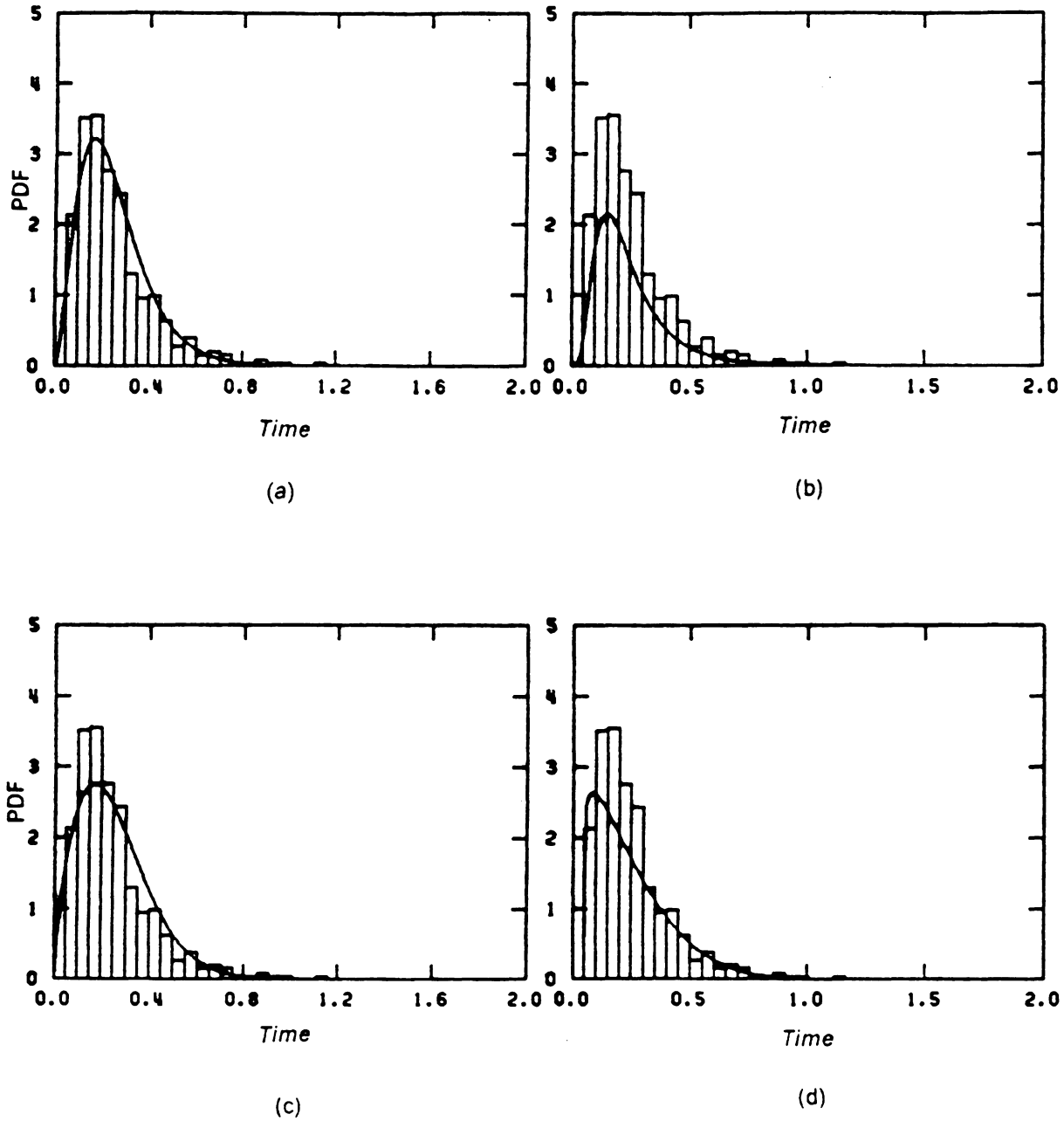

Figure 26. Histogram of time to first snap-through for Case 4: (a) the gamma distribution, (b) the lognormal distribution, (c) the Weibull distribution, and (d) the beta distribution

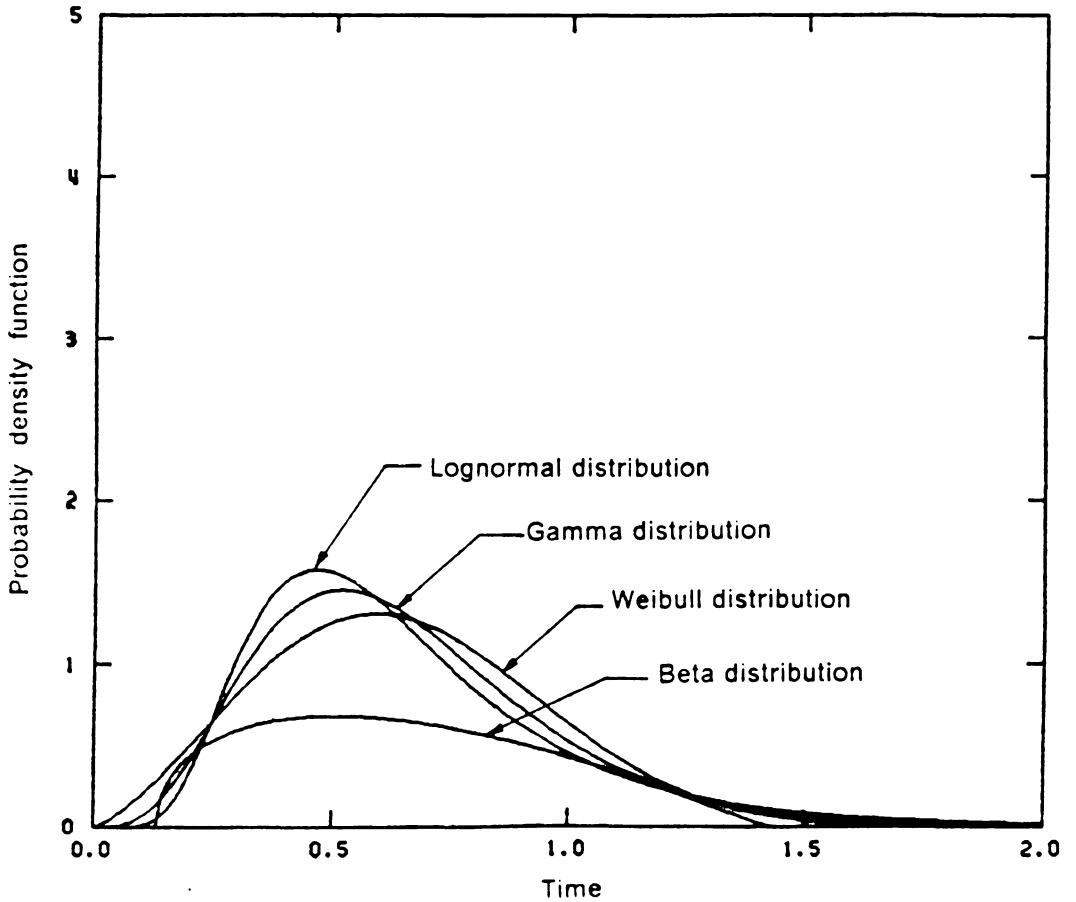

Figure 27. Probability density function of first-passage time: Case 2, $\Phi_0 = 1.0$

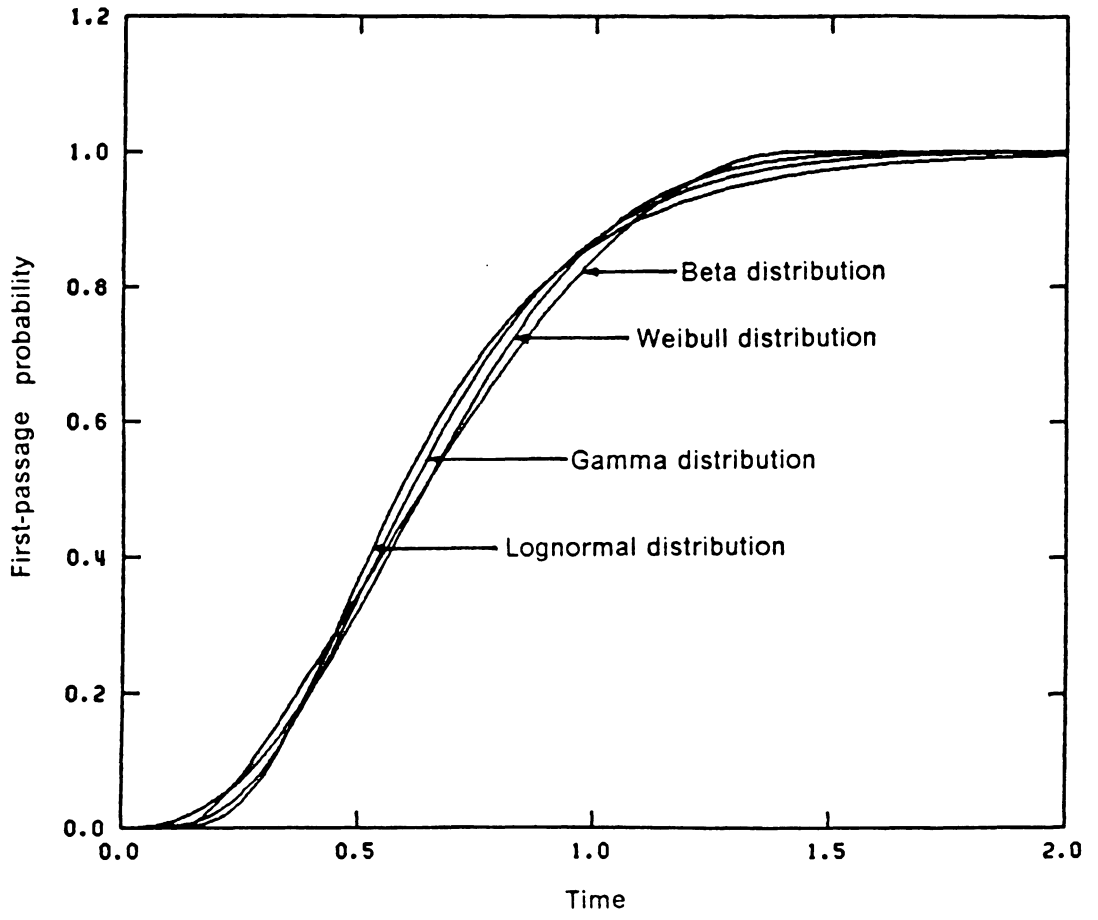

Figure 28. Probability of first-passage failure: Case 2, $\Phi_0 = 1.0$

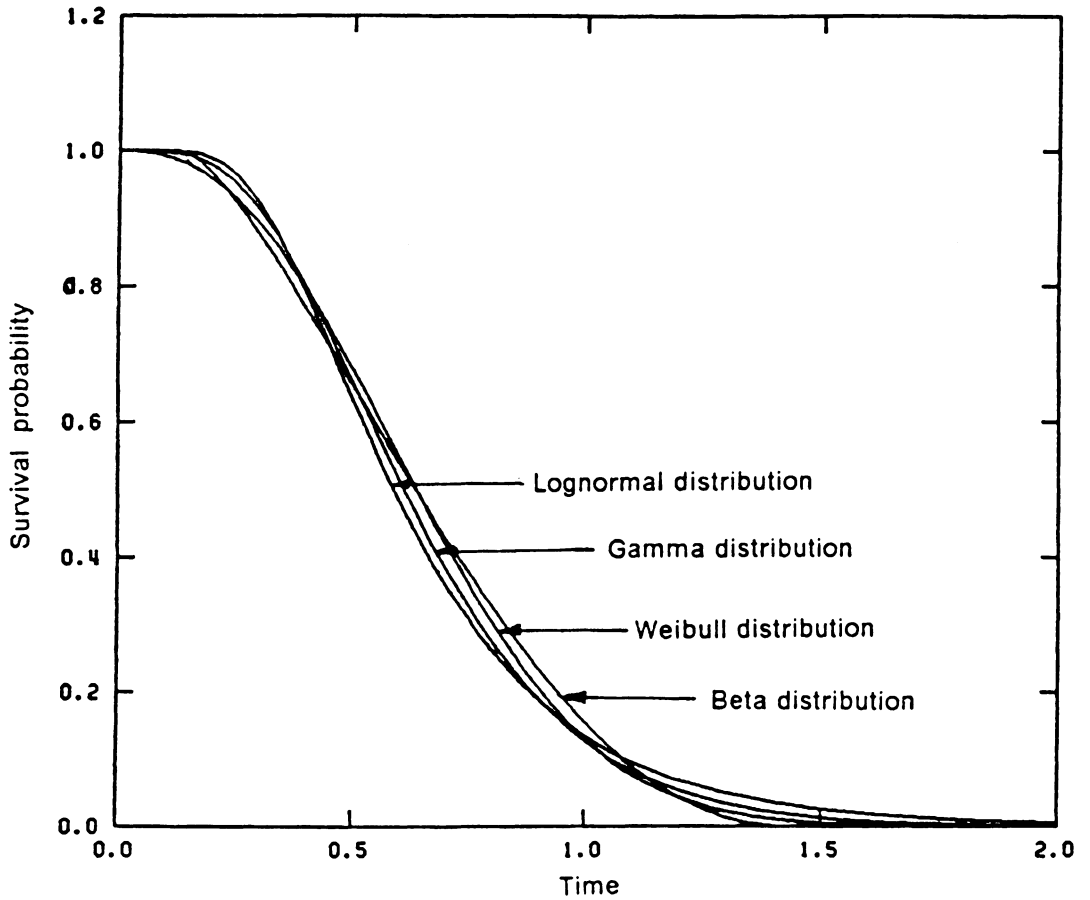

Figure 29. Survival probability: Case 2, $\Phi_0 = 1.0$

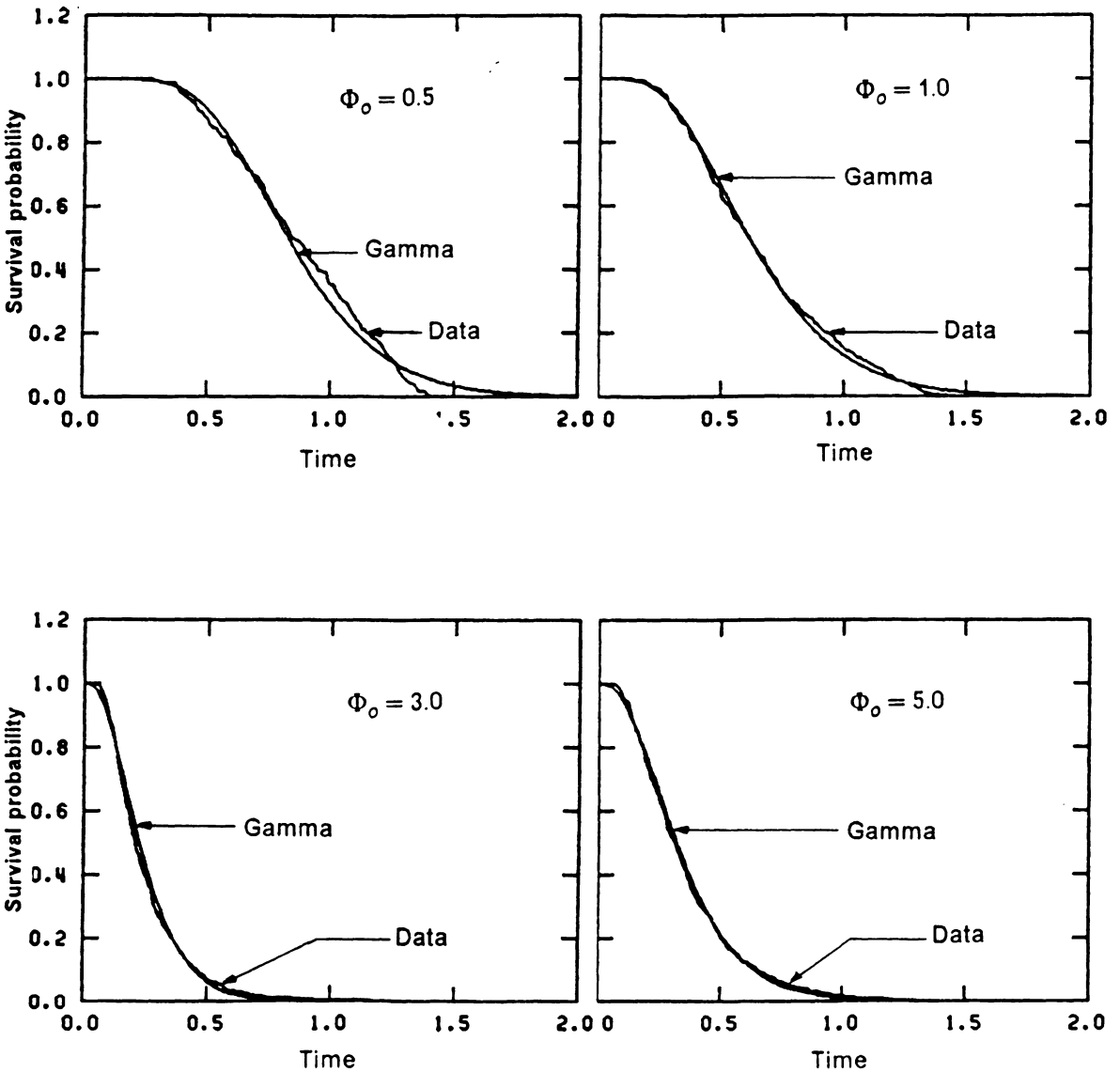

Figure 30. Survival probability using the gamma distribution compared with the data

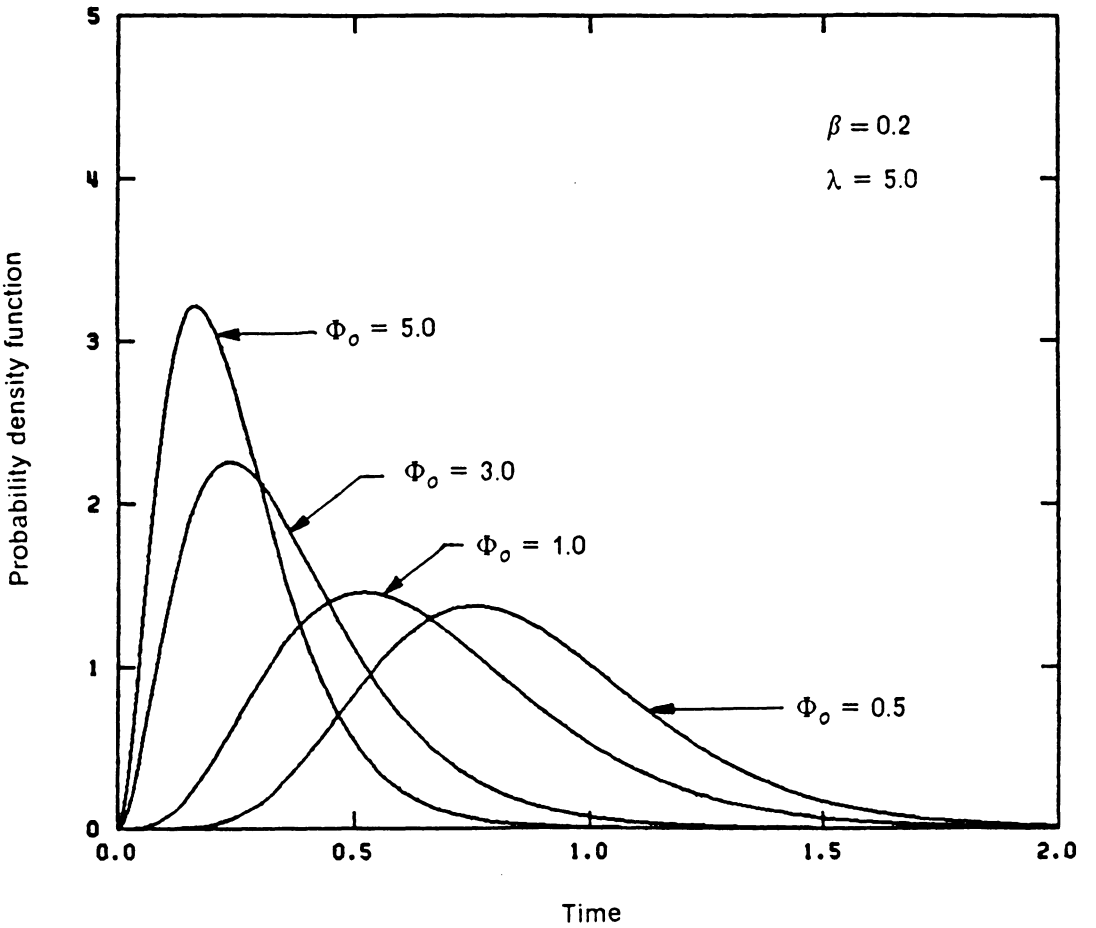

Figure 31. Effect of the intensity of random loading on the probability density function of first-passage failure

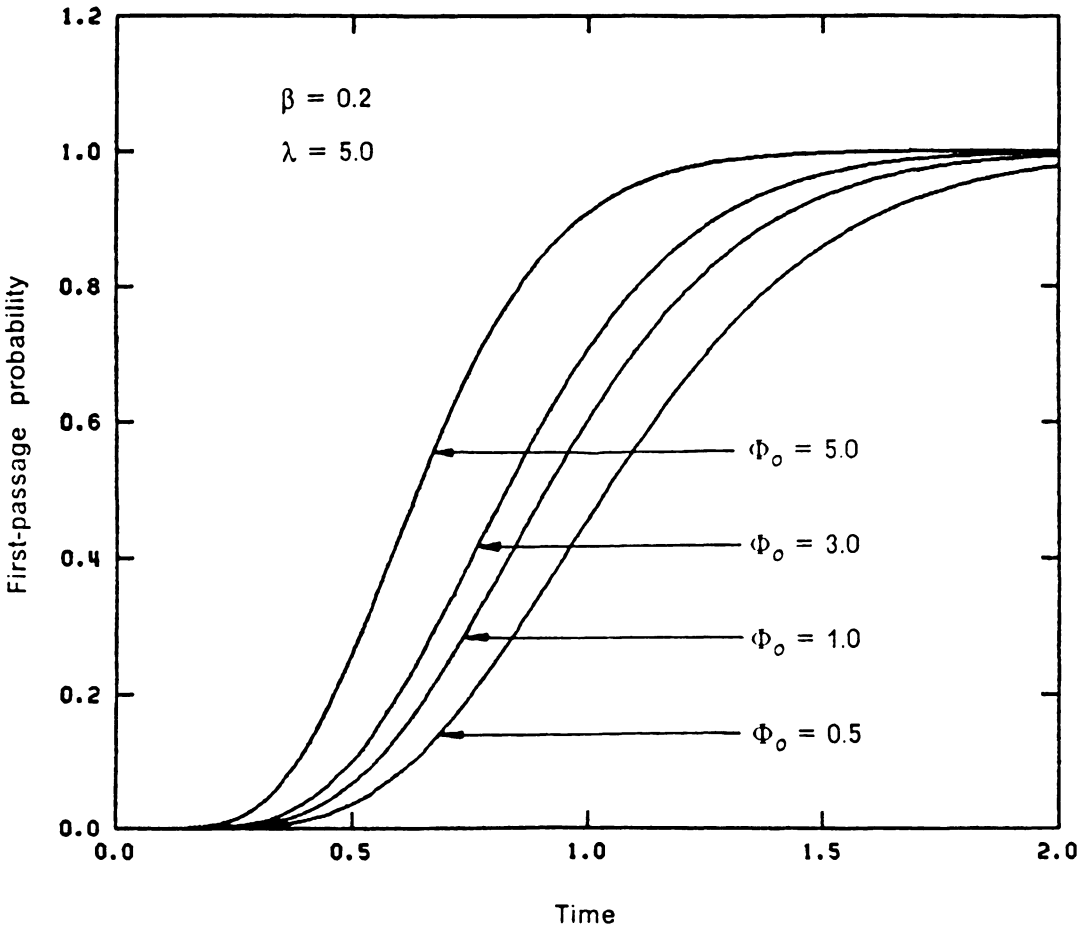

Figure 32. Effect of the intensity of random loading on the probability distribution of first-passage failure

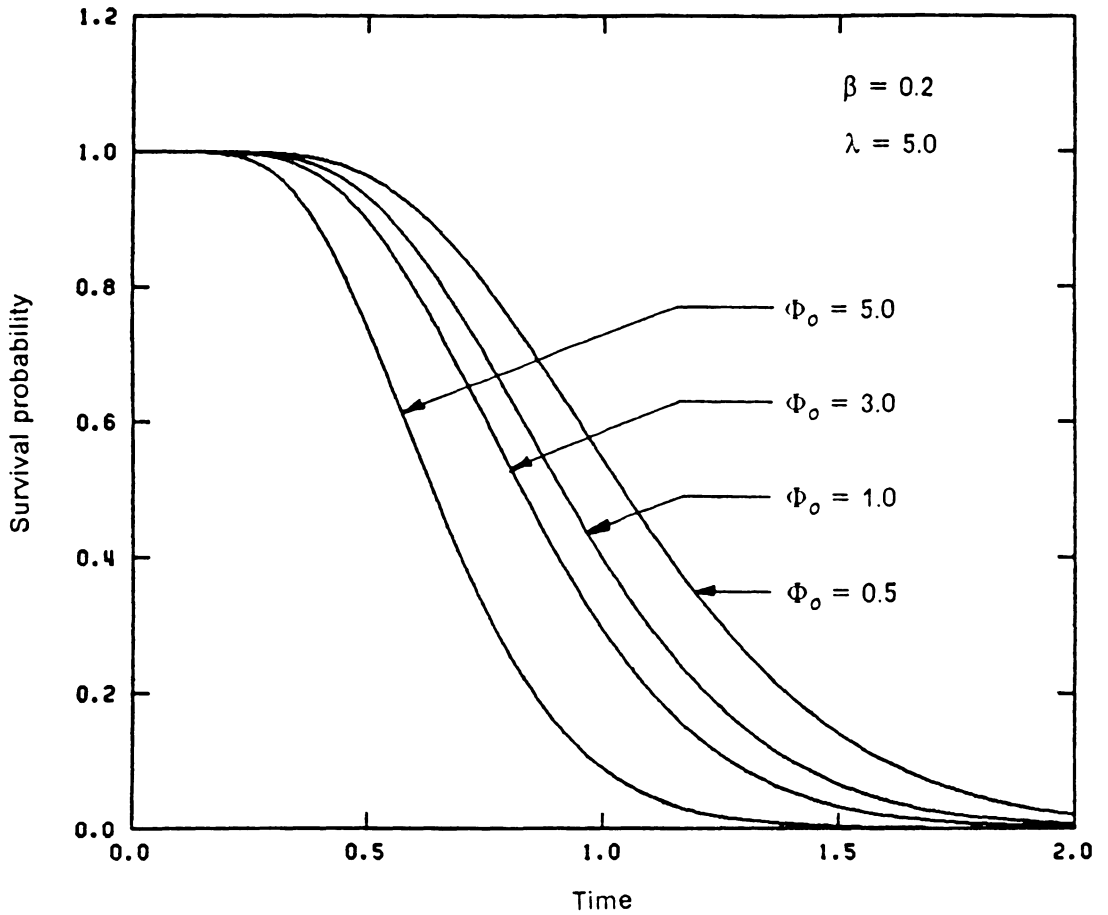

Figure 33. Effect of the intensity of random loading on the survival probability

Table 5.1

Ranked Data--Time of First Snap-Through, $n = 284$, $\Phi = 0.50$

0.2790	0.2790	0.2925	0.3600	0.3600	0.3600	0.3645	0.3690
0.3735	0.3780	0.3780	0.3780	0.3870	0.3960	0.3960	0.4005
0.4095	0.4140	0.4230	0.4275	0.4320	0.4410	0.4455	0.4455
0.4455	0.4455	0.4455	0.4500	0.4500	0.4725	0.4725	0.4770
0.4770	0.4860	0.4860	0.4950	0.4995	0.4995	0.4995	0.5040
0.5040	0.5085	0.5130	0.5265	0.5310	0.5310	0.5310	0.5400
0.5400	0.5445	0.5445	0.5625	0.5670	0.5715	0.5760	0.5805
0.5850	0.5850	0.5895	0.5895	0.5895	0.5940	0.5940	0.5985
0.5985	0.6030	0.6030	0.6075	0.6120	0.6255	0.6255	0.6300
0.6390	0.6390	0.6435	0.6480	0.6480	0.6480	0.6525	0.6525
0.6525	0.6660	0.6705	0.6705	0.6750	0.6750	0.6930	0.6975
0.7020	0.7020	0.7065	0.7110	0.7155	0.7155	0.7200	0.7200
0.7200	0.7200	0.7290	0.7290	0.7290	0.7290	0.7335	0.7335
0.7425	0.7425	0.7425	0.7470	0.7470	0.7515	0.7515	0.7560
0.7560	0.7650	0.7695	0.7695	0.7740	0.7740	0.7785	0.7785
0.7830	0.7830	0.7875	0.7920	0.7920	0.7920	0.8055	0.8100
0.8100	0.8190	0.8190	0.8190	0.8235	0.8235	0.8235	0.8235
0.8280	0.8280	0.8325	0.8325	0.8370	0.8460	0.8460	0.8505
0.8685	0.8730	0.8775	0.8865	0.8865	0.8910	0.8955	0.8955
0.8955	0.8955	0.9000	0.9000	0.9000	0.9045	0.9135	0.9180
0.9180	0.9180	0.9270	0.9270	0.9315	0.9315	0.9405	0.9405
0.9450	0.9450	0.9495	0.9630	0.9675	0.9810	0.9810	0.9810
0.9855	0.9855	0.9855	0.9855	0.9855	0.9945	0.9945	0.9990
1.0125	1.0125	1.0125	1.0170	1.0170	1.0215	1.0215	1.0215
1.0305	1.0305	1.0305	1.0350	1.0440	1.0440	1.0485	1.0530
1.0665	1.0710	1.0710	1.0710	1.0755	1.0755	1.0800	1.0800
1.0800	1.0890	1.0890	1.0935	1.0980	1.1025	1.1025	1.1025
1.1070	1.1115	1.1115	1.1205	1.1205	1.1205	1.1295	1.1295
1.1430	1.1430	1.1475	1.1520	1.1610	1.1610	1.1655	1.1745
1.1835	1.1880	1.1970	1.1970	1.2060	1.2060	1.2105	1.2150
1.2195	1.2195	1.2195	1.2240	1.2240	1.2285	1.2330	1.2330
1.2375	1.2420	1.2510	1.2555	1.2645	1.2645	1.2690	1.2735
1.2735	1.2780	1.2780	1.2780	1.2780	1.2825	1.2825	1.2825
1.2915	1.2960	1.2960	1.3005	1.3050	1.3140	1.3140	1.3230
1.3320	1.3410	1.3410	1.3410	1.3545	1.3590	1.3590	1.3815
1.3995	1.3995	1.4040	1.4085				

Table 5.2

Time of First Snap-Through of a Shallow Arch
Under Stationary White-Noise Excitations Using Monte Carlo Method

	Case 1 $\Phi_o = 0.5$	Case 2 $\Phi_o = 1.0$	Case 3 $\Phi_o = 3.0$	Case 4 $\Phi_o = 5.0$
No. of simulations	500	500	500	500
No. of snap-through events	284	435	496	500
Mean value	0.8621	0.6568	0.3595	0.2510
Standard deviation	0.2906	0.2968	0.2214	0.1617
Skewness coefficient	0.0000	0.5531	1.3728	1.7318
Kurtosis	1.9556	2.4695	5.1811	7.1232
Minimum time	0.2790	0.1305	0.0630	0.0450
Maximum time	1.4085	1.4220	1.3095	1.1610

Number of modes = 1
Arch rise parameter = 5.00
Damping coefficient = 0.20

Table 5.3

Statistical Properties of the Time to First Snap-Through From Observed Data and the Proposed Distribution Models for Case 1, $\Phi_o = 0.5$

Statistical Properties	Observed Data	Distribution Model			
		Lognormal	Gamma	Weibull	Beta
Mean value	0.8621	0.8671	0.8621	0.8646	0.8621
Variance	0.0844	0.1134	0.0950	0.0811	0.0844
Skewness coefficient	0.0000	1.2235	0.7150	0.0645	-0.0470
Kurtosis	1.9556	5.7747	3.7667	2.7105	6.8939
		Goodness-of-Fit Test			
Chi-square value		64.35 (16)	35.84 (15)	29.87 (17)	15.87 (17)
KS value		0.0847	0.0744	0.0302	0.0487

Note: Numbers in parentheses are the numbers of degrees of freedom.

Table 5.4

Statistical Properties of the Time to First Snap-Through From Observed Data and the Proposed Distribution Models for Case 2, $\Phi_o = 1.0$

Statistical Properties	Observed Data	Distribution Model			
		Lognormal	Gamma	Weibull	Beta
Mean value	0.6568	0.6616	0.6568	0.6590	0.6568
Variance	0.0881	0.1141	0.0911	0.0867	0.0881
Skewness coefficient	0.5551	1.6647	0.9192	0.4126	0.2238
Kurtosis	2.4695	8.3003	4.2673	2.9145	6.6881
		Goodness-of-Fit Test			
Chi-square value		28.09 (17)	21.30 (17)	35.94 (17)	very high
KS value		0.0403	0.0378	0.0570	0.0477

Note: Numbers in parentheses are the numbers of degrees of freedom.

Table 5.5

Statistical Properties of the Time to First Snap-Through From Observed Data and the Proposed Distribution Models for Case 3, $\Phi_o = 3.0$

Statistical Properties	Observed Data	Distribution Model			
		Lognormal	Gamma	Weibull	Beta
Mean value	0.3593	0.3614	0.3593	0.3616	0.3593
Variance	0.0490	0.0578	0.0437	0.0456	0.0490
Skewness coefficient	1.3769	2.2896	1.1632	0.8220	0.7028
Kurtosis	5.1811	13.5715	5.0294	3.6617	7.1878
		Goodness-of-Fit Test			
Chi-square value		5.97 (14)	13.65 (12)	33.50 (12)	very high
KS value		0.0335	0.0403	0.0629	0.0613

Note: Numbers in parentheses are the numbers of degrees of freedom.

Table 5.6

Statistical Properties of the Time to First Snap-Through From Observed Data and the Proposed Distribution Models for Case 4, $\Phi_o = 5.0$

Statistical Properties	Observed Data	Distribution Model			
		Lognormal	Gamma	Weibull	Beta
Mean value	0.2510	0.2507	0.2510	0.2530	0.2510
Variance	0.0262	0.0266	0.0214	0.0236	0.0262
Skewness coefficient	1.7370	2.2281	1.1645	0.8700	0.9552
Kurtosis	7.1232	12.9562	5.0341	3.7855	7.3104
		Goodness-of-Fit Test			
Chi-square value		8.75 (11)	21.15 (10)	41.22 (10)	very high
KS value		0.0352	0.0651	0.0740	0.0856

Note: Numbers in parentheses are the numbers of degrees of freedom.

Table 5.7

Percentile Value of the Chi-Square Distribution *

	α						
f	0.05	0.9	0.95	0.975	0.990	0.995	0.999
10	3.94	16.0	18.3	20.5	23.2	25.2	29.6
11	4.57	17.3	19.7	21.9	24.7	26.8	31.3
12	5.23	18.5	21.0	23.3	26.2	28.3	32.9
14	6.59	21.1	23.7	26.1	29.1	31.3	36.1
15	7.26	22.3	25.0	27.5	30.6	32.8	37.7
16	7.96	23.5	26.3	28.8	32.0	34.3	39.3
17	8.67	24.8	27.6	30.2	33.4	35.7	40.8

*Abridged from Table A.3 of Ref. 4.

Table 5.8

Critical Values of D_n^a from Refs. 4 and 30

	α			
	0.20	0.10	0.05	0.01
Case 1				
Lognormal	0.0437	0.0484	0.0527	0.0618
Gamma	0.0445	0.0493	0.0540	0.0629
Weibull	0.0438*	0.0484	0.0527	0.0618
Standard value, beta	0.0635*	0.0724	0.0807	0.0967
Case 2				
Lognormal	0.0353	0.0391	0.0426*	0.0499
Gamma	0.0360	0.0398*	0.0436	0.0508
Weibull	0.0354	0.0391	0.0426	0.0499
Standard value, beta	0.0513*	0.0585	0.0652	0.0782
Case 3				
Lognormal	0.0330	0.0367*	0.0399	0.0467
Gamma	0.0346	0.0386	0.0422*	0.0485
Weibull	0.0331	0.0367	0.0399	0.0469
Standard value, beta	0.0480	0.0548	0.0611	0.0732*
Case 4				
Lognormal	0.0329	0.0365*	0.0397	0.0466
Gamma	0.0344	0.0385	0.0422	0.0483
Weibull	0.0330	0.0365	0.0397	0.0466
Standard value,beta	0.0479	0.0546	0.0608	0.0729

Table 5.9

Validity of The Assumed Distribution for the Time to First Snap-Through

Case	Distribution Model			
	Lognormal	Gamma	Weibull	Beta
(1). The Chi-Square Test				
1). $\Phi_o = 0.5$	GOOD	POOR	GOOD	BEST
2). $\Phi_o = 1.0$	BEST	GOOD	GOOD	POOR
3). $\Phi_o = 3.0$	GOOD	BEST	POOR	POOR
4). $\Phi_o = 5.0$	GOOD	BEST	POOR	POOR
(1). The Kolmogorov-Smirnov Test				
1). $\Phi_o = 0.5$	GOOD	GOOD	GOOD	BEST
2). $\Phi_o = 1.0$	BEST	GOOD	GOOD	GOOD
3). $\Phi_o = 3.0$	GOOD	BEST	POOR	GOOD
4). $\Phi_o = 5.0$	GOOD	BEST	POOR	POOR

Chapter VI

Results and Further Study on Nonstationary Random Excitation

The snap-through of a shallow arch subjected to wide-band, stationary random excitation was studied in the previous chapters. The random excitation was assumed to be a white-noise process. In Chapter 4, the energy envelope process of the displacement and velocity was used to approximate the governing Fokker-Planck-Kolmogorov equation. It was assumed that the damping was light, so the energy envelope process could be modelled, to a close approximation, as a one-dimensional Markov process. The implicit finite difference scheme, of the Crank-Nicolson type, was used to approximate the diffusion process of the FPK equation. Results were presented in the form of the mean time to first-passage failure and the probability distribution function.

In Chapter 5, the Monte Carlo simulation method was used to solve the same problem. The equation of motion was solved numerically using the Runge-Kutta method for each record of random excitations. A large number of realizations of the time to first snap-through was collected. Statistics of the time to first snap-through, i.e., the mean value, the standard deviation, and higher moments, were estimated from these realizations. These statistics were then used to select the empirical probability distribution model. The gamma distribution was found to be the appropriate model for the probability distribution of the time to first snap-through.

6.1 Reliability of Energy Envelope Approximation

The method of computer simulation is frequently used to assess the reliability of the approximation technique, since the simulation method solves the equation of motion directly, and is usually applicable. In this section, the results of the energy envelope approximation are compared with those of the Monte Carlo simulation method.

A further investigation of the Monte Carlo simulation method is conducted before the comparison can be reasonably made. Reliable results of the simulation method and a numerical step-by-step integration depend greatly on the time increment, Δt. Table 6.1 shows the effect of Δt on the solution of computer simulation. It can be verified that the value of Δt approximately equal to $\frac{1}{20}$ of the period of free oscillation of the structure usually gives reliable results [65]. The values of $\Delta t < 0.004$ do not significantly improve the results. Very small values of Δt will require much more computer time. Table 6.2 presents the investigation of the number of snap-through realizations on the simulation results. It is indicated that 500 realizations may give satisfactory results. Therefore, the value of $\Delta t = 0.004$ with 500 realizations of the first snap-through will be used in the rest of this study.

It is noted that solutions of the computer simulation obtained here are different from those presented in Chapter 5, where the time length of the applied random excitation was definite and less than the time length of a step-by-step integration. In this section, both time lengths are the same since the random excitation was assumed to act on the system for the entire time in the method of energy envelope approximation. The time length must be sufficiently long for all simulation records to have at least one event of snap-through or the number of snap-through realizations to converge to a constant value, which means that the snap-through will not occur at all for some particular records of random excitation. The unrealization of the snap-through event may happen if the intensity of the random excitation is sufficiently low.

The comparison of the results between the method of Monte Carlo simulation and the method of energy envelope approximation is given in Tables 6.3 and 6.4, and also in Figs. 34 to 43. The mean time to first-passage failure and curves of the probability distribution function

are used as the basis for comparison. The mean time to first-passage, for the case of $\lambda = 5.0$ and $\beta = 0.2$, for various values of Φ_o is given in Table 6.3. The results for this case are also shown in Fig. 34. The effect of β on the mean time using both techniques, for the case of $\lambda = 5.0$ and $\Phi_o = 5.0$, is given in Table 6.4 and Fig. 35. It is observed that the difference in the results between both methods is small for the range of Φ_o and β considered in this study.

The comparison between results of the computer simulation and those of the energy envelope approximation can also be accomplished based on the probability distribution function of the first-passage failure. For the energy envelope approximation method, the probability distribution can be obtained directly, as described in Chapter 4, in the form of the reliability function, $P_s(t)$. The probability of first-passage failure, $P_f(t)$, and its density function, $p_f(t)$, can then be estimated from $P_s(t)$.

For the method of Monte Carlo simulation, results are data sets of a large number of realizations of the time to first snap-through and their statistics such as the mean value and the standard deviation. The investigation in Chapter 5 indicated that the gamma model can be used to represent adequately the probability distribution of time to the first snap-through. Therefore, the gamma distribution model will be used in this section.

When the mean time to first-passage failure is large, the probability distribution function seems to have an exponential form. The shape of the exponential distribution was also suggested by the results of Chapter 4. Therefore, the exponential distribution model is also used, in addition to the gamma model, to represent solutions of the computer simulation. The probability density function of the exponential model is given as [4]

$$p_e(t) = \nu e^{-\nu t} \tag{6.1}$$

where ν is its scale parameter. ν can be simply estimated from the random data as follows:

$$\nu = \frac{1}{\bar{T}} \tag{6.2}$$

where $\bar{T}$ is the mean value.

The comparison of both techniques based on the probability distribution function is given in Figs. 36 to 43. These figures compare curves of the reliability function and the probability density function. There are 3 curves in each figure, which are: a curve obtained directly from the results of the energy envelope approximation, and two curves obtained from the solutions of Monte Carlo simulation using the gamma and exponential models.

The probability distribution function for the case of $\lambda = 5.0$ and $\beta = 0.2$ is shown in Figs. 36, 37, 38, and 39 for the values of $\Phi_o = 5.0$, 3.0, 1.0, and 0.5 , respectively. The effect of the damping parameter on the probability distribution for the case of $\lambda = 5.0$ and $\Phi_o = 5.0$ is shown in Figs. 36, 40, 41, 42, and 43, respectively, for the values of β = 0.2, 2.0, 5.0, 10.0, and 20.0. It is indicated from these figures that results obtained using both methods are in close agreement for a range of Φ_o and β considered in this study. In summary, the energy envelope approximation gives reliable results in the range of parameters considered here. It is also indicated that the energy envelope process may be modelled as a one-dimensional Markov process as assumed, especially for a system with light damping. The energy envelope approximation with the implicit finite difference method can be used in solving first-passage time problems associated with the displacement response of a system with nonlinear restoring forces, such as the equation of motion governing the response of shallow structures subjected to wide-band, stationary random excitation.

6.2 Multi-Mode Analysis-Monte Carlo Simulation

In all previous studies on the snap-through of a shallow arch subjected to random excitation, a single-mode approximation of the governing equation of motion, Eq. (3.19), was used. In the one-mode approximation, only the response of the first mode, $q_1(t)$, was considered. Note that the downward deflection of the arch is defined by Eq. (3.16), where it is given as

$$w(x,t) = \sum_{i=1}^{N} q_i(t)\sqrt{2}\ \sin i\pi x \tag{3.16}$$

where N is a number of modes.

In this section, multi-mode response of the arch is investigated using the method of Monte Carlo simulation. The procedure is similar to the study in Chapter 5. The equation of motion, for the N-mode approximation, is given in Eq. (3.19), and rewritten here: for $j = 1, \ldots, N$

$$\ddot{q}_j(t) + \beta\dot{q}_j(t) + \left[j^4\pi^4 - j^2\pi^2 m\right]q_j(t) + \frac{\sqrt{2}}{2}\lambda\pi^2 m\delta_{1j} = f_j(t) \tag{6.3}$$

where m and $f_j(t)$ are defined as

$$m = 2\left[\sqrt{2}\,\lambda\pi^2 q_1(t) - \sum_{i=1}^{N} i^2\pi^2 q_i^2(t)\right] \tag{6.4}$$

$$f_j(t) = \sqrt{2}\,\pi^4 \int_0^1 f_j(x,t)\sin j\pi x\ dx \tag{6.5}$$

The displacement response of the arch is now given by N generalized coordinates, $q_i(t)$ for $i = 1, 2, \ldots, N$. The response measure at an instant of time can be given in the form of the root-mean-square (rms) response, $\rho(t)$, which is defined as

$$\rho(t) = \left[\sum_{i=1}^{N} q_i^2(t)\right]^{1/2} \tag{6.6}$$

The rms response $\rho(t)$ is a random process. For the first-passage time problem, the critical barrier becomes $\rho(t) = b$. The failure criterion can be stated as follows: the arch fails when $\rho(t)$ first takes on a value of $\rho = b$. It is noted that the safe domain in this case is similar

to a double-sided barrier of the first-passage problem described in Chapter 4. It is assumed that after the total response, $\rho(t)$, passes out of the safe domain, $\rho < b$, the response will increase gradually or abruptly and become so large that the arch snaps-through to the other side of the horizontal axis. Therefore, the snap-through event of the arch occurs. The parameter of interest here is the time to first snap-through or the time when the rms response first exceeds the value of $\rho = b$.

A sinusoidal loading is considered, where the random excitation can be expressed as follows:

$$f_j(x,t) = F(t) \sin \pi x \tag{6.7}$$

where $F(t)$ is a time-dependent random excitation. F(t) is assumed to be a white-noise process. The random excitation defined by Eq. (6.7) is a symmetric load corresponding to the first mode of the sinusoidal loading. The shape of this symmetric load is shown in Fig. 44(a). Hence, the forcing function, $f_j(t)$, becomes

$$f_1(t) = \sqrt{2}\,\pi^4 F(t) \int_0^1 \sin \pi x \, \sin \pi x \, dx = \frac{\sqrt{2}\,\pi^4 F(t)}{2} \tag{6.8}$$

and

$$f_j(t) = 0, \quad \text{for } j = 2, \ldots, N. \tag{6.9}$$

The N-mode approximation, where $N = 1, 2, 3, 4$, is considered in this study. The initial rise of the arch is assumed to be $\lambda = 5.0$, and the damping coefficient is taken to be 0.2. Results are obtained for various values of intensity of random load, i.e., $\Phi_o = 0.5, 1.0, 3.0$, and 5.0. The complete equation of motion is described in detail as follows:

For $j = 1$:

$$\ddot{q}_1(t) + \beta\dot{q}_1(t) + [\pi^4 - \pi^2 m]q_1(t) + \frac{\sqrt{2}}{2}\lambda\pi^2 m = \frac{\sqrt{2}\,\pi^4 F(t)}{2}$$

For $j = 2$:

$$\ddot{q}_2(t) + \beta\dot{q}_2(t) + [16\pi^4 - 4\pi^2 m]q_2(t) = 0$$

And for $j = N$:

$$\ddot{q}_N(t) + \beta\dot{q}_N(t) + [N^4\pi^4 - N^2\pi^2 m]q_N(t) = 0$$

where $m = 2\left[\sqrt{2}\,\lambda\pi^2 q_1(t) - \{\pi^2 q_1^2(t) + 4\pi^2 q_2^2(t) + \cdots + N^2\pi^2 q_N^2(t)\}\right]$.

The following initial conditions are employed for the 4-mode analysis:

$$q_1(0) = 0.0,\ q_i(t) = 0.01,\ \text{for } i = 2,\ 3,\ 4, \tag{6.10}$$

and

$$\dot{q}_i(0) = 0.0,\ \text{for } i = 1,\ 2,\ 3,\ \text{and } 4 \tag{6.11}$$

It is noted that the nonzero initial conditions for higher modes are required to insure that the antisymmetric modes participate in the response of the arch to symmetric loading.

For the 4-mode approximation, the response for each mode, $q_j(t)$, for $j = 1,\ 2,\ 3,\ 4$, and the rms response, $\rho(t)$, as a function of time is shown in Fig. 44(b). It is observed that the response of the first mode is predominant in the total response. The contribution of the higher modes to the total response is small.

Results of the Monte Carlo simulation are presented in Table 6.5 for the multi-mode analysis. The difference between the results of the 2-mode and 4-mode analyses is small. In Fig. 45, values of the mean time to first snap-through for 1-mode and 2-mode analyses are plotted versus the intensity of random loadings. Curves of the probability density function of the time to first snap-through are compared in Fig. 46. For an arch under symmetric loading,

the higher modes than two modes offer small contribution to the total response. It is indicated that the second mode does have a significant effect on the mean time to first snap-through.

6.3 Nonstationary Random Excitation - Monte Carlo Simulation.

In this section, the snap-through of a shallow arch subjected to nonstationary random excitation of an earthquake-type disturbance is considered. There are several approaches that attempt to define and generate artificial earthquake ground motions for use in the time domain analysis of nonlinear response of structures. The simplest method is to express the nonstationary earthquake excitation as a modulated white noise. The random forcing function, $F(t)$, of the one-mode approximation of the equation of motion, can be expressed as [81]

$$F(t) = \psi(t)n(t) \tag{6.12}$$

where $\psi(t)$ is a deterministic modulating function of time and $n(t)$ is a stationary white-noise process. This approach is also known as the separable nonstationary stochastic model of seismic motions, where the modulating function is also called an enveloping function. The enveloping function is used to represent the nonstationary properties and duration of the earthquake excitation. The enveloping function is generally expressed in the form of [81]

$$\psi(t) = e^{-\beta_1 t} - e^{\beta_2 t} \tag{6.13}$$

The parameters β_1 and β_2 are usually chosen to give the desired nonstationary properties and duration. β_1 and β_2 are simply used to control the build up, decay, and duration of the artificial accelerograms. Using the past records of ground motions, such as the time to peak, the amplitude of peak, and the duration of the actual accelerograms, the parameters β_1 and β_2 can be estimated.

The following enveloping functions are used in this study:

$$
\begin{aligned}
\psi_1(t) &= 1 \\
\psi_2(t) &= 2.32\left[e^{-1.50t} - e^{-24.83t}\right] \\
\psi_3(t) &= 12.8\left[e^{-2.33t} - e^{-3.17t}\right]
\end{aligned}
\tag{6.14}
$$

The modulating functions are obtained for a 20-sec. duration of strong ground motions. In this study, the duration of the applied random loadings is taken as 1.2, in a nondimensional time scale. Therefore, the parameters β_1 and β_2 are estimated proportionally. The first enveloping function, $\psi_1(t)$, yields a white-noise excitation for the arch, which has been used in all previous works. The second enveloping function, $\psi_2(t)$, represents an earthquake with a fast rise time [18], approximately 0.1200 in a nondimensional time, i.e., about 2 sec. for a 20-sec. duration of an earthquake. The third one, $\psi_3(t)$, is associated with a moderate rise time earthquake with a time to peak of about 0.36 [18]. $\psi_2(t)$ and $\psi_3(t)$ are derived from the accelerograms of the El Centro and Taft earthquakes [18,95]. The shapes of the enveloping functions are shown in Fig. 47. Typical samples of artificial earthquake excitations in the form of a modulated white noise are shown in Fig. 48.

The method of Monte Carlo simulation is used to obtain the probabilistic information of time to the first snap-through. Numerical results are obtained for the case of $\lambda = 5.0$, $\beta = 0.2$, and $\Phi_o = 5.0$, and given in Table 6.6. A minimum time, in Table 6.6, represents the fastest time at which any record of the first snap-through occurs, while a maximum time is the latest time. Curves of probability distribution of the first-passage failure are presented in Figs. 49 and 50, for the reliability function and the probability density function, respectively. Results indicate the effect of the nonstationary nature of an earthquake excitation on the curves of reliability function and on the mean time. The rise time to peak clearly affects the mean time and the fast drop of the reliability function is indicated for the fast rise time earthquake. The minimum time for the fast rise enveloping function is about one-half less than the minimum time for the moderate rise case.

Table 6.1

Effect of Δt on the Monte Carlo Simulation Results
($\lambda = 5.0$, $\beta = 0.20$, $\Phi_o = 5.0$, 500 realizations)

Δt	$\bar{T}$	σ_T
0.01	0.2717	0.1695
0.009	0.2671	0.1682
0.005	0.2582	0.1717
0.0045***	0.2510	0.1617
0.004	0.2486	0.1660
0.002	0.2486	0.1699
0.001	0.2367	0.1506

*** $\Delta t = \frac{1}{20}\frac{2\pi}{\omega_o}$

Table 6.2

Effect of Number of Snap-Through Realizations on the Monte Carlo Simulation Results
($\lambda = 5.0,\ \beta = 0.20,\ \Phi_o = 5.0, \Delta t = 0.0045$)

Number of Realizations	Mean Time	Standard Deviation
500	0.2510	0.1617
1000	0.2499	0.1649
2000	0.2468	0.1579
3000	0.2470	0.1606

Table 6.3

Effect of Φ_o on the Mean Time to First-Passage Failure
($\lambda = 5.0$, $\beta = 0.2$)

Φ_o	Monte Carlo Simulation	Energy Envelope Approximation
0.5	1.5649	1.5002
1.0	0.8525	0.7944
3.0	0.3550	0.3207
5.0	0.2442	0.2398

Table 6.4

Effect of β on the Mean Time to First-Passage Failure
($\lambda = 5.0$, $\Phi_o = 5.0$)

β	Monte Carlo Simulation	Energy Envelope Approximation
0.2	0.2442	0.2398
1.0	0.2511	0.2479
2.0	0.2682	0.2601
5.0	0.3240	0.3118
10.0	0.4675	0.4598
20.0	1.0882	1.1311

Table 6.5

Solutions of Monte Carlo Simulation For Multi-Mode Approximations
($\lambda = 5.0$, $\beta = 0.2$, $b = 3.5355$, $\Delta t = 0.004$, 500 realizations)

Case	Mean Time to First Snap-Through		
	1-Mode	2-Mode	4-Mode
1). $\Phi_o = 0.5$	0.8019	0.6920	0.6967
2). $\Phi_o = 1.0$	0.6092	0.5056	0.5130
3). $\Phi_o = 3.0$	0.3524	0.2860	0.2846
4). $\Phi_o = 5.0$	0.2442	0.2130	0.2124

Table 6.6

Effect of Nonstationary Properties of the Random Excitations
($\lambda = 5.0$, $\Phi_o = 5.0$, $\beta = 0.2$, $b = 3.5355$, $\Delta t = 0.004$, 1-mode, 500 realizations)

Enveloping Function No.	Mean Time	Standard Deviation	Minimum Time	Maximum Time
1	0.2442	0.1589	0.0360	1.1280
2	0.1631	0.0861	0.0520	0.7720
3	0.2878	0.1073	0.1160	0.7520

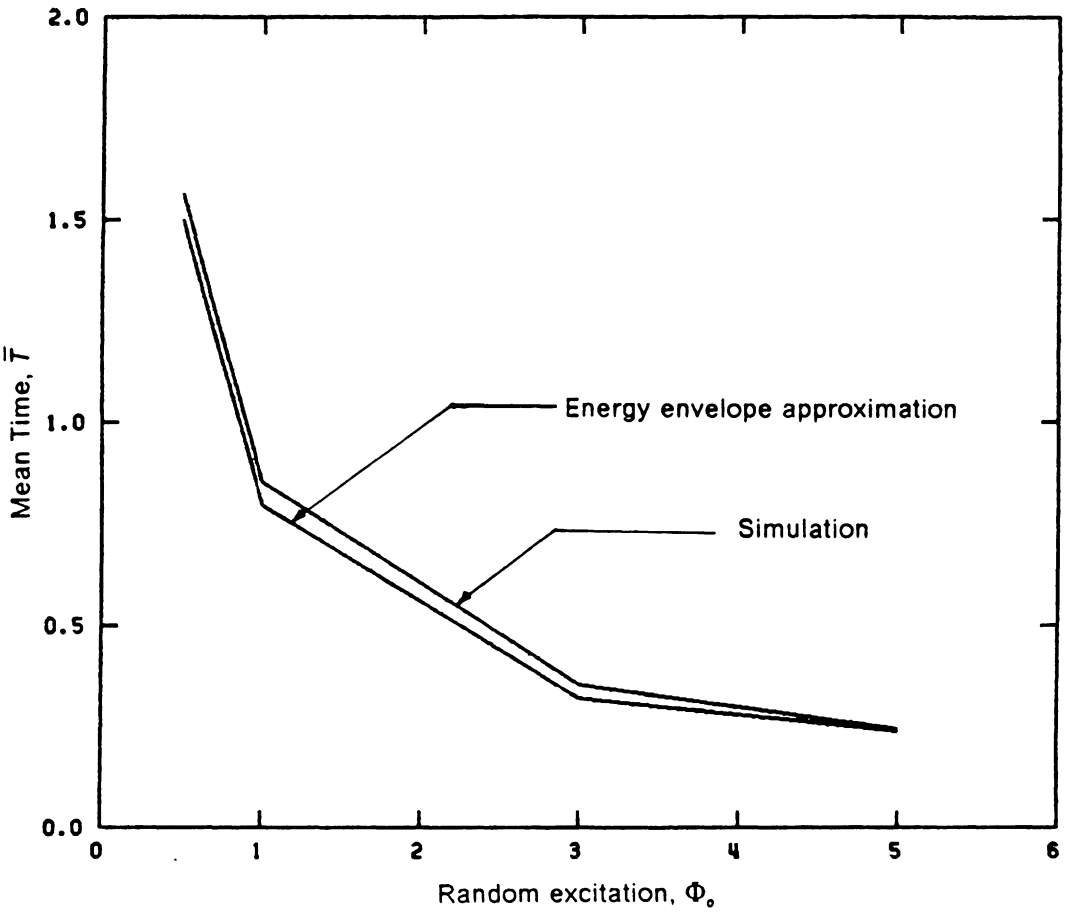

Figure 34. Variation of the mean time to first-passage failure for various values of random excitation: $\lambda = 5.0$ and $\beta = 0.2$.

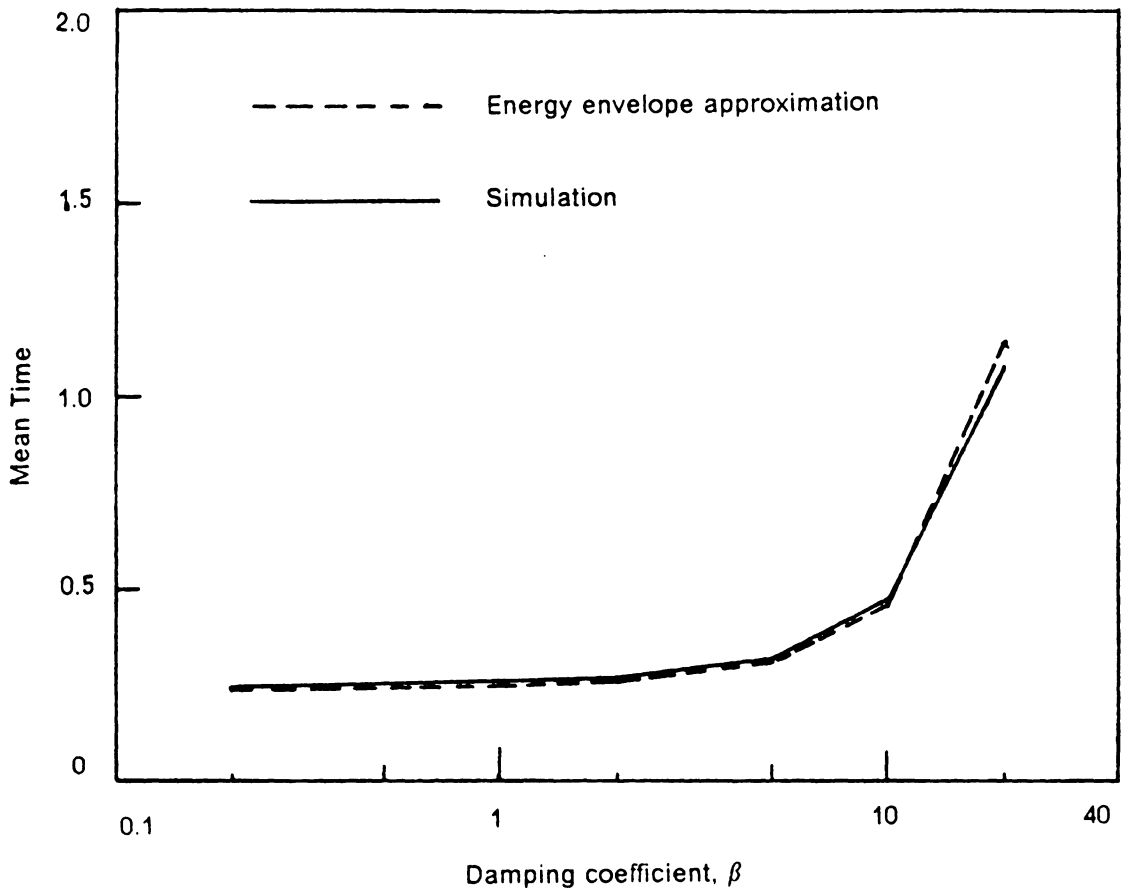

Figure 35. Variation of the mean time to first-passage failure for various values of damping parameter: $\lambda = 5.0$ and $\Phi_0 = 5.0$.

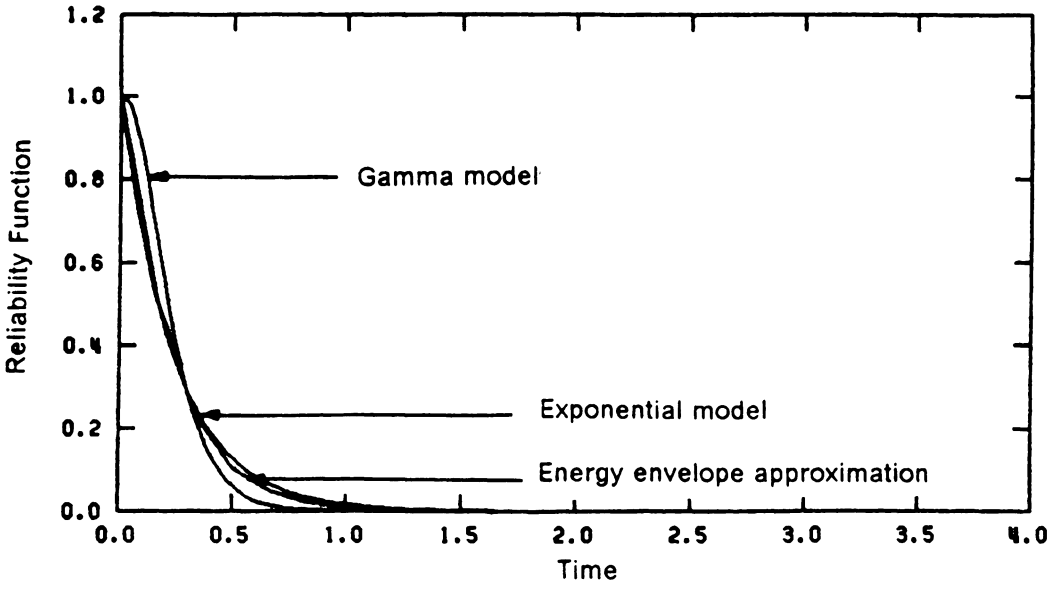

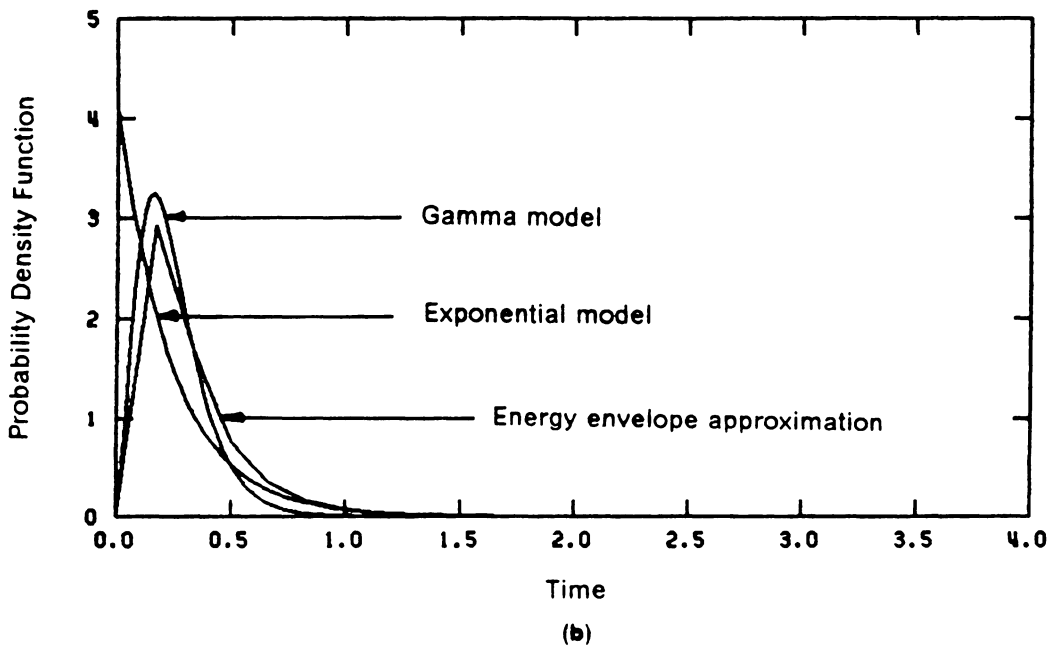

Figure 36. **Probability distribution of the first-passage failure for $\Phi_0 = 5.0$, $\beta = 0.2$:** (a). reliability function, (b). probability density function.

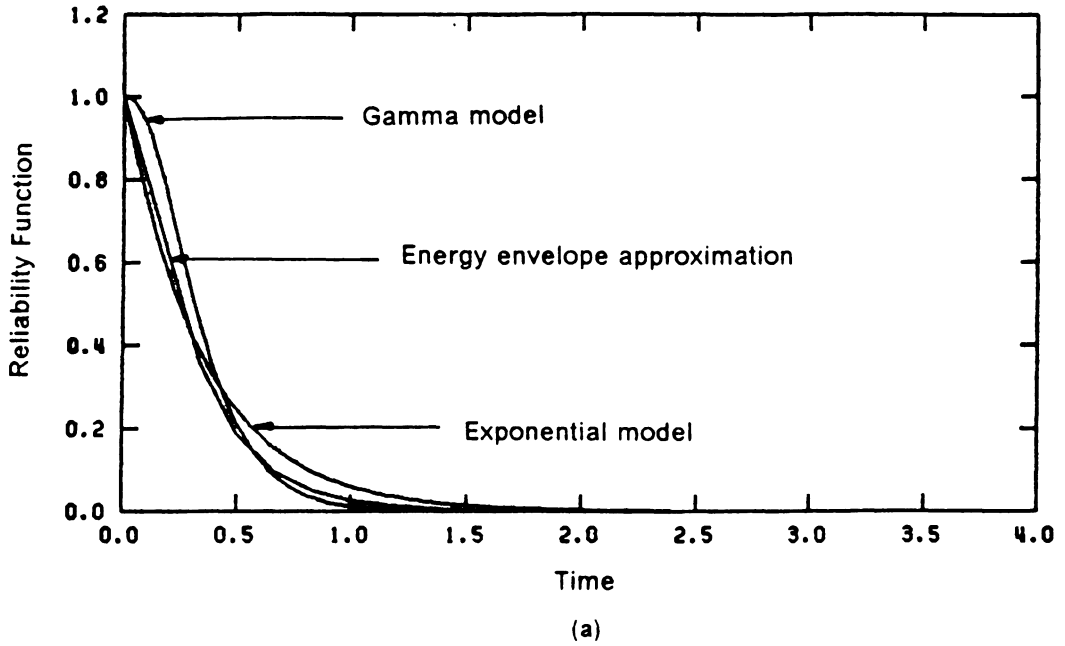

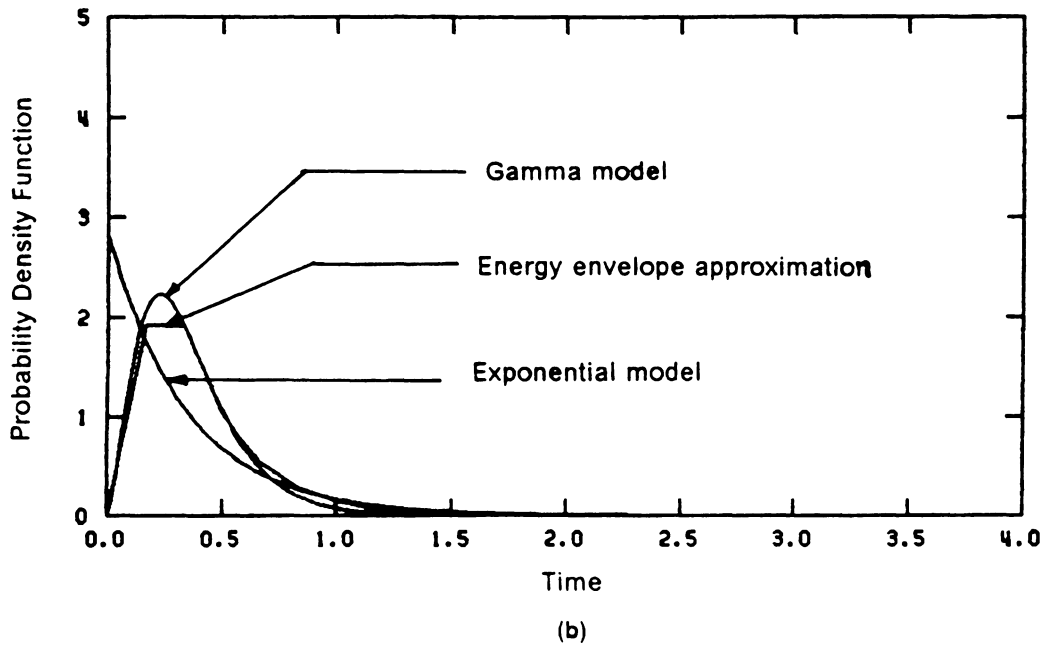

Figure 37. **Probability distribution of the first-passage failure for $\Phi_0 = 3.0$, $\beta = 0.2$:** (a). reliability function, (b). probability density function.

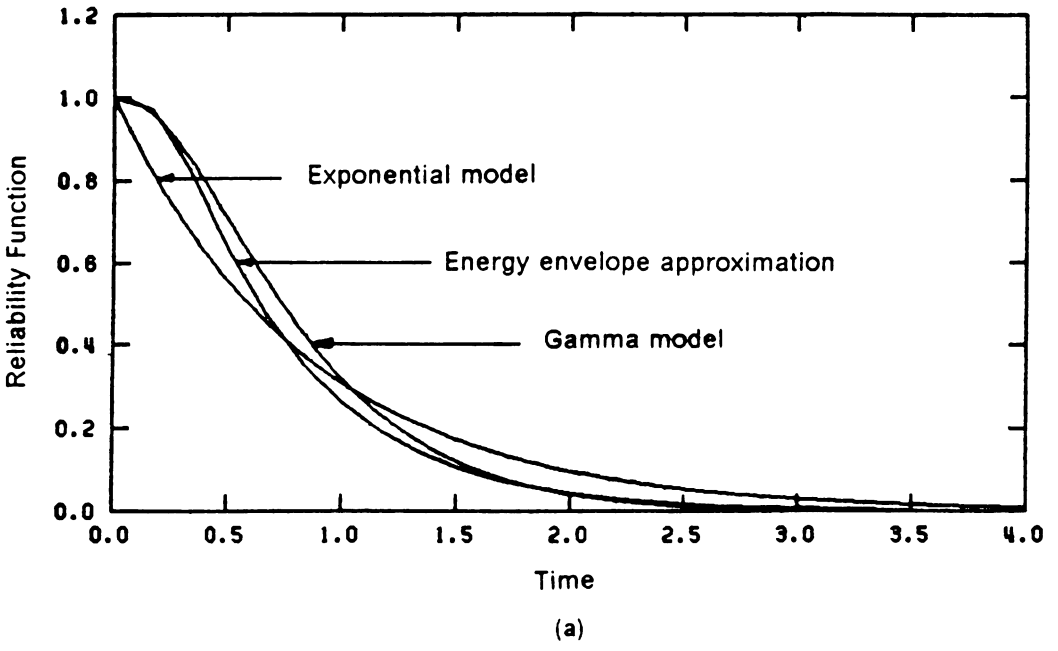

(a)

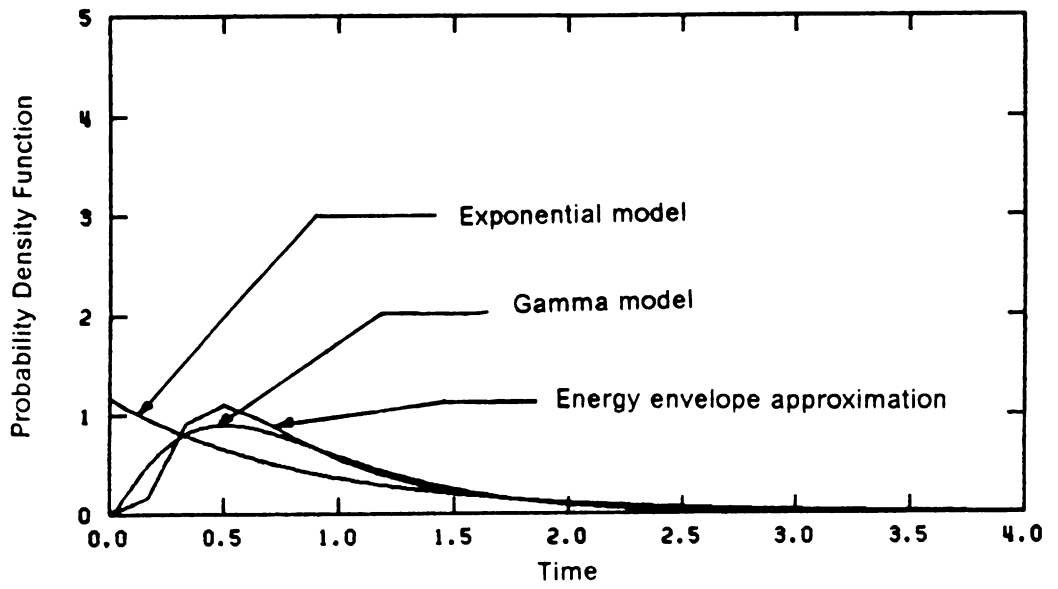

(b)

Figure 38. **Probability distribution of the first-passage failure for $\Phi_0 = 1.0$, $\beta = 0.2$:** (a). reliability function, (b). probability density function.

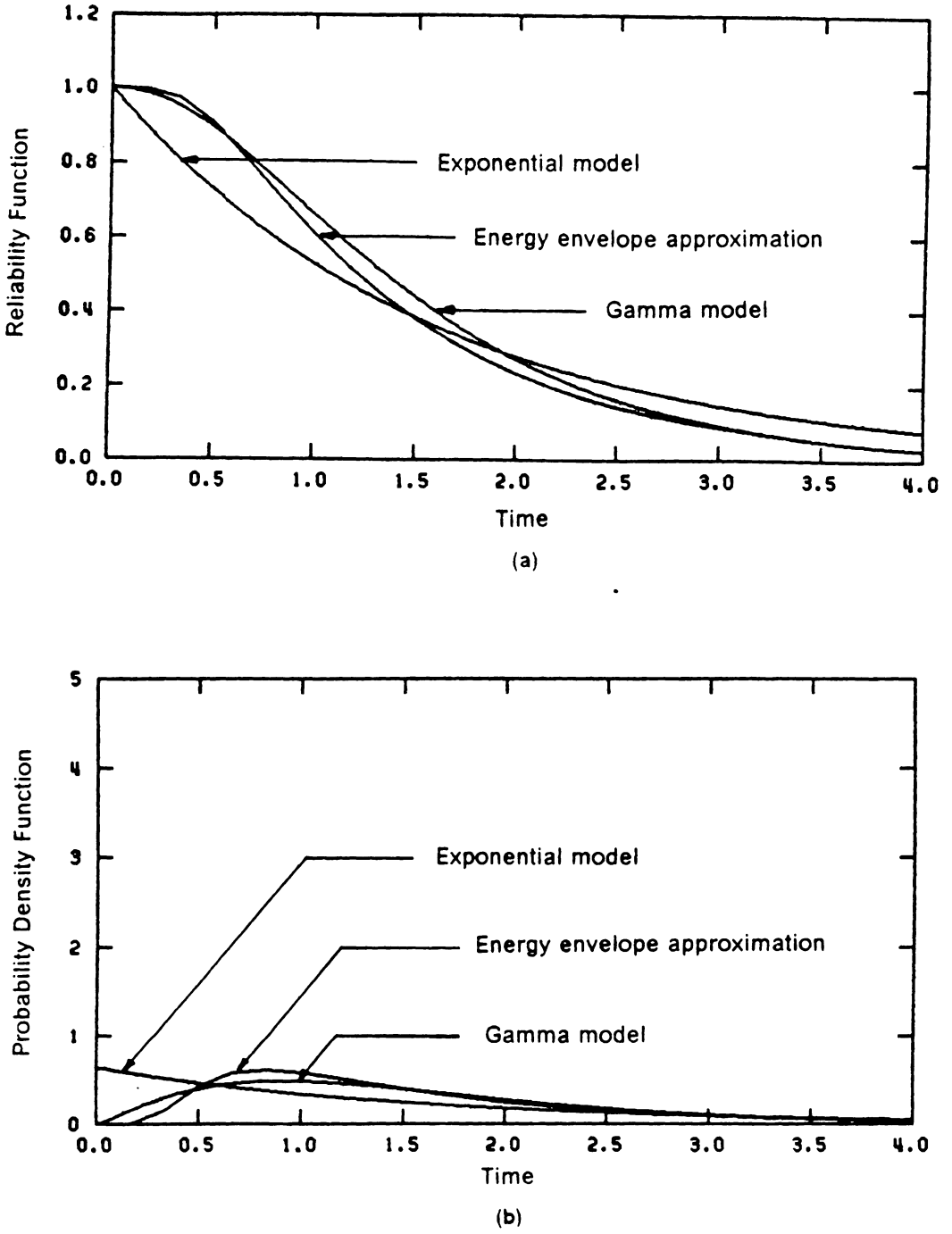

Figure 39. **Probability distribution of the first-passage failure for $\Phi_0 = 0.5$, $\beta = 0.2$:** (a). reliability function, (b). probability density function.

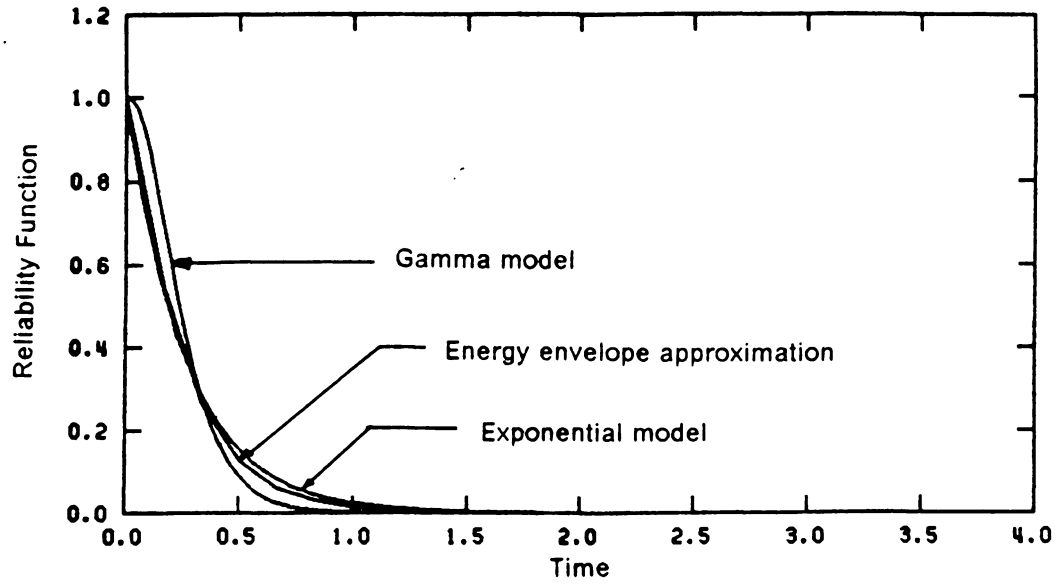

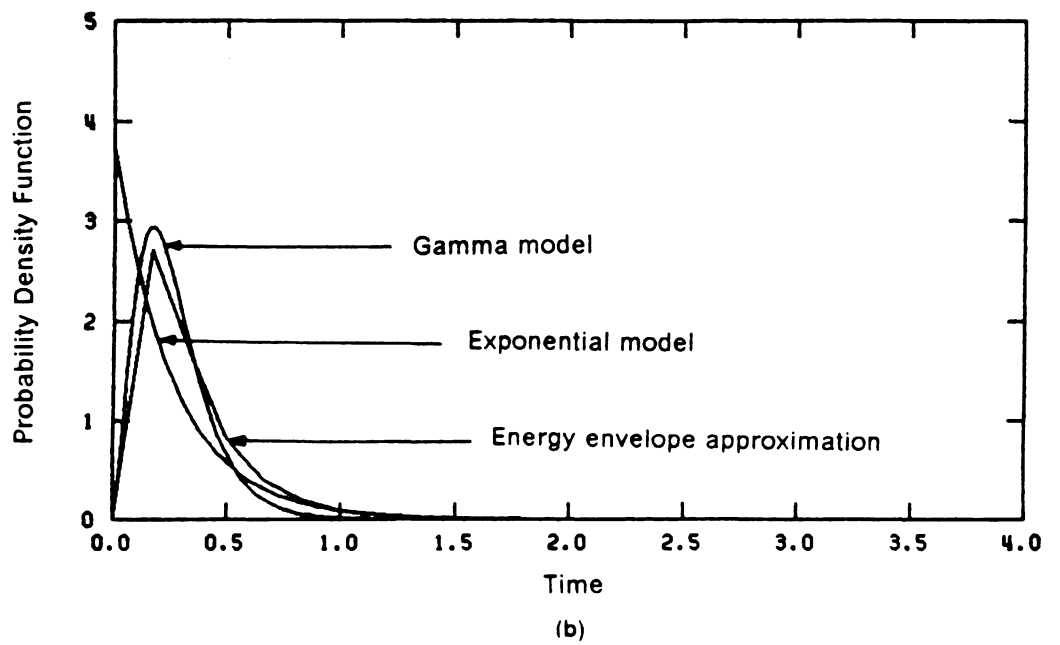

Figure 40. **Probability distribution of the first-passage failure for $\Phi_o = 5.0$, $\beta = 2.0$:** (a). reliability function, (b). probability density function.

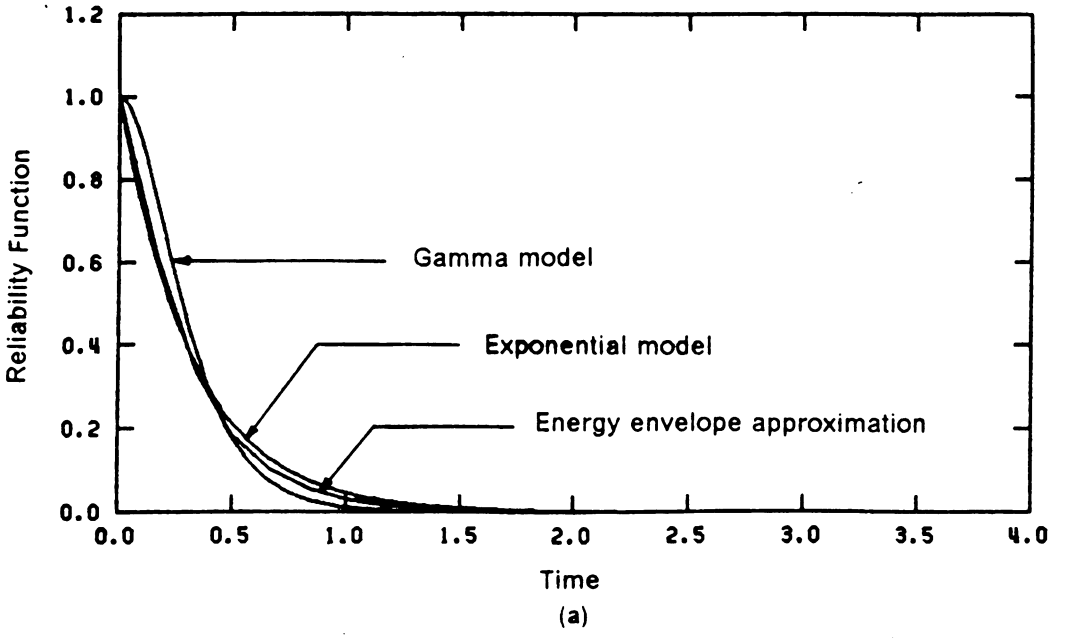

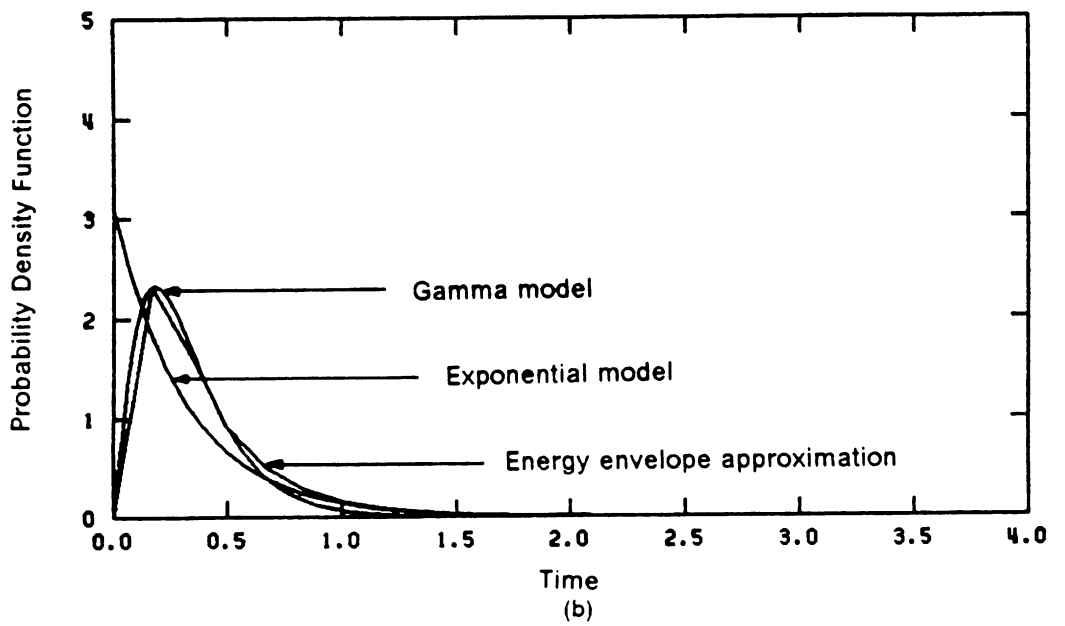

Figure 41. **Probability distribution of the first-passage failure for $\Phi_0 = 5.0$, $\beta = 5.0$:** (a). reliability function, (b). probability density function.

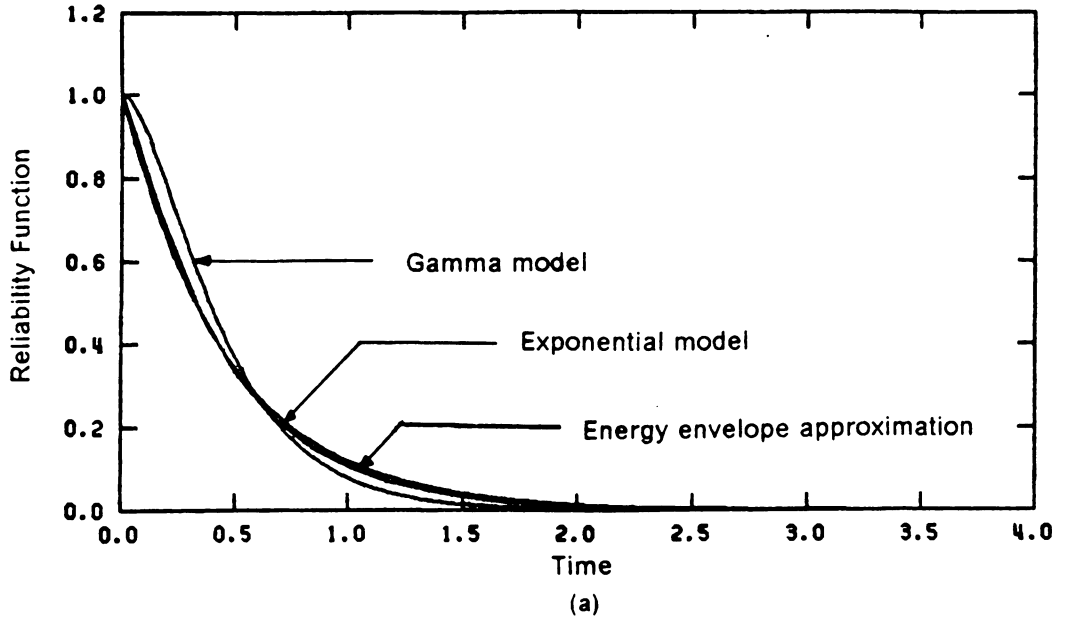

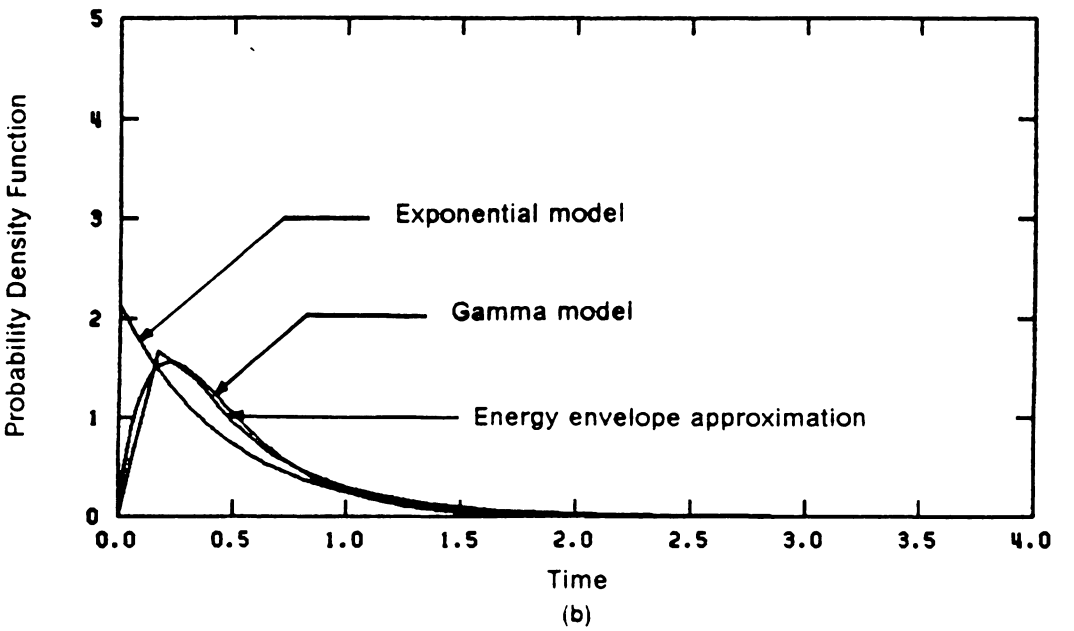

Figure 42. **Probability distribution of the first-passage failure for $\Phi_o = 5.0$, $\beta = 10.0$:** (a). reliability function, (b). probability density function.

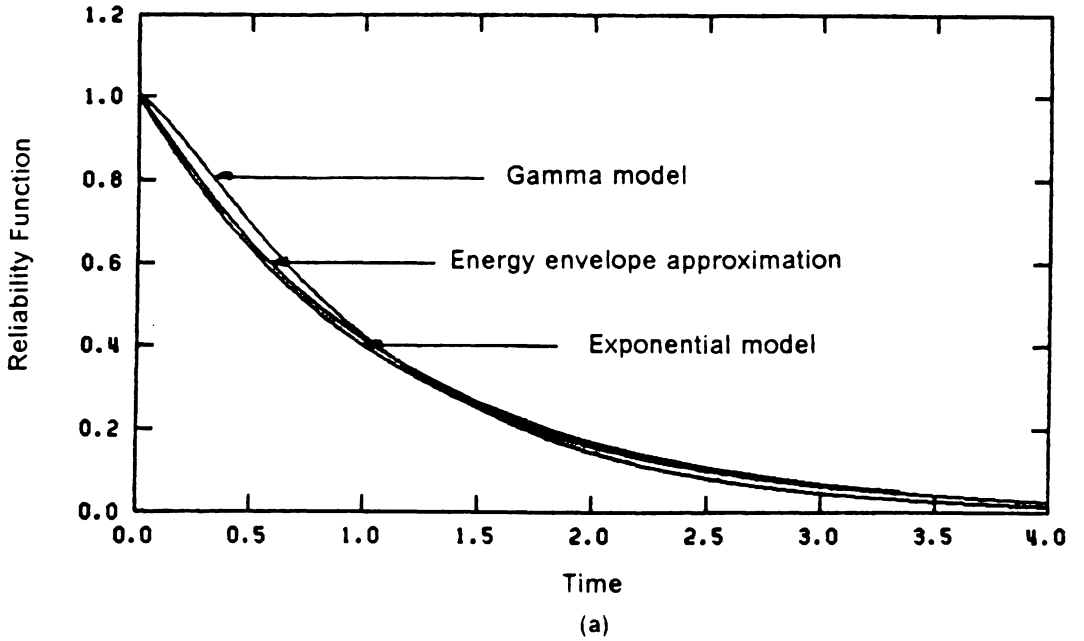

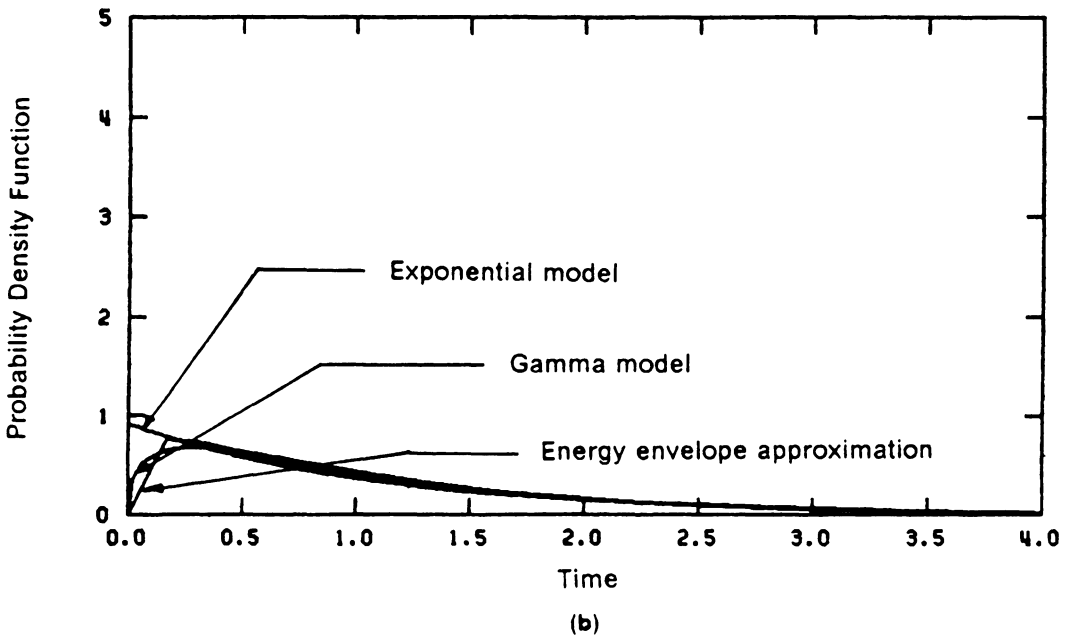

Figure 43. **Probability distribution of the first-passage failure for $\Phi_0 = 5.0$, $\beta = 20.0$:** (a). reliability function, (b). probability density function.

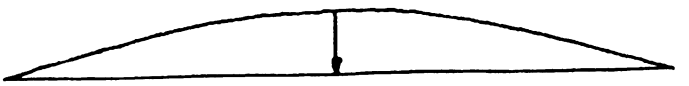

(a)

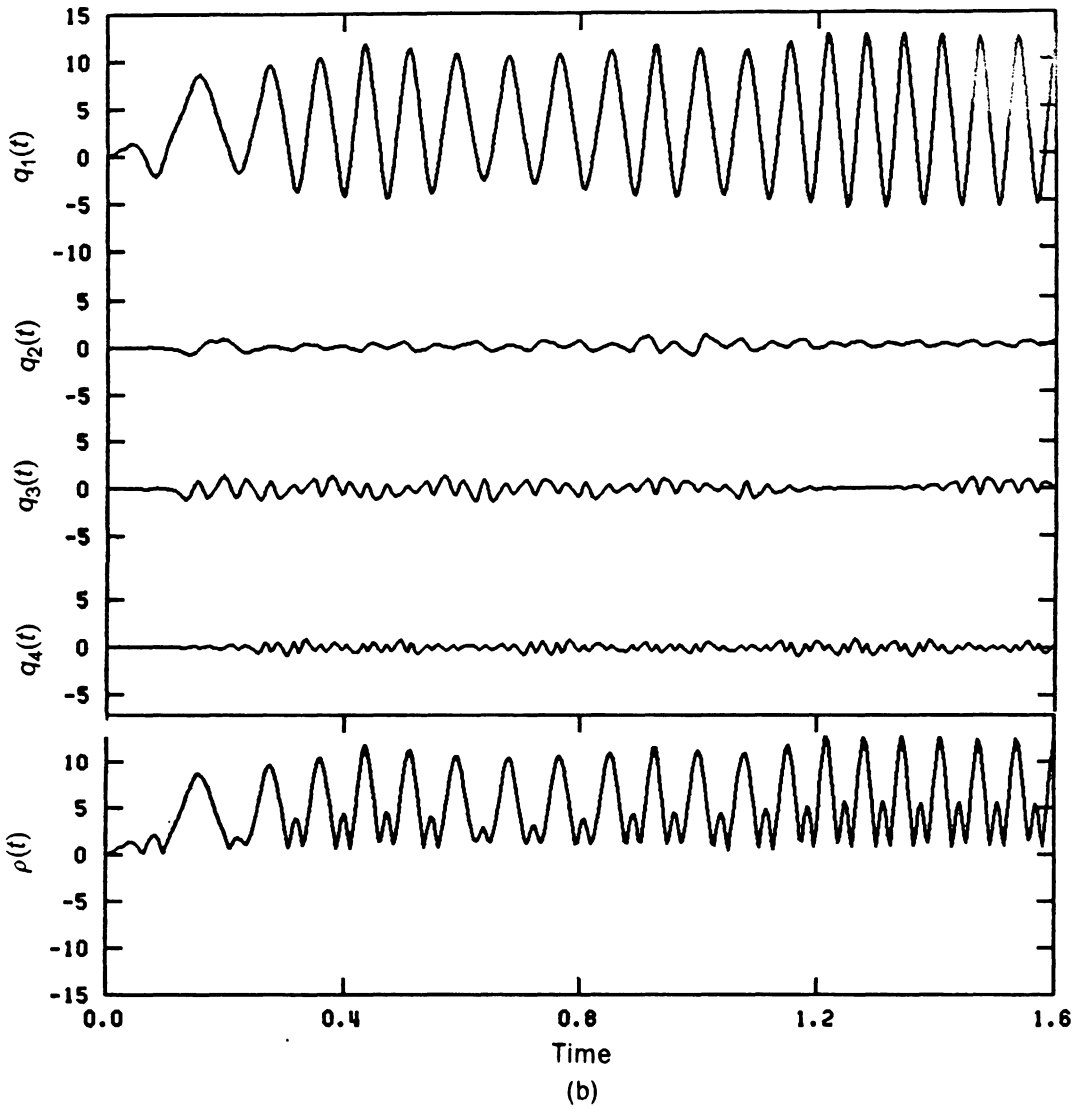

(b)

Figure 44. (a). Shape of the symmetric load corresponding to 1 mode of sinusoidal load, (b). Time history of response processes.

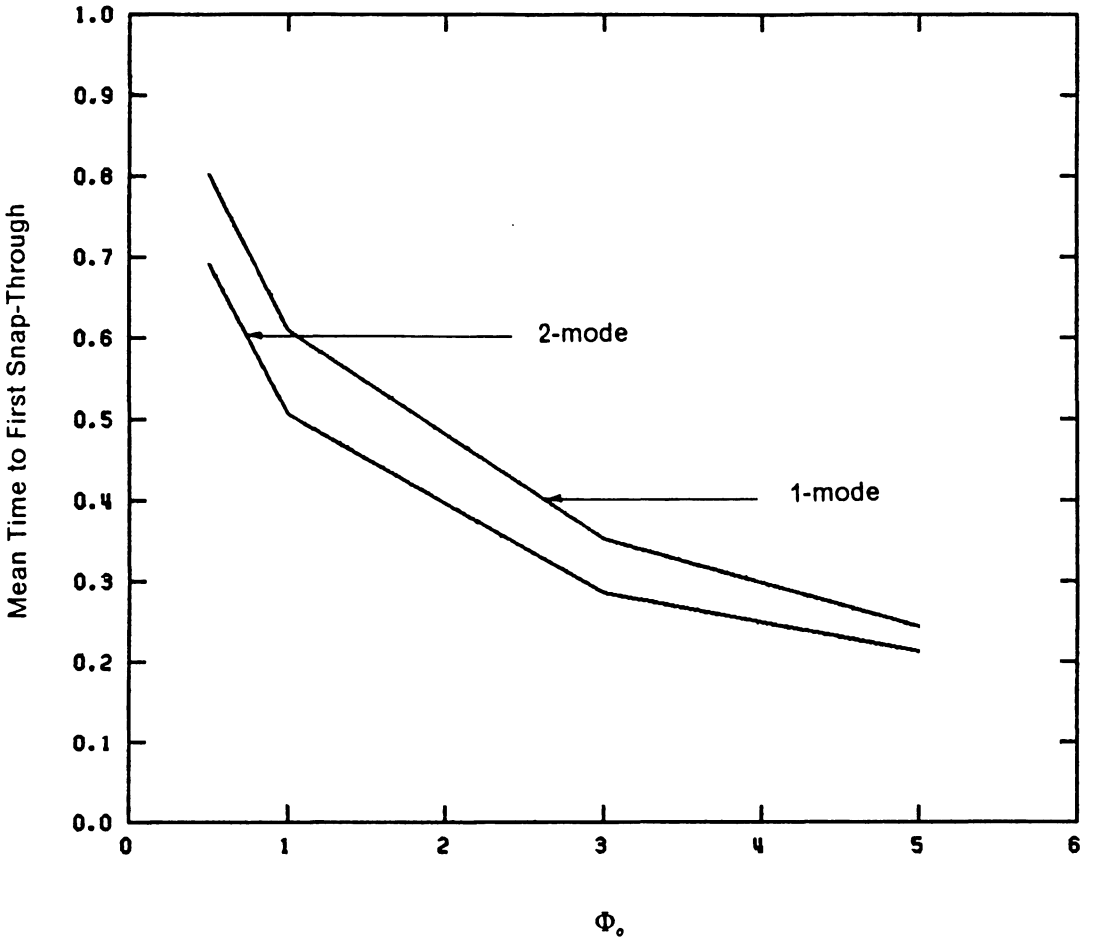

Figure 45. Effect of including 2-mode response on the mean time to first snap-through.

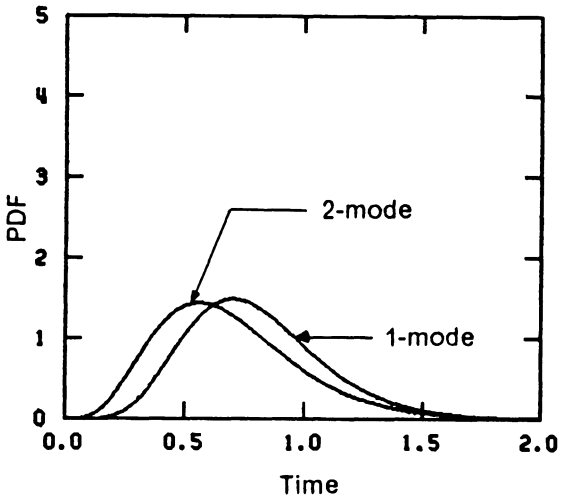

(a). $\Phi_o = 0.5$

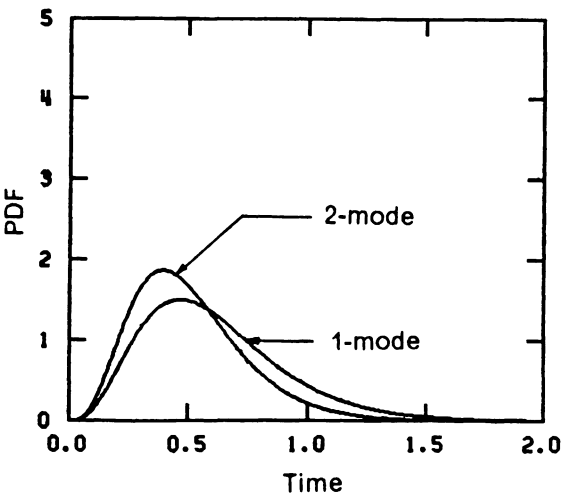

(b). $\Phi_o = 1.0$

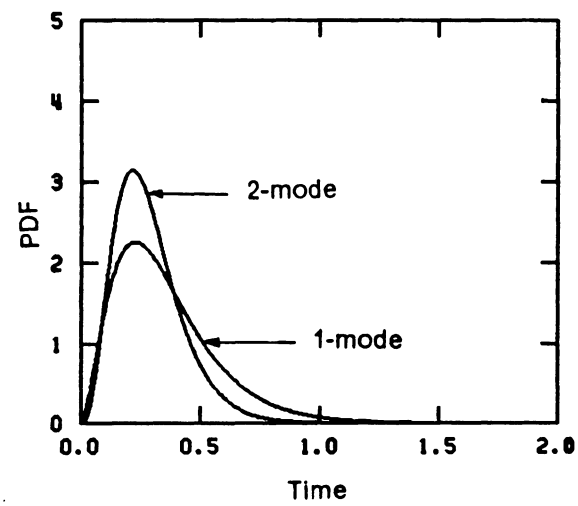

(c). $\Phi_o = 3.0$

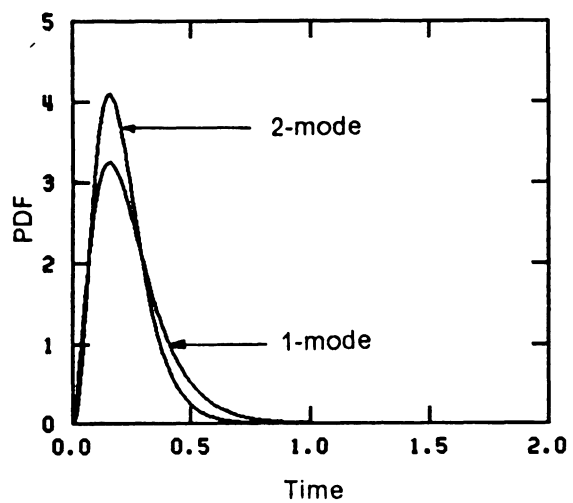

(d). $\Phi_o = 5.0$

Figure 46. Probability density function of time to first snap-through for various values of random excitation.

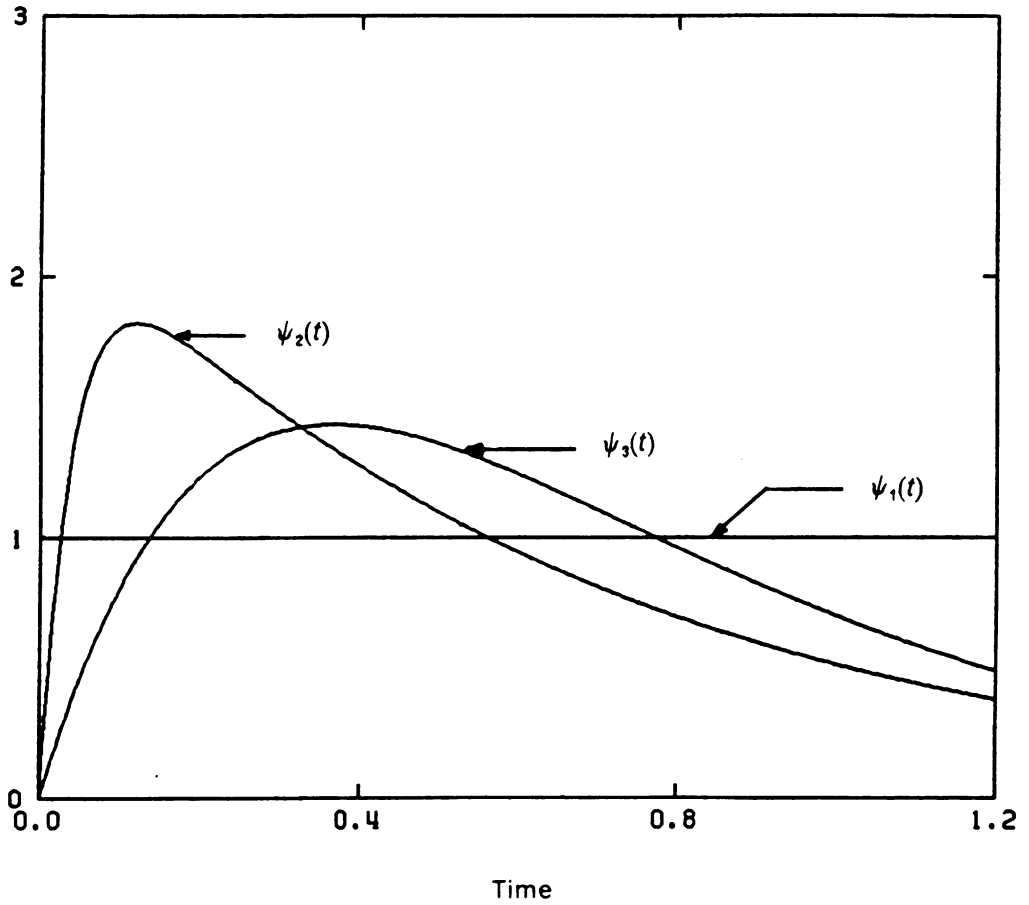

Figure 47. Shapes of the enveloping functions

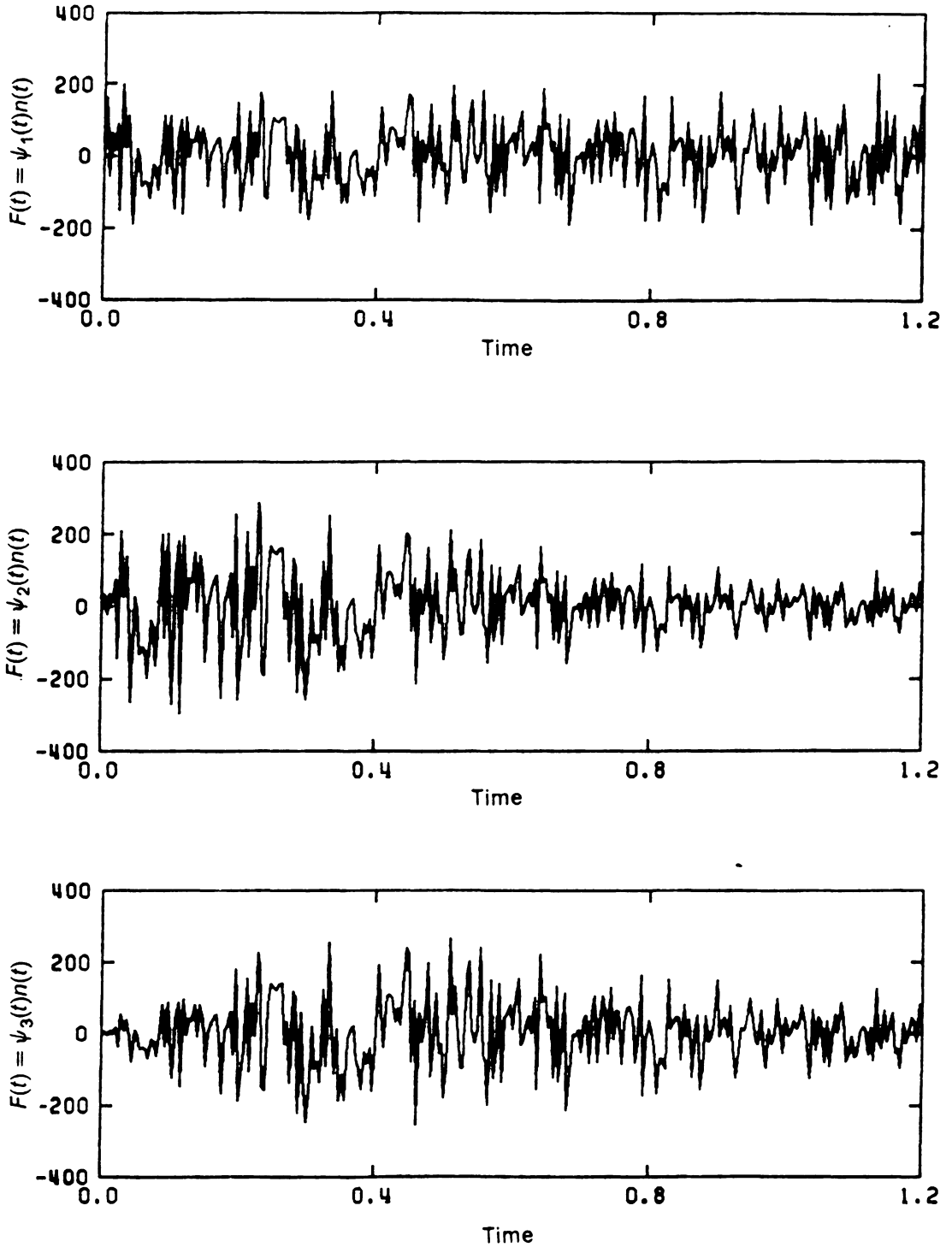

Figure 48. Typical samples of artificial earthquake excitation

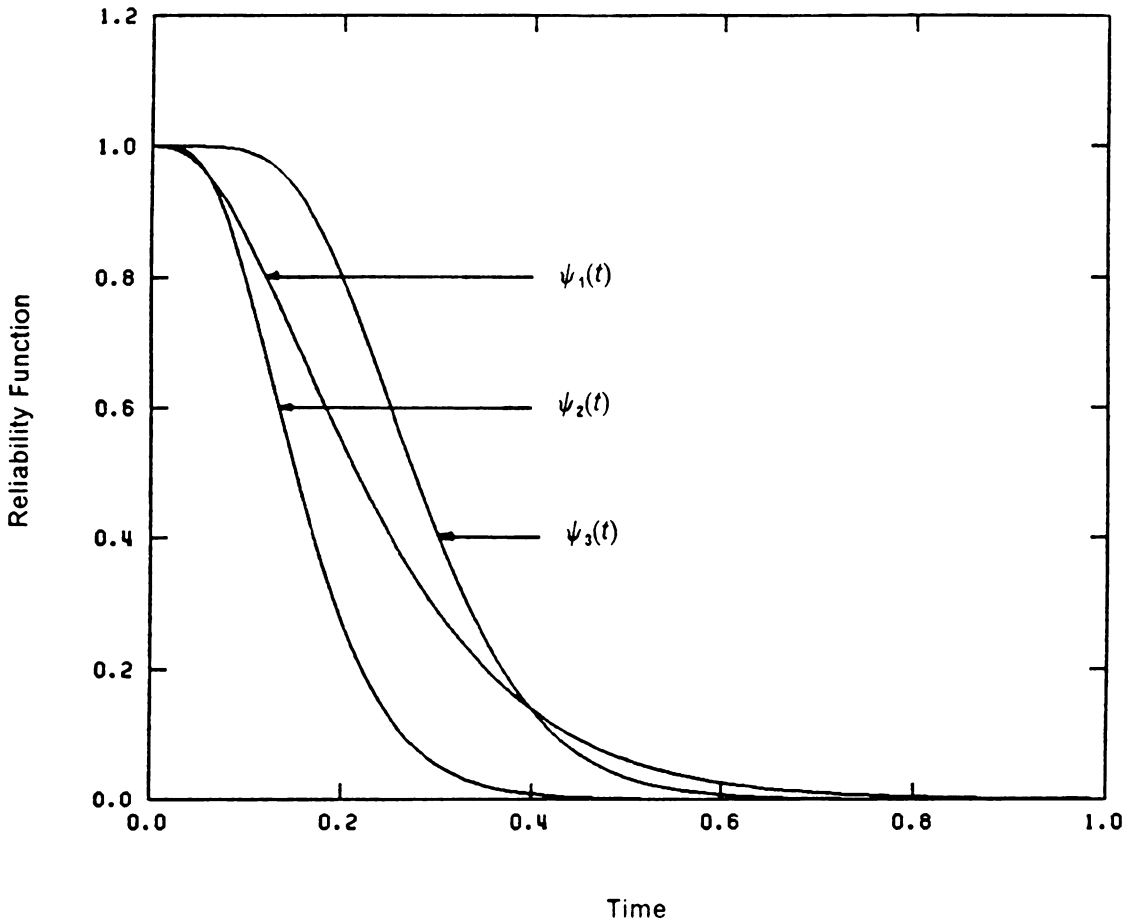

Figure 49. Effect of modulating functions on the reliability function

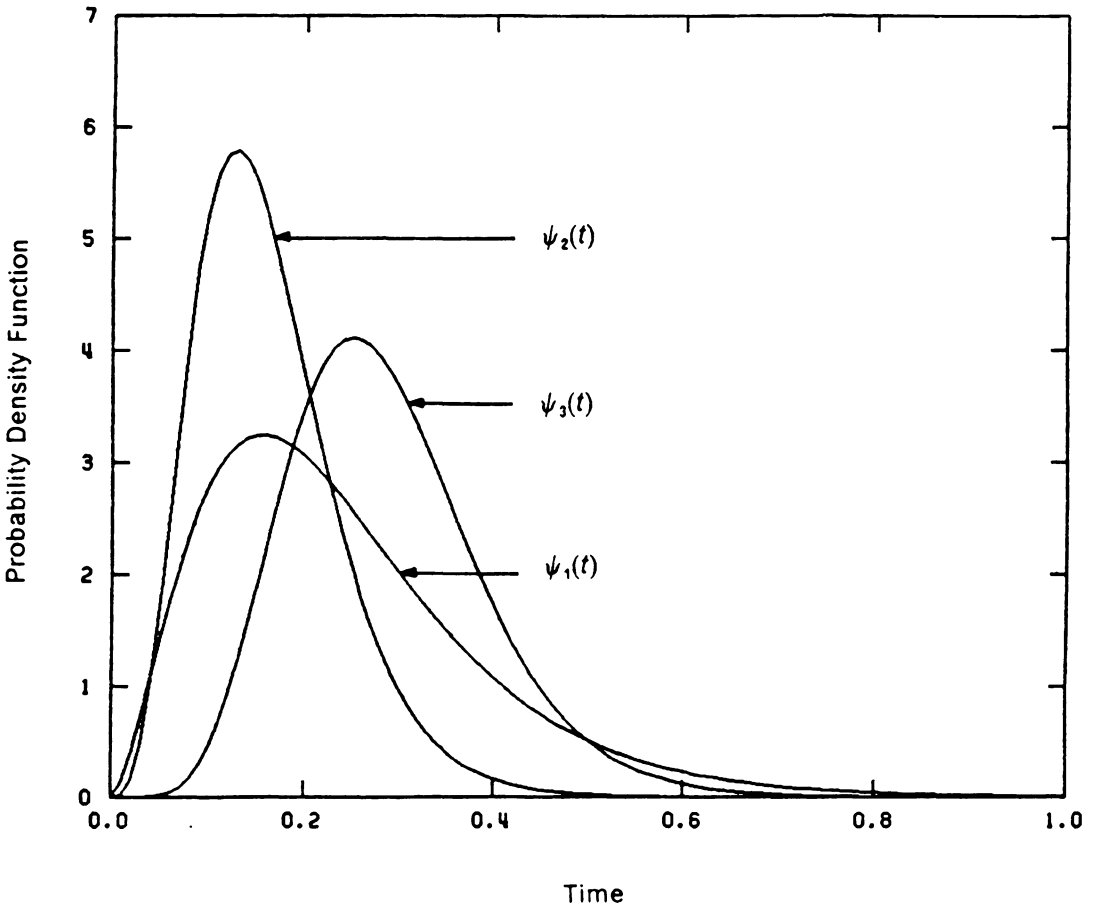

Figure 50. Effect of modulating functions on the density function of the probability of time to first snap-through.

Chapter VII

Conclusions

The snap-through of a shallow arch subjected to random excitation was investigated. This type of problem is also known as the first-passage time problem. The arch is assumed to fail by dynamic snap-through when its displacement response crosses a given threshold. The given threshold is usually defined by some critical barrier, such as a single-sided barrier or a double-sided barrier. This study used a single-sided barrier. The parameter of interest is the time when the response exceeds the critical barrier for the first time, which is also known as the first-passage time or the time to first snap-through. The reliability of the structure or the survival probability is the probability that the response stays within the safe domain throughout the considered time interval. Probability distributions of the first-passage failure and the mean time to failure are the quantities of interest.

The structure considered in this study was a shallow arch with deterministic properties, such as known initial rise and initial shape. The initial rise of the arch was small, so the arch was shallow and capable of failure due to dynamic snap-through. The arch was simply supported and had a sinusoidal initial shape. The arch was subjected to a time-dependent sinusoidal loading applied at time zero. There was no initial static load and the arch was assumed to start from rest. The governing equation of motion of the arch was nonlinear in the restoring forces of the softening type.

In the first part of the study, the critical random loading for the dynamic snap-through of the shallow arch was investigated using the method of computer simulation. The random excitation was assumed to be a stationary white-noise process. The primary object was the determination of the critical power spectral density parameter of the random excitations. The vanishing or diminishing of the average frequency of snap-through or zero-crossing, which was defined as the number of zero crossings of the maximum response of the arch divided by the time period, was used to estimate this parameter. A precise or exact value of the critical random loading could not be obtained using this criterion, since it was based on numerical integration of the nonlinear equation of motion and a computer simulation which was expensive and time-consuming. However, the critical value or range of critical values of the intensity of random excitations could be estimated with a reasonable degree of accuracy.

The second part of this study was related to the first-passage time problem of a shallow arch subjected to white noise. For an oscillator subjected to white noise, the displacement and velocity processes are governed by the Fokker-Planck-Kolmogorov (FPK) equation. In this study, an energy envelope process was used to approximate the first-passage failure associated with the displacement process. The approximate FPK equation governing the energy envelope process was derived based on the assumption that, for a system with light damping, the energy envelope process could be modelled, to a close approximation, as a one-dimensional Markov process. The implicit finite difference technique , of the Crank-Nicolson type, was used to solve the diffusion process. Solutions were obtained in the form of the mean time to first-passage failure and curves of probability distribution function.

The method of Monte Carlo simulation was then used to solve the same problem. A large number of records of the random forcing function was simulated and used as input in the numerical integration of the nonlinear equation of motion. For each record of excitation, the Runge-Kutta method was used to obtain the time history of the displacement response, and the time at which the response exceeded the critical barrier for the first time was recorded. 500 realizations of time to the first snap-through were collected. Then statistics of the time to first snap-through, such as the mean time and standard deviation, were estimated. Data of

realizations and statistical properties were then used to select an empirical distribution model to represent the probability distribution of the time to first snap-through.

Results of the method of the energy envelope approximation were compared with those of the computer simulation. Comparisons were accomplished based on the mean time to failure and curves of the probability distribution of first-passage failure. Results of both methods were in close agreement. Then, Monte Carlo simulation was used to examine the effect of including more than one mode in the equation of motion. Multi-mode approximations up to 4 modes were considered. Finally, the effect of nonstationary random excitation on the first-passage failure was studied using the computer simulation. The random excitation was taken as a modulated white-noise process.

Results of this study can be summarized as follows:

(1). An increase in the initial rise parameter of the arch increased the critical power spectral density parameter of the random excitations, and a decrease in the damping coefficient reduced the critical intensity of random loading.

(2). An estimate of the critical power spectral density parameter for the snap-through of a shallow arch subjected to white-noise excitation is given by

$$\Phi_{cr} = (10 \times 10^{-5})\, \lambda^4,$$

where λ is the initial rise parameter.

(3). The energy envelope approximation greatly simplified the first-passage failure problems associated with the displacement process. An increase in the damping coefficient increased the mean time to failure, while an increase in the strength of random excitations reduced the mean time. The mean time to failure tended to increase rapidly with increase in the damping when the damping coefficient was greater than 2.0. The values of damping less than 2.0 had an insignificant effect of the first-passage failure. Curves of probability distribution were observed to be of the exponential form.

(4). For all ranges of parameters considered in this study, results of the computer simulation indicated that the gamma distribution was the most appropriate distribution for the time to first snap-through.

(5). The difference of results between the method of energy envelope approximation and the computer simulation method was small. Therefore, the method of energy envelope approximation was reliable and efficient for the range of parameters considered in this study, especially for small values of damping coefficient.

(6). Results of the 2-mode approximation of the equation of motion were significantly different from the one-mode approximation. For the arch under the symmetric load corresponding to the first mode of sinusoidal loading, the higher modes than two modes offer small contribution to the total response.

(7). The nonstationary properties of random excitation had some effect on the response of the arch and the first-passage probability. Results depended on the time to peak and the amplitude of peak of the ground accerelations. Therefore, variability in the nonstationary properties of the actual earthquake excitation is very important in the nonlinear analysis of structures, since a small magnitude of variability might significantly alter the response of the structure.

References

1. Abramowitz, M., and Stegun, I. A., *Handbook of Mathematical Functions with Formulas, Graphs, and Mathematical Tables*, Dover Publications, Inc., New York, 1972.

2. Amin, M., and Ang, A. H-S., "Nonstationary Stochastic Model of Earthquake Motions," *Journal of the Engineering Mechanics Division, ASCE,* Vol. 94, No. EM2, 1968, pp. 559-583.

3. Ang, A. H-S., "Probability Concepts in Earthquake Engineering," in *Applied Mechanics in Earthquake Engineering*, edited by W. D. Iwan, ASME, AMD, Vol. 8, 1974, pp. 225-259.

4. Ang, A. H-S., and Tang, W. H., *Probability Concepts in Engineering Planning and Design, Volumn I-Basic Principles*, John Wiley and Sons, New York, 1975.

5. Ariaratnam, S. T., and Sankar, T. S., "Dynamic Snap-Through of Shallow Arches Under Stochastic Loads," *AIAA Journal*, Vol. 6, 1968, pp. 798-802.

6. Atkinson, J. D., "Eigenfunction Expansions for Randomly Excited Nonlinear Systems," *Journal of Sound and Vibration*, Vol. 30, No. 2, 1973, pp. 153-172.

7. Augusti, G., Baratta, A., and Casciati, F., *Probabilistic Methods in Structural Engineering*, Chapman and Hall, New York, 1983, pp. 51-106.

8. Bergman, L. A., and Heinrich, J. C., "Solution of the Pontriagin-Vitt Equation for the Moments of Time to First-Passage of the Randomly Accelerated Particle by the Finite Element Method," *International Journal for Numerical Methods in Engineering*, Vol. 15, 1980, pp. 1408-1412.

9. Bergman, L. A., and Spencer, B. F., "Solution of the First-Passage Problem for Simple Linear and Nonlinear Oscillators by the Finite Element Method," *Department of Theoretical and Applied Mechanics, University of Illinois at Urbana-Champaign*, T & M Report No. 461, 1983.

10. Bogdanoff, J. L., Goldberg, J. E., and Bernard, M. C., "Response of a Simple Structure to a Random Earthquake-Type Disturbance" *Bulletin of the Seismological Society of America*, Vol. 51, No. 2, April, 1961, pp. 293-310.

11. Bolotin, V. V., "Statistical Aspects in the Theory of Structural Stability," *Dynamic Stability of Structures*, edited by G. Herrmann, Pergamon Press, London, 1967, pp. 67-81.

12. Budiansky, B., and Roth, R. S., "Axisymmetric Dynamic Buckling of Clamped Spherical Caps," *U.S. NASA Technical Note D-1510,* December, 1962, pp. 597-606.

13. Bycroft, G. N., "White Noise Representation of Earthquakes," *Journal of the Engineering Mechanics Division, ASCE,* Vol. 86, No. EM2, April, 1960, pp. 1-16.

14. Caughey, T. K., "Equivalent Linearization Techniques," *Journal of the Acoustical Society of America*, Vol. 35, No. 11, 1963, pp. 1706-1711.

15. Caughey, T. K., "On the Response of a Class of Nonlinear Oscillators to Stochastic Excitation," *Proc. Colloquium Internationale du Centre National de le Recherche Scientifique*, No. 148, Marseille, France, September, 1964, pp. 393-402.

16. Caughey, T. K., "Nonlinear Theory of Random Vibrations," *Advances in Applied Mechanics*, Vol. 11, 1971, pp. 209-253.

17. Clough, R. W., and Penzien, J., *Dynamics of Structures,* McGraw-Hill, New York, 1975.

18. Corotis, R. B., and Marshall, T. A., "Oscillator Response to Modulated Random Excitation," *Journal of the Engineering Mechanics Division, ASCE,* Vol. 103, No. EM4, 1977, pp. 501-513.

19. Crandall, S. H., "Perturbation Techniques for Random Vibrations of Nonlinear Systems," *Journal of the Acoustical Society of America*, Vol. 35, No. 11, 1963, pp. 1700-1705.

20. Crandall, S. H., Chandiramani, K. L., and Cook, R. G., "Some First-Passage Problems in Random Vibration," *Journal of Applied Mechanics*, Vol. 33, September, 1966, pp. 532-538.

21. Crandall, S. H., "Correlation and Spectra of Nonlinear System Response," *Nonlinear Vibration Problems*, Vol. 14, 1973, pp. 39-53.

22. Crandall, S. H., "Non-Gaussian Closure Techniques for Stationary Random Vibration," *International Journal of Non-linear Mechanics*, Vol. 20, No. 4, 1985, pp. 1-8.

23. Dimentberg, M. F., "An Exact Solution to a Certain Non-linear Random Vibration Problem," *International Journal of Non-linear Mechanics*, Vol. 17, No. 4, 1982, pp.231-236.

24. Donaldson, M. T., "Dynamic Stability Boundaries for Shallow Arches Under Step, Impulse, and Pulse Loads," *M. S. Thesis*, Virginia Polytechnic Institute and State University, Blacksburg, Virginia, July, 1981.

25. Evan-iwanowski, R. M., *Resonance Oscillations in Mechanical Systems,* Elsevier Scientific Publishing Co., New York, 1976, pp. 158-173.

26. Fulton, R. E., and Barton, F. W., "Dynamic Buckling of Shallow Arches," *Journal of the Engineering Mechanics Division*,ASCE, Vol. 97, No. EM3, Proc. Paper 8214, June, 1971, pp.865-877.

27. Fung, Y. C., and Kaplan, A., "Buckling of Low Arches or Curved Beams of Small Curvature," TN2840, NACA, Nov. 1952.

28. Goldberg, J. E., Bogdanoff, J. L., and Sharpe, D. R., "The Response of Simple Nonlinear Systems to a Random Disturbance of the Earthquake Type," *Bulletin of the Seismological Society of America*, Vol. 54, 1964, pp. 263-276.

29. Greenwood, J. A., and Durand, D., "Aids for Fitting the Gamma Distribution by Maximum Likelihood," *Technometrics*, Vol. 2, No. 1, February, 1960, pp. 55-65.

30. Grutcher, H. L., "A Note on the Possible Misuse of the Kolmogorov-Smirnov Test," *Journal of Applied Meteorology*, Vol. 14, No. 8, December, 1975, pp. 1600-1603.

31. Hahn, G. J., and Godfrey, J. T., "Estimation of Weibull Distribution Parameters with Differing Test Times for Unfailed Units," *Technometrics*, Vol. 6, No. 1, 1964, pp. 118 (abstract).

32. Hahn, G. J., and Shapiro, S. S., *Statistical Models in Engineering*, John Wiley and Sons, New York, 1967.

33. Hoel, P. G., *Introduction to Mathematical Statistics*, 3rd Edition, John Wiley and Sons, New York, 1962.

34. Housner, G. W., "Characteristics of Strong Motion Earthquakes," *Bulletin of the Seismological Society of America*, Vol. 37, 1947, pp. 19-31.

35. Housner, G. W., "Behavior of Structures During Earthquakes," *Journal of the Engineering Mechanics Division, ASCE,* Vol. 85, No. EM4, 1959, pp. 109-129.

36. Housner, G. W., and Jennings, P. C., "Generation of Artificial Earthquakes," *Journal of the Engineering Mechanics Division, ASCE,* Vol. 90, No. EM1, February, 1964, pp. 113-150.

37. Hsu, C. S., "On Dynamic Stability of Elastic Bodies with Prescribed Initial Conditions," *International Journal of Engineering Science*, Vol. 4, No. 1, March, 1966, pp. 1-21.

38. Huang, N. C., and Nachbar, W., "Dynamic Snap-Through of Imperfect Viscoelastic Shallow Arches," *Journal of Applied Mechanics*, Vol. 35, No. 2, June, 1968, pp. 289-296.

39. Hull, T. E., Enright, W. H., and Jackson, K. R., "User's Guide for DVERK-A Subroutine for Solving Non-Stiff ODE's," TR No. 100, Department of Computer Science, University of Toronto, October, 1976.

40. Humphreys, J. S., "On Dynamic Snap Buckling of Shallow Arches," *AIAA Journal*, Vol. 4, No. 5, 1966, pp. 878-886.

41. Ilin, A. M., and Khasminski, R. Z., "On Equations of Brownian Motion," *Theory of Probability and Its Applications*, Vol. 9, 1964, pp.421-444.

42. *IMSL User's Guide*, DVERK Subroutine, Publication of User Services Department, VPI Computer Center Library, 1982.

43. *IMSL User's Guide*, GNNML Subroutine, Publication of User Services Department, VPI Computer Center Library, 1982.

44. *IMSL User's Guide*, MDBETA Subroutine, Publication of User Services Department, VPI Computer Center Library, 1982.

45. *IMSL User's Guide*, MDGAM Subroutine, Publication of User Services Department, VPI Computer Center Library, 1982.

46. Iwan, W. D., and Yang, I. M., "Application of Statistical Linearization Techniques to Nonlinear Multi-degree-of-freedom Systems," *Journal of Applied Mechanics*, Vol. 39, 1972, pp. 545-550.

47. Iwan, W. D., "A Generalization of the Method of Equivalent Linearization," *International Journal of Non-linear Mechanics*, Vol. 8, 1973, pp. 279-287.

48. Iwan, W. D., "Application of Nonlinear Analysis Techniques," in *Applied Mechanics in Earthquake Engineering*, edited by W. D. Iwan, ASME, AMD, Vol. 8, 1974, pp. 135-162.

49. Iwan, W. D., and Mason, A. B. Jr., "Equivalent Linearization of Systems Subjected to Nonstationary Random Excitation," *International Journal of Non-linear Mechanics*, Vol. 15, 1980, pp. 71-82.

50. Iyengar, R. N., and Dash, P. K., "Study of Random Vibration of Nonlinear Systems by Gaussian Closure Technique," *Journal of Applied Mechanics*, Vol. 45, 1978, pp. 393-399.

51. Iyengar, R. N., and Rao, P. N., "Generation of Spectrum Compatible Accelerograms," *Earthquake Engineering and Structural Dynamics*, Vol. 7, 1979, pp. 253-263.

52. Iyengar, R. N., and Prodhan, K. C., "Classification and Rating of Strong-Motion Earthquake Records," *Earthquake Engineering and Structural Dynamics*, Vol. 11, 1983, pp. 415-426.

53. Johnson, N. L., and Kotz, S., *Continuous Univariate Distributions-I, Distributions in Statistics*, John Wiley and Sons, New York, 1970.

54. Kanai, K., "Semi-Empirical Formula for the Seismic Characteristics of the Ground," *Bulletin of the Earthquake Research Institute*, University of Tokyo, Vol. 35, 1957, pp. 309-325.

55. Kao, J. H. K., "Computer Methods for Estimating Weibull Parameters in Reliability Studies," *IRE Trans. Reliability Quality Control*, Vol. 13, July, 1958, pp. 15-22.

56. Kuak, Y. C., and Lennox, W. C., "First Passage Probability for Snap-Through of a Cylindrical Shell Using Finite Elements," *Developments in Mechanics*, Vol. 11, Proceedings of the 17th Midwestern Mechanics Conference held at the University of Michigan, Ann Arbor, Michigan, May 6-8, 1981, pp. 155-156. (abstract)

57. Kushner, H. J., "The Cauchy Problem for a Class of Degenerate Parabolic Equations and Asymptotic Properties of Related Diffusion Process," *Journal of Differential Equations*, Vol. 6, No. 2, 1969, pp. 209-231.

58. Lennox, W. C., and Sykes, J. F., "First Passage Problem for a Linear Oscillator Using Finite Elements,"presented at the U.S.-Japan Seminar on Interdisciplinary Finite Element Analysis, Cornell University, August, 1978.

59. Lo, D. L. C., and Masur, E. F., "Dynamic Buckling of Shallow Arches," *Journal of the Engineering Mechanics Division, ASCE*, Vol. 102, No. EM5, Proc. Paper 12493, October, 1976, pp. 901-917.

60. Lock, M. H., "Snapping of a Shallow Sinusoidal Arch Under a Step Pressure Load," *AIAA Journal*, Vol. 4, No. 7, July 1966, pp. 1249-1256.

61. Mettler, E., "Stability and Vibration Problems of Mechanical Systems under Harmonic Excitation," *Dynamic Stability of Structures*, edited by G. Herrmann, Pergamon Press, London, 1967, pp. 169-188.

62. Nayfeh, A. H., "Combination of Tones in the Response of Simple Degree of Freedom Systems With Quadratic and Cubic Non-Linearities," *Journal of Sound and Vibration*, Vol. 92, No. 3, 1984,pp 379-386.

63. Nigam, N. C., *Introduction to Random Vibrations*, The MIT Press, Massachusetts, 1983.

64. Pi, H. N., Ariaratnam, S. T., and Lennox, W. C., "Numerical Solution for the Mean First-Passage Time for Snap-Through of Shells," *Developments in Theoretical and Applied Mechanics*, Vol. 5, Proceeding of the 5th Conference on Theoretical and Applied Mechanics held in Raleigh-Durham, North Carolina, April 16-17, 1970, pp. 235-253.

65. Pi, H. N., Ariaratnam, S. T., and Lennox, W. C., "First-Passage Time for Snap-Through of a Shell-Type Structure," *Journal of Sound and Vibration*, Vol. 14, No. 3, 1971, pp. 375-384.

66. Plaut, R. H., and Johnson, E. R., "The Effects of Initial Thrust and Elastic Foundation on the Vibration Frequencies of a Shallow Arch," *Journal of Sound and Vibration*, Vol. 78, No. 4, 1981, pp. 565-571.

67. Plaut, R. H., and Hsieh, J. -C., "Oscillations and Instability of a Shallow Arch Under Two-Frequency Excitation," *Journal of Sound and Vibration*, Vol. 102, No. 2, 1985, pp. 189-201.

68. Popelar, C. H., and Abraham, G. M., "A Comparison of Initial Velocities for Dynamic Instability of a Shallow Arch," *Developments in Theoretical and Applied Mechanics*, Vol. 5, Proceeding of the 5th Conference on Theoretical and Applied Mechanics held in Raleigh-Durham, North Carolina, April 16-17, 1970, pp. 745-762.

69. Rehak, M.,and Benaroya, H., "Simulation of a Random Differential Equation," *Proc., AIAA/ASME/ASCE/AHS 27rd Structures, Structural Dynamics and Materials Conference*, Vol. 2, 1986, pp. 464-473.

70. Roberts, J. B., "First-Passage Time for the Envelope of a Randomly Excited Linear Oscillator," *Journal of Sound and Vibration*, Vol. 46, No. 1, May, 1976, pp. 1-14.

71. Roberts, J. B., "First-Passage Probability for Nonlinear Oscillators," *Journal of the Engineering Mechanics Division, ASCE*, Vol. 102, No. EM5, October, 1976, pp. 851-866.

72. Roberts, J. B., "First-Passage Time for Oscillators with Nonlinear Restoring Forces," *Journal of Sound and Vibration*, Vol 56, 1978, pp. 71-86.

73. Roberts, J. B., "The Energy Envelope of a Randomly Excited Non-linear Oscillator," *Journal of Sound and Vibration*, Vol. 60, 1978, pp. 177-185.

74. Roberts, J. B., "Techniques for Nonlinear Random Vibration Problems," *Shock and Vibration Digest*, Vol. 16, No. 9, 1984, pp. 3-14.

75. Roberts, J. B., and Spanos, P. -T. D., "Stochastic Averaging: An Approximate Method of Solving Random Vibration Problems," *International Journal of Non-linear Mechanics*, Vol. 21, No. 2, 1986, pp. 111-134.

76. Roberts, J. B., "First-Passage Time for Randomly Excited Non-linear Oscillators," *Journal of Sound and Vibration*, Vol. 109, No. 1, 1986, pp. 33-50.

77. Sakata, M., and Kimura, K., "The Use of Moment Equations for Calculating the Mean Square Response of a Linear System to Nonstationary Random Excitation," *Journal of Sound and Vibration*, Vol. 67, No. 3, 1979, pp. 383-393.

78. Seide, P., "RMS Response of Initially Buckled Beams Subjected to Random Time Dependent Uniform Pressure," *Proc., AIAA/ASME/ASCE/AHS 23rd Structures, Structural Dynamics and Materials Conference*, Part 1, New Orleans ,May 1982, pp. 506-510.

79. Seide, P., "Snap-Through of Initially Buckled Beams Under Uniform Pressure," *Recent Advances in Structural Dynamics*, Southhampton, 2nd Conf., 1984, pp. 329-340.

80. Shinozuka, M., "On the Two-sided Barrier Problem," *Journal of Applied Probability*, Vol. 2, 1965, pp. 79-87.

81. Shinozuka, M., and Sato, Y., "Simulation of Nonstationary Random Process," *Journal of the Engineering Mechanics Division, ASCE,* Vol. 93, No. EM1, February, 1967, pp. 11-40.

82. Shinozuka, M., "Monte Carlo Simulation of Structural Dynamics," *Computers & Structures*, Vol. 2, 1972, pp. 855-874.

83. Shinozuka, M., and Wen, Y. -K., "Monte Carlo Solution of Nonlinear Vibrations," *AIAA Journal*, Vol. 10, No. 1, January , 1972, pp. 37-40.

84. Shinozuka, M., and Jan, C. -M., "Digital Simulation of Random Processes and Its Applications" *Journal of Sound and Vibration*, Vol. 25, No. 1, 1972, pp. 111-128.

85. Smith, G. D., *Numerical Solution of Partial Differential Equations-Finite Difference Method*, 2nd Ed., Clarendon Press, Oxford, 1978.

86. Solomos, G. P., and Spanos, P.-T. D., "Structural Reliability Under Evolutionary Seismic Excitation," in *Stochastic Methods in Earthquake Engineering*, edited by Cakmak, A. S., A Computational Mechanics Publication, Southampton, Great Britain, 1986, pp. 97-103.

87. Spanos, P.-T. D., "Monte Carlo Simulation of Response of Non-symmetric Dynamic System to Random Excitations," *Computers & Structures*, Vol. 13, 1981, pp. 371-376.

88. Spanos, P.-T. D., "Survival Probability of Nonlinear Oscillators Subjected to Broad-Band Random Disturbances," *International Journal of Non-linear Mechanics*, Vol. 17, No. 5/6 , 1982, pp. 303-317.

89. Tajimi, H., "A Statistical Method of Determining the Maximum Response of a Building Structure During an Earthquake," *Proc. 2nd World Conference on Earthquake Engineering*, Vol. 11, Tokyo and Kyoto, Japan, 1960.

90. To, C. W. S., "The Response of Nonlinear Structures to Random Excitation," *Shock and Vibration Digest*, Vol. 16, No. 4, 1984, pp. 13-33.

91. Toland, R. H., and Yang, C. Y., "Random Walk Model for First-passage Probability," *Journal of the Engineering Mechanics Division, ASCE*, Vol. 97, No. EM3, June, 1971, pp. 791-807.

92. Vaicaitis, R., Dowell, E. H., and Ventres, C. S., "Nonlinear Panel Response by a Monte Carlo Approach," *AIAA Journal*, Vol. 12, No. 5, May, 1974, pp. 685-691.

93. Vanmarcke, E. H., "Structural Response to Earthquakes," in Chapter 8 of *Seismic Risk and Engineering Decisions*, edited by Lomnitz, C. and Rosenblueth, E., Elsevier Scientific Publishing Co., New York, 1976, pp. 287-337.

94. Wen, Y. K., "Approximate Method for Nonlinear Random Vibration." *Journal of the Engineering Mechanics Division, ASCE*, Vol. 101, No. EM4, August, 1975, pp. 389-401.

95. Wiegel, R. L., *Earthquake Engineering and Structural Dynamics*, Prentice Hall, Inc., Englewood Cliffs, New Jersey, 1970

96. Wirsching, P. H., and Yao, J. T. P., "Monte Carlo Study of Seismic Structural Safety," *Journal of the Structural Division, ASCE*, Vol. 97, No. ST5, May, 1971, pp. 1497-1519.

97. Yang, J. N., and Shinozuka, M., "First-Passage Time Problem," *Journal of the Acoustical Society of America*, Vol. 47, 1970, pp. 393-394.

The vita has been removed from the scanned document